DEVELOPMENT OF SELF SENSING CEMENTITIOUS COMPOSITE SENSOR USING CARBON BLACK FOR PERFORMANCE MONITORING OF CONCRETE

A Seminar Report Submitted in Partial Fulfillment of the requirement for the Award of the Degree of

Master of Engineering

in

Structural Engineering

Submitted by

ASHANK DOGRA

(802224005)

Under Supervision of

DR. SHRUTI SHARMA
Professor
Department of Civil Engineering
TIET, Patiala

DR. ARPIT GOYAL
Assistant Professor
Department of Civil Engineering
TIET, Patiala

Department of Civil Engineering
Thapar Institute of Engineering &Technology
(Deemed to be University)
Patiala-147004 (Punjab)

August 2024

DECLARATION

I hereby declare that this is a bonafide work which is presented in this minor design project report/seminar report entitled **"DEVELOPMENT OF SELF SENSING CEMENTITIOUS COMPOSITE SENSOR USING CARBON BLACK FOR PERFORMANCE MONITORING OF CONCRETE"** as per the requirements for the award of **Master of Engineering** in **Structural Engineering,** submitted in the Department of Civil Engineering, Thapar Institute of Engineering and Technology (TIET), Patiala. This work is carried out under the guidance and supervision of **Dr. Shruti Sharma** and **Dr. Arpit Goyal.** It is declared that this work is original and has not been submitted anywhere else for the award of any other degree or certificate.

Date: 20/09/24.

Ashank.

(Ashank Dogra)

(802224005)

CERTIFICATE

This is to certify that the above statement made by the candidate is correct to the best of our knowledge.

Shruti Sharma 20/9/2024

(DR. SHRUTI SHARMA)

Professor

Department of Civil Engineering

TIET, Patiala

Arpit

(DR. ARPIT GOYAL)

Assistant Professor

Department of Civil Engineering

TIET, Patiala

i

ACKNOWLEDGEMENT

This research thesis would not have been done without the help and guidance of several individuals who provided valuable input, whether directly or indirectly, via their honest criticism. I want to express my deep thanks to Dr. Shruti Sharma, a Professor in the Department of Civil Engineering at Thapar Institute of Engineering and Technology, Patiala, and Dr. Arpit Goyal, an Assistant Professor in the same department, for their essential guidance, support, attentive listening to my ideas, and creative ideas for implementing them. For the enthusiasm and inspiration that pushed me throughout my job. I would like to express my gratitude to every staff member at the Institute for their invaluable assistance and provision of necessary resources, which were important in the successful completion of my study. I am unable to find the words that fully express my greatest appreciation for what they have done in conducting a variety of trials and procedures. Finally, I would want to express my gratitude to my family, who have always provided me with constant support and encouragement, particularly in my studies.

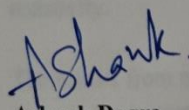

Ashank Dogra
(802224005)

ABSTRACT

In recent years, an innovative method has been used to detect different structural conditions by incorporating steel and carbon fibers into a cementitious composite. This technique aims to reduce the resistivity of the composite and establish a piezoresistive matrix. Smart cement-based nanomaterials, such as graphene derivatives like carbon fiber or carbon nanotube cementitious hybrids, or a combination of both, function as sensors for structural health monitoring (SHM). These materials are piezo-resistive, meaning that their resistivity changes in response to applied stress or strain. This signifies that a cement sample or construction does not need the external or supplementary connection of any sensor. On the other hand, the cement composite has the capability to sense its own tension as well as several other elements.

The current research describes the several tests conducted to assess the mechanical and electrical characteristics of cementitious mortar samples containing different proportions of CB (Carbon Black). Testing was conducted at intervals of 28, and 56 days throughout the curing process. The mechanical qualities were assessed by compressive strength and flexural strength tests, while the electrical properties were evaluated through electrical resistivity and piezo resistivity tests. The self-sensing capacity of the composite phase is due to the piezoresistive action of functional filler particles, which are uniformly distributed and establish a conductive link. Therefore, when a cementitious composite is subjected to external forces, the structure of the material changes, leading to a change in its electrical resistivity.

The results from many experiments indicate that the addition of CB led to an improvement in both the compressive strength and flexural strength of the cementitious mortar after 28 days and 56 days. When CB is added at all addition percentages, the FCR (Fractional Change in Resistivity) lowers as the load increases. This drop correlates with an increase in electrical conductivity. After the sample fails under monotonic loading, the FCR returns to its previous value, which corresponds to a decrease in conductivity. Therefore, the piezoresistive behaviour consistently adheres to the overall pattern.

TABLE OF CONTENT

LIST OF FIGURES

LIST OF TABLES

CHAPTER 1 INTRODUCTION

1.1 GENERAL

Over time, there has been a growing focus on monitoring and analyzing concrete performance utilizing condition assessment methods and various materials. Structural Health Monitoring (SHM) is a novel technology that may identify performance issues in structures before they cause significant capacity loss. "SHM" is a technique that continuously monitors a structure's state to detect faults and prevent collapse or failure. By using an early damage monitoring method for load-bearing structural systems. Identifying vulnerabilities early on allows for early assessment and potential damage restoration. SHM analyzes a structure's functioning, monitors its performance, and provides real-time information on its current status. SHM can monitor several parameters, including corrosion, alkali reactions, humidity, ionic strength, loads, accelerations, strains, and fractures. Structural health monitoring uses a sensory method to accurately quantify the functioning of structures. Recently proposed cement-based sensors may detect stress/strain directly via electrical resistance analysis due to their piezoresistive properties. Smart sensors, also known as self-sensing structural composites, may be integrated into a structure to provide structural capabilities and respond to stress and damage (Azhari & Banthia, 2012).

In recent decades, there has been a growing interest in the ability of cementitious materials with conductive particles to feel themselves for SHM. Previous research suggests that many materials and sensors have emerged, but their practical usage remains limited due to the high cost of conductive materials. Nanoscale materials, such as carbon nanotubes (CNTs), may be difficult to disseminate in cementitious matrix.

Electric-resistivity strain gauges, piezo-resistivity detectors, and optic sensors are often used in construction to analyze and monitor conditions. However, their usage has considerable drawbacks, including limited sensitivity and low durability. Advancements in smart materials, such as cement-based sensors, may alleviate these worries (wang, et al., 2015).

1.1 SELF SENSING CONCRETE.

Self-sensing concrete (SSC) is a smart material that can detect and send real-time information on its own structural health and performance. It is a cutting-edge technology that blends concrete, sensors, and electronics to create a new generation of intelligent structures. SSC sensors are often inserted in the concrete matrix during the mixing process or affixed to the concrete's surface after it has hardened. Mechanical loads such as compression, tension, shear, and bending, as well as environmental parameters such as temperature, humidity, and moisture content, may be detected by the sensors (Han, et al., 2015).

Self-Sensing cementitious concrete (SSC) has been thoroughly studied because it might provide a realistic and cheap solution for civil infrastructure structural health monitoring. Concrete self-sensing is caused by the piezoresistive action of functional filler particles that generate a conductive connection throughout the composite phase. Thus, when concrete is

pushed, the network and electrical resistance change. The structure of self-sensing concrete is complex. By detecting and monitoring them, self-sensing concrete may improve structural concrete safety, durability, service life, and reliability. Conductive functional fillers including carbon black (CB), carbon fibers (CF), graphite nanofibers (GNF), and carbon nanoparticles like CNT and CNF provide self-sensing concrete its properties. Some hybrids can provide tangible sensing capabilities that classic fillers couldn't. The cementing matrix and conductive networks transmit electricity (Monteiro, et al., 2017). Filling the specimen under compression or stress tests fractional change in resistance (FCR) or cement-based sensor sensitivity. The sensing behaviour of conductive components in a cement-based composite under pure compression or stress may be examined using piezo resistivity, electrical resistivity, conductivity, etc (Han, et al., 2015). Since cement-based sensors must be employed on beams and bridge decks, strain under flexure must be sensed.

1.2 NEED OF SELF SENSING CONCRETE.

Self-sensing concrete is a smart substance that incorporates the ability to sense into the actual mixture of concrete. This concept shows potential for several significant reasons:

1.Structural Health Monitoring: Prompt Identification of Structural Damage: Self-sensing concrete has the capability to promptly identify fractures, strain, or other types of damage in real-time. This facilitates prompt intervention and upkeep, perhaps averting more profound structural problems. Continuous monitoring enables the collection of consistent and up-to-date information on the condition of a building, facilitating better decision-making when it comes to repairs and maintenance.

2.Improved Safety: Instantaneous Notifications: Early discovery of faults in vital infrastructure, such as bridges or buildings, is crucial for ensuring safety. Self-sensing concrete has the ability to detect and notify about any damage or weakening in its structure, hence enhancing the overall level of safety.

3.Cost Savings: Decreased expenses for inspections: By using integrated sensors, the frequency of human inspections may be minimized, resulting in cost savings for maintenance and monitoring. Preventive maintenance involves detecting problems in advance to minimize maintenance expenses and prolong the lifetime of the building.

4.Enhanced Durability: Self-sensing concretes has the capacity to modify their characteristics in response to identified stress or damage, hence possibly improving their durability and overall performance.

5.Sustainability: Self-sensing concrete may promote sustainable building practices by minimizing excessive wear and tear and optimizing maintenance.

6.Smart Infrastructure Integration: Self-sensing concrete may be included into smart

infrastructure systems, enabling advanced data analysis and management.

7.Advancements in Construction: The advancement and utilization of self-sensing concrete enables the exploration of groundbreaking building methods and applications, which have the potential to enhance the durability and adaptability of infrastructure.
Self-sensing concrete is now undergoing active research and development. However, its potential advantages position it as a viable technology for the future of building and infrastructure management.

1.3 PROCESS OF MAKING SELF-SENSING CONCRETE

- The first step is to mix the concrete according to the manufacturer's instructions. Cement, water, aggregates (such as sand and gravel), and admixtures are common components in concrete mixes. During this phase, the sensor materials are added to the mix.
- Using a high-shear mixer or a paddle mixer, the sensor materials are equally distributed throughout the concrete mix. This ensures that the sensors are evenly dispersed and do not cluster together.
- After mixing, the concrete is placed in molds and allowed to solidify for several days. During this period, the sensor materials must be kept dry and free of contamination.
- After the concrete has hardened, the sensors must be calibrated to guarantee that they are measuring the appropriate values properly. The sensor output is measured after applying known loads or stresses to the concrete.
- Wires or fiber optic cables link the sensors to a data acquisition system. This permits sensor data to be transferred and analyzed by a computer or other monitoring equipment.
- To evaluate its functionality and precision, the self-sensing concrete is tested under various loading circumstances. Applying varying loads or stresses to the concrete and monitoring the sensor output may be involved.
- The sensors may deteriorate or get damaged over time owing to environmental variables or wear and tear. Regular sensor maintenance and replacement may be required to guarantee that they continue to perform properly and dependably.

1.4 CHALLENGES WHILE MAKING SELF SENSING CONCRETE

The development of self-sensing concrete faces multiple challenges, which have a direct influence on the material's efficiency, expense, and acceptability. Here is a thorough examination of the primary obstacles:

1. Material Integration:

   Achieving a consistent and even distribution of materials: Obtaining a homogeneous dispersion of conductive fillers throughout the concrete mixture is a difficult task. Uneven distribution might result in regions with inadequate sensing capability. Compatibility refers to the assurance that conductive fillers blend with other components of concrete and do not have any negative impact on its mechanical qualities or durability.

2. Performance and Sensitivity: Comparing Sensitivity and Noise: Ensuring the self-sensing concrete's sensitivity while effectively eliminating external noise or interference. Excessive sensitivity might result in inaccurate positive results or readings that are not meaningful.
Calibration and accuracy include the process of ensuring that the sensors integrated into the concrete provide precise and dependable measurements. This includes adjusting the sensors to accommodate changes in the environment and variations in the characteristics of the concrete.

3.The capacity to withstand wear and tear and last for a long time:
Environmental Exposure: The conductive fillers and sensing systems need to resist exposure to moisture, temperature changes, and other environmental variables without deteriorating.
Material degradation refers to the process of ensuring that the conductive network stays efficient and functional for a prolonged period, taking into account the possibility of damage and deterioration.

4. Cost:
Material Costs: The use of high-quality conductive fillers, such as carbon nanotubes or graphene, might result in a significant expense. Discovering economical materials that provide the required performance is a substantial obstacle.
Production prices: The intricacy involved in blending and incorporating conductive fillers into concrete might escalate production prices, thus impeding its wider use.

5. Manufacturing Process:
Methods of blending: Creating dependable mixing methods that guarantee uniform dispersion of conductive additives while preserving the structural integrity of the concrete's mechanical characteristics.
Scaling Up: The process of transitioning from small-scale laboratory studies to large-scale manufacturing, while ensuring consistency and maintaining high quality standards.

6. Data Management and Interpretation: Dealing with the vast amounts of data produced by self-sensing concrete systems may be challenging, as it necessitates the use of advanced technologies for data processing and analysis.
Integration with Monitoring Systems: The process of combining self-sensing tangible data with pre-existing structural health monitoring systems and assuring compatibility.

7. Adherence to regulations and standards:
Standards Development: The process of creating and following industry standards and regulations for self-sensing concrete, which may still be in the early stages of development.

Acceptance: Obtaining clearance and recognition from regulatory organizations and industry experts who may have reservations about embracing novel technology.

8. Factors to Consider Regarding the Environment and Health:
Environmental Impact: Evaluating and reducing any possible environmental consequences of the conductive fillers, particularly if they are obtained from non-sustainable sources or if they potentially present risks during disposal.
Health Hazards: Ensuring that the materials used, particularly in substantial amounts, do not provide any health hazards to workers or consumers.

9. User Training and Adoption:
Training Requirements: Ensuring engineers and construction professionals get comprehensive training on the use, upkeep, and analysis of self-sensing concrete systems.
Market Acceptance: Promoting the acceptance and comprehension of the advantages of self-sensing concrete within the building sector.

The goal is to provide real solutions that are both practical and efficient in terms of self-sensing capabilities.

1.5 USE OF CONDUCTIVE FILLERS IN SSC.

Conductive fillers are materials with high electrical conductivity that are used to build a conductive network in concrete. Carbon fibers, carbon nanotubes (CNTs), graphene, and carbon black are examples of carbon-based fillers. Filler selection is influenced by a variety of criteria including as electrical conductivity, mechanical strength, cost, and environmental compatibility.

Understanding the Mechanism of Conductive Fillers:

Establishing an Electrically Conductive Network: Conductive fillers disperse evenly throughout the concrete matrix, forming a network of pathways that allow for conductivity (Han, et al., 2015). When stress or strain is present, the electrical resistance of this network changes, enabling the concrete to detect these alterations.
Monitoring Changes: When the concrete undergoes deformation or stress, the conductive network alters its electrical characteristics, such as resistance or capacitance. The structural state may be evaluated by monitoring these changes (wang & zhang, 2022).
Data Collection: The electrical reactions are quantified using sensors or measuring equipment that are included into the concrete. This data aids in evaluating the state of the structure and identifying possible problems.

Advantages of Conductive Fillers:

Improved Sensing Capacity: Incorporating conductive fillers greatly enhances the concrete's capacity to detect and quantify stress, strain, and possible harm.
Real-Time Monitoring: The inclusion of conductive fillers in concrete enables the

continuous monitoring of its structural health, facilitating the early identification of problems and prompt repair.
Enhanced Resilience: Through the use of conductive fillers, the ability to consistently monitor the state of the concrete is facilitated, hence aiding in the preservation of its structural soundness throughout its lifespan.
Cost efficiency may be achieved by minimizing the reliance on external sensors and human inspections, resulting in long-term cost reductions.
Conductive fillers provide adaptability, since they may be customized to suit various applications, accommodating the individual needs of the building or environment.

Applications:
Bridges and Highways: Used to monitor stress levels and identify any damage in essential infrastructure.
Buildings: Designed to enhance safety and durability by providing timely alerts for structural concerns.
Smart Cities: Incorporating self-sensing concrete into urban infrastructure to enhance management and maintenance.
Conductive fillers play a crucial role in the creation of self-sensing concrete, enhancing the intelligence, responsiveness, and longevity of building materials.

1.6 TYPES OF CONDUCTIVE FILLERS.

1.6.1 CARBON-BLACK FILLER :- Carbon black does not have intrinsic sensing qualities, but it can improve the sensing properties of other materials such as polymers or composites by boosting electrical conductivity and mechanical strength.
Because of its high degree of graphitization and tiny particle size, carbon black offers outstanding mechanical qualities such as high strength-to-weight ratio, stiffness, and flexibility. Because of its high degree of graphitization and tiny particle size, carbon black has a high electrical conductivity. This strong electrical conductivity assures SSC's self-sensing capabilities and dependability across a variety of environmental situations.
Because of its high degree of graphitization and tiny particle size, carbon black offers outstanding mechanical qualities such as high strength-to-weight ratio, stiffness, and flexibility.

Fig1. 1Carbon black (Alshammari, et al., 2023)

1.6.2 CARBON NANOTUBES (CNTS):- CNTs are cylindrical nanomaterials composed of rolled-up sheets of graphene ranging in diameter from 1 nm to several micrometers. Because of its high aspect ratio, carbon nanotubes have been employed in a variety of applications including electronics, sensors, batteries, and composites.

Because of their one-dimensional structure and high degree of graphitization, carbon nanotubes exhibit extraordinarily high electrical conductivity.

Because of their one-dimensional structure and high degree of graphitization, carbon nanotubes offer exceptional mechanical qualities such as high strength-to-weight ratio, stiffness, and flexibility.

Because of its one-dimensional structure and high degree of graphitization, carbon nanotubes have a high heat conductivity.

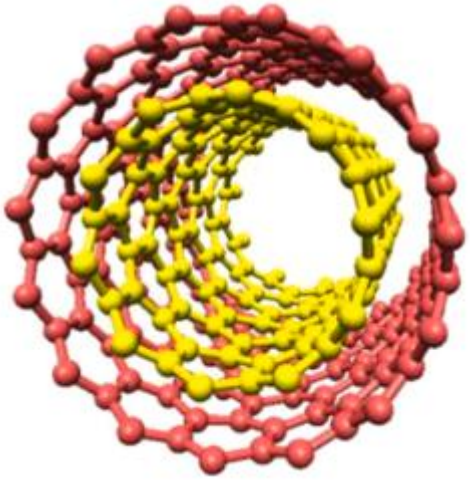

Fig1. 2 Multilayer Carbon nanotubes (Rathinavel, et al., 2021)

1.6.3 SILICON NANO-POWDER:- In SSC, silicon nanopowder may be introduced to the concrete mix in a variety of ways, including direct mixing, sonication, and ball milling.

Although silicon nanopowder does not have intrinsic sensing qualities, it can improve the sensing properties of other materials such as polymers or composites by boosting electrical conductivity and mechanical strength.

Because of its tiny particle size and large surface area, silicon nanopowder has a high heat conductivity.

Because of its tiny particle size and large surface area, silicon nanopowder has a high

electrical conductivity.
Because of its tiny particle size and large surface area, silicon nanopowder offers exceptional mechanical qualities such as high strength-to-weight ratio, stiffness, and flexibility.

Fig1. 3 Silicon nanopowder

1.6.4 CARBON FIBER :- Because of its crystalline structure and high degree of graphitization, carbon fiber possesses remarkable mechanical qualities such as high strength-to-weight ratio, stiffness, and durability.
Because of its amorphous structure and low degree of graphitization, carbon fiber has limited electrical conductivity. It can, however, increase concrete's electrical conductivity by providing a conductive channel for electrical impulses. SSC's low electrical conductivity assures its safety and dependability in a variety of environmental circumstances.
Because of its crystalline structure and high degree of graphitization, carbon fiber has a high heat conductivity.

Fig1. 4Carbon fiber.

1.6.5 GRAPHENE OXIDE :-(GO) is a two-dimensional substance created by chemical oxidation of graphite. GO is made up of a single layer of graphene sheets that have been functionalized with oxygen-containing groups like hydroxyl, epoxy, and carboxyl. The functionalization of GO gives it certain features that make it appealing as a reinforcing

material in self-sensing concrete (SSC). because of the presence of oxygen-containing groups on its surface, which function as insulating barriers, GO has low electrical conductivity. However, by providing a conductive channel for electrical impulses, GO can still increase the electrical conductivity of concrete. SSC's low electrical conductivity assures its safety and dependability in a variety of environmental circumstances. because of its two-dimensional structure and high degree of functionalization, GO has exceptional mechanical qualities such as high strength-to-weight ratio, stiffness, and flexibility. SSC's strong mechanical strength assures its longevity and integrity under a variety of loading circumstances. because of its huge surface area and functional groups, GO has great sensing capabilities that allow it to interact with a variety of environmental stimuli such as strain, temperature, and humidity.

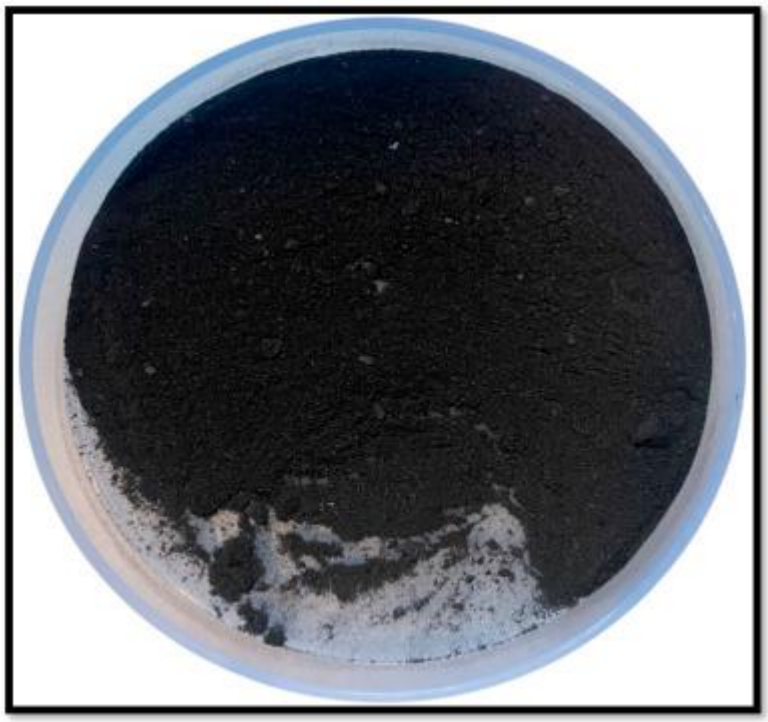

Fig1. 5 Graphene oxide (Singh, et al., 2022)

1.7 MEASUREMENT OF SENSING SIGNAL OF CEMENT MORTAR COMPOSITE.

The sensitivity of the concrete may be assessed using many measures, such as piezoresistivity, electrical resistivity, dielectric constant, conductivity, and capacitance (Han, et al., 2015)One of the most straightforward approaches is using electrical resistance or resistivity as a sensitivity indicator. The electrical resistivity of cement-based composites is affected by changes in compression, temperature, or damage, and is impacted by the conductivity of the fibers present. In order to assess electrical conductivity in different configurations, electrodes made from appropriate materials are used (Han, et al., 2015)Prior to choosing an electrode, it is important to consider three parameters: material, fixing site,

and pattern. The material should possess two primary characteristics: a low electrical resistance and a consistent conductive quality. The electrodes may be attached to the surface of the composite, implanted into the composite at a significant depth, or arranged in a clipping pattern. Out of these options, embedding and attaching are the two most widely used procedures. Experiments may be conducted using either a two-probe approach or a four-probe setup, where both electrodes serve as the current and voltage poles (Han, et al., 2015)Unlike a two-probe approach, a four-probe method utilizes inner probes to measure voltage and outside probes to detect current. When comparing the two-probe technique to the four-probe method, it can be concluded that the two-probe method is more practical and simpler to implement (Figure 1.6). Nevertheless, the four-probe method is often used for measuring low resistance values because of its superior accuracy in obtaining accurate findings (Han, et al., 2015)

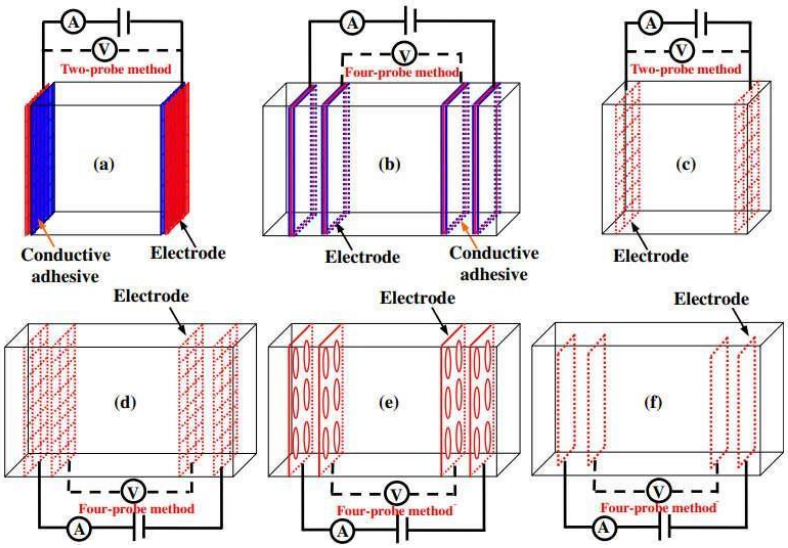

Fig1. 6Setting the electrode configuration and style in self-sensing concrete (a, b): surface-mounted electrodes; (c–f): embedded mesh, perforated plate, or loop electrode. (Han, et al., 2015)

1.8 OBJECTIVES OF THE WORK

The objective of the study is to create self-sensing cementitious (SSC) composites by including industrial-based nanofillers, such as carbon black (CB), for the purpose of smart structural health monitoring. The primary goals of the planned research may be summarized as follows:

- To study the influence of addition of carbon black on the mechanical properties of cementitious composite.
- To study electrical characteristics of carbon black cementitious composites such as electrical resistivity and piezo-resistivity.
- To develop self-sensing cementitious sensor using carbon black for monitoring stress in concrete.
- To evaluate the performance of developed sensor for monitoring flexural stresses in reinforced concrete beam.

1.9 ORGANISATION OF THESIS

The thesis report has five chapters.

Chapter 1- Introduces SSC composites and explores several kinds of nanomaterials along with their respective characteristics.

Chapter 2- Focuses on the examination of different researchers' studies on various nanofillers, including CB, rGO, CNTs, GNPs, GP, and other carbon-based nanomaterial. The chapter explores the impact of these nanofillers on several self-sensing characteristics, such as electrical resistivity and piezo-resistivity, as well as mechanical properties.

Chapter 3- Provides a comprehensive explanation of the experimental design, including the materials used and the factors considered. This chapter also provides an illustration of mortar mix design.

Chapter 4- Presents the findings and analysis of mechanical characteristics, namely compressive strength and flexural strength. This chapter further discusses the findings and examination of electrical characteristics, including electrical resistivity and piezo resistivity.

Chapter 5- Provides a summary and conclusion of the study's results, and also discusses the potential future directions of the research.

References are often placed at the conclusion of a document.

CHAPTER 2 LITERATURE REVIEW

2.1 GENERAL

This chapter addresses the literature work done by many authors over the years on the properties of Graphene oxide (GO), Reduced Graphene oxide (rGO), Carbon nanotubes (CNTs), Carbon black (CB), Graphene nanoplates (GNP) and other carbon derivatives when added to cementitious composites. Two primary groups were formed from studies properties: mechanical properties and self-sensing characteristics. While self-sensing qualities encompass the examination of the principal sensing mechanism by means of piezo-resistivity and electrical resistivity, mechanical properties comprise compressive and flexural strength.

2.2 EFFECT OF NANOMATERIALS ON MECHANICAL PROPERTIES ON CEMENTITIOUS COMPOSITES

(Li , et al., 2024) Fig2.1 displays the compressive strengths of each group. The compressive strengths of samples filled with pure CB and hybrid CB/CNF show a minor rise at 0.5% CB content, followed by a notable drop at 1.0% and 2.0% CB content. The research on CB-filled cement composites with different CB contents is consistent with this variance pattern. Based on quantitative findings from earlier research, the filling impact of CB and decrease effect of harmful pores are mostly responsible for the first rise in compressive strength. The cement matrix is densified and the particle size distribution is altered by the appropriate concentration of nanoscale CB particles. The absorbance of free water, CB agglomerations, and superplasticizer are mostly responsible for the significantly decreased compressive strength. These factors negatively impact cement hydration and fluidity, which in turn affects the particle size distribution and compressive strength. Furthermore, research suggests that CB weakens the bonds between the hydration products. Furthermore, the dilution effect, in which the lower cement concentration prevents the development of strength, is most likely the cause of the decreased compressive strength.

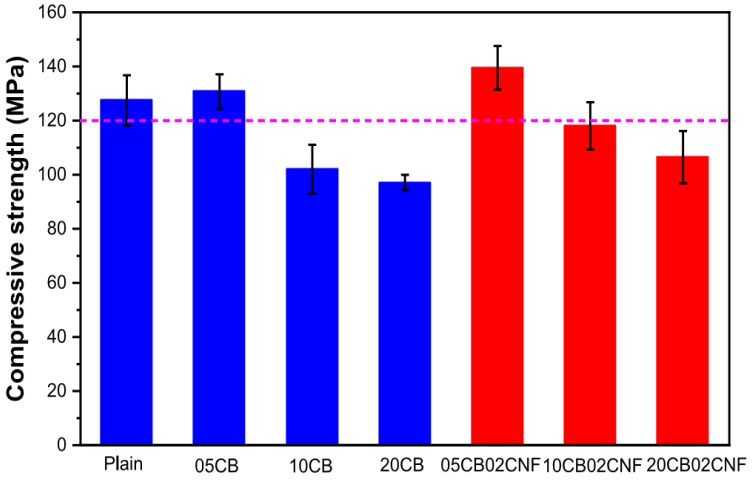

Fig2. 1 UHPC filled with CB or a mix of CB and CNF compressive strength (Li , et al., 2024).

(Qi, et al., 2023) Compared to the Blank group, rGO-HO had a much greater flexural and compressive strength, with growth rates of 20.0% and 14.0%, respectively, at 3d and 10.8% and 11.7% at 28d. There was no obvious increase in rGO-LO's strength. This suggests that, when the sheet size is the same, rGO-HO with a greater oxygen concentration adds more to the strength of cement composite, but rGO-LO with a lower oxygen content contributes less. This could be because rGO-HO disperses more readily in the cement matrix than rGO-LO does, and this makes it easier to provide sites for the nucleation of hydration products during crystallization.

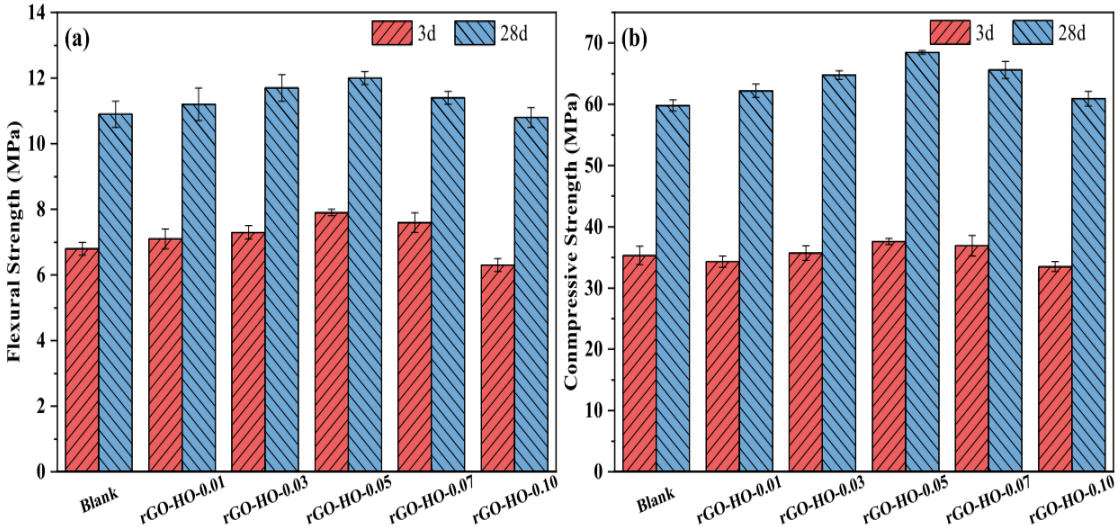

Fig2. 2 Effect of graphene dosage on mechanical properties of cement (Qi, et al., 2023).

(Monteiro, et al., 2017) The compressive strength of Portland cement (PCSS) increases with time due to the conventional hydration process. The CB4 sample exhibited the highest compressive strength, indicating an optimal ratio of binder to filler for achieving the maximum PCSS compressive strength. The rise in efficacy from CB0 to CB4 at 28 and 120 days confirms the mechanical reinforcement impact of the addition. CB4 exhibited worse compressive strength compared to CB1 and CB7 at the 14-day mark. The mechanical benefits of the material decrease as it becomes more brittle, maybe due to an excessive amount of filler particles that hinder proper bonding within the cement matrix. Tests with a CB loading of more than 10% showed both segregation and significantly reduced strength values. The modulus exhibited an increase from CB0 to CB4, however the CB7 and CB10 specimens showed lower values compared to the control sample. CB4 had the greatest overall value among the specimens. It is important to analyse the filler's inefficient dispersion method and the water-binder ratio. Further investigation is necessary to determine the optimal hydration level of the cement.

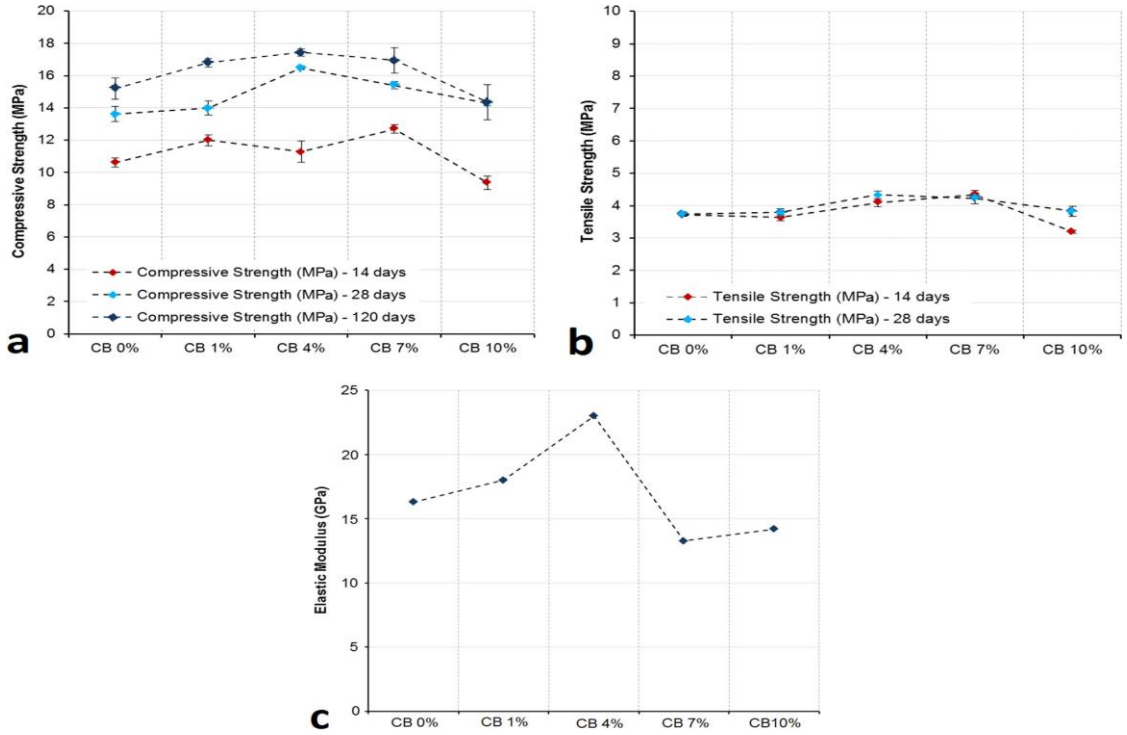

Fig2. 3 Shows (a) compressive strength, (b) tensile strength and (c) Elastic modulus of the different composite at 120 days of curing (Monteiro, et al., 2017)

(wang & zhang, 2022) Following 28 days of monotonic compression, the stress-strain curves of a cementitious composite containing 8GNPs/CNTs are shown. The stress-strain curves for M0 and M6 exhibit almost linear behaviour throughout the loading period, demonstrating a positive link between stress and strain. There had been no change prior to the most recent stressful event. The specimen suddenly broke as it reached its breaking point. After that, the force was progressively reduced as the specimen was crushed. For M0 and M6, the maximum stress values are 96.5 (MPa) and 66 MPa, respectively. The ultimate stress of M0 and M6 have standard deviations of 4.68% and 3.25%, respectively. M0's compressive strength is 30.5% greater than M6's.

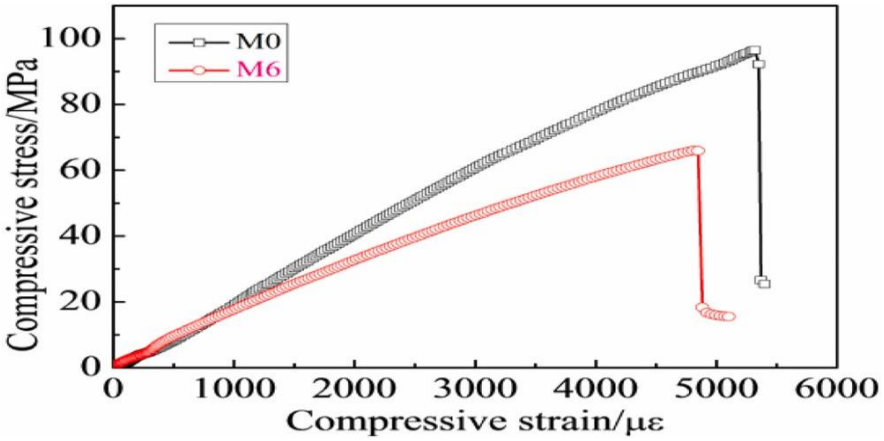

Fig2. 4 M0 and M6 specimen stress and strain curves under monotonic compression to failure (wang & zhang, 2022).

(Tao, et al., 2019) As the (GNP) increases, the compressive and flexural strength first increases and then decreases. M0 exhibits compressive strength of 49.5 MPa and flexural strength of 7.7 MPa. The compressive strength of M1 is increased to 53.6 MPa, while its flexural strength is improved to 8.9 MPa. But when the concentration reaches 0.05%, both compressive and flexural strength decrease, as seen in the figure.

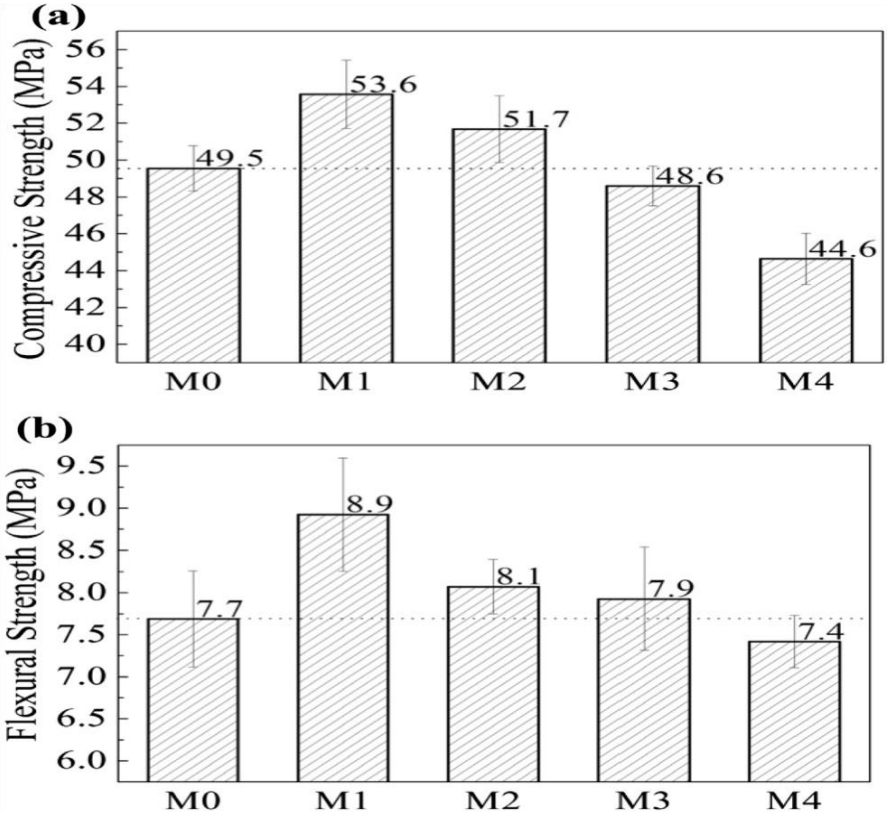

Fig2. 5(a) Compressive and (b) flexural strengths of the GNP-modified cement mortars (Tao, et al., 2019)

(Dong, et al., 2021) Increasing the GNP content to 2% results in a rise in compressive strength. The specimen filled with 1% SHP has a compressive strength of 62.6 Mpa. The reason is that the GNP enhances the compactness of the cementitious composites composed of densely packed calcium silicate hydrate and calcium hydroxide. Nevertheless, as the SHP reaches a level of 2%, the compressive strength experiences a decrease. The cement hydration process is disrupted when excessive addition limits the water channel or the water needed by the SHP dissolves.

Increasing the GNP content to 2% while maintaining a SHP of 1% leads to a rise in flexural strength. The pressure reaches a maximum of 8.9(Mpa). Nevertheless, when the SHP fraction is raised to 2%, the strength decreases to 6.9Mpa, which remains greater than the specimen without the GNP.

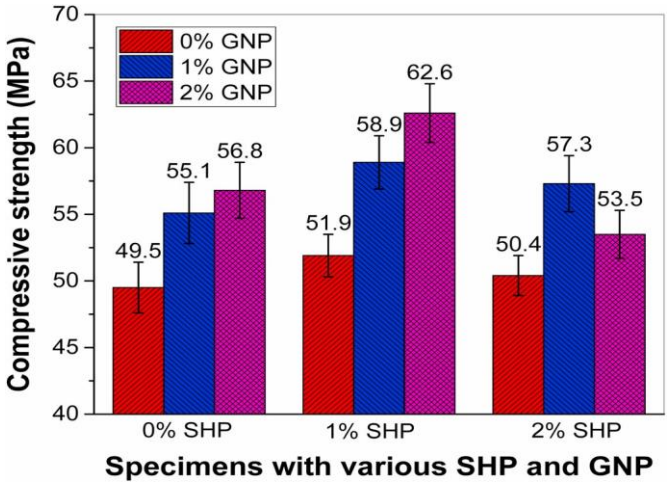

Fig2. 6 Cementitious composite's compressive strength with different SHP and GNP concentrations (Dong, et al., 2021)

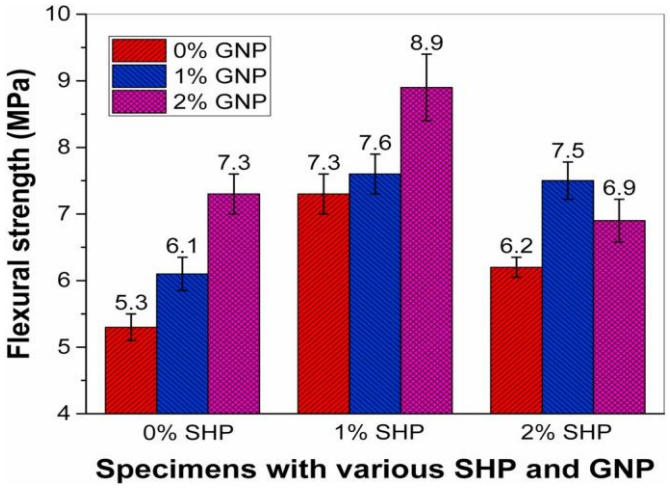

Fig2. 7 Cementitious composite's flexural strength at different SHP and GNP concentrations (Dong, et al., 2021)

(wang, et al., 2018) The study examines the flexural and compressive strength of CNF-RPC samples after a 28-day curing period. The results indicate that the flexural and compressive strength first decrease but subsequently increase with an increase in the concentration of CNFs. The specimen achieved its highest mechanical strength when the amount of carbon nanofibers (CNFs) reached 0.5%. The reason for this rise is the ability of CNFs to connect microcracks, fill gaps, and accelerate the hydration process of cement-based materials. Carbon nanofibers (CNFs) also limit the formation and uncontrolled expansion of microcracks. Carbon nanofibers (CNFs) reduced the amount of empty space and made the size of the pores smaller, resulting in enhanced mechanical properties of CNF-reinforced polymer composites (CNF-RPC). Nevertheless, the presence of weak sections in carbon nanofibers (CNFs) and the inhibitory effect of carbon nanoparticles on cement hydration might lead to reduced strength. An increase in CNFs content from 0.5% to 2.0% may lead to the entrapment of additional air bubbles in cement paste when fibers or nanomaterials are used. This can result in a decrease in strength.

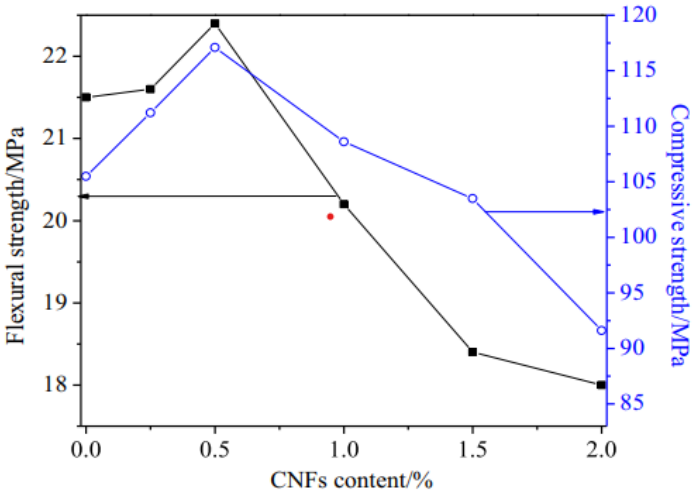

Fig2. 8 Mechanical Strength of CNF-RPC (wang, et al., 2018)

2.3 EFFECT OF NANOMATERIAL ON SELF-SENSING BEHAVIOUR

(Tao, et al., 2019) Evaluated through the four-probe methodology. When the concentration of GNP is below 0.1%, the initial resistance is 300 kohm. But the initial opposition decreases as the GNP content increases. The electrical resistance of GNP 1% is about 19 kohm. When the concentration of GNP is high, the electrical resistance decreases significantly and conductive channels start to appear. When the spacing between GNPs is sufficiently close to allow for tunneling, the GNPs have achieved a particular amount.

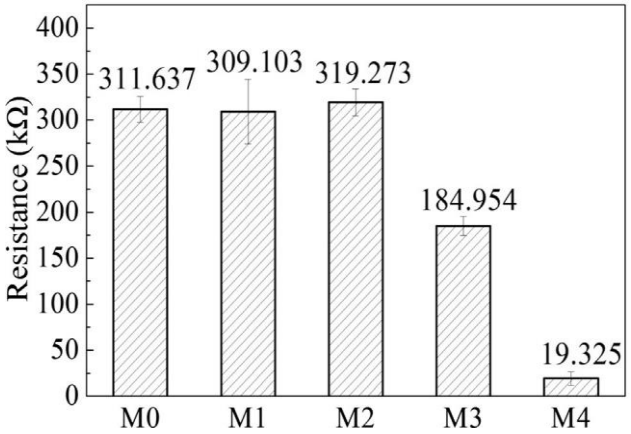

Fig2. 9 Initial electric resistance of the GNP-modified cement mortars (Tao, et al., 2019)

(Li , et al., 2024) As a function of CB doses, the resistivity of samples filled with single CB and hybrid CB/CNF is displayed in Fig. 8(a). The percolation thresholds for single CB filled cement composites from previously published publications are summarized in Fig. 8(b). According to several research, the percolation zone was unusually high. The major cause of

the difference is the various structural characteristics of CB particles, including size and dibutyl phthalate (DBP), considering the variety of CB varieties that are marketed commercially. Lower percolation thresholds are frequently the result of CB particles with smaller size (higher specific area) and stronger DBP absorption (large number of CB nanoparticles formed for the main aggregate), also referred to as higher structure. The percolation zone can also be determined by the presence of coarse and fine particles. However, it is clear that the majority of research reported a beginning percolation threshold of about 0.5-0.7%, which supports the findings of the current investigation. Although the percolation trend in the hybrid CB/CNF filled UHPC is identical, the resistivity of the single CB filled UHPC is greatly reduced by the addition of 0.2% CNF as additive nanofillers, with approximately one order and two thirds, respectively, for the instances of 2.0% and 1.0 % CB. It is seen that resistivity increases for the 0.5% CB case. The combined impact of the more compact matrix and the increased superplasticizer inclusion is probably what is causing the rise in resistance. The silica sand mortar's microstructural and interfacial properties will be changed by the superplasticizer, causing the mortar to become superplasticized and always show greater electrical resistivity than the control samples. Overall, the much decreased resistivity provides proof of the advantageous synergistic effects of using hybrid nanofillers that differ in size and dimension.

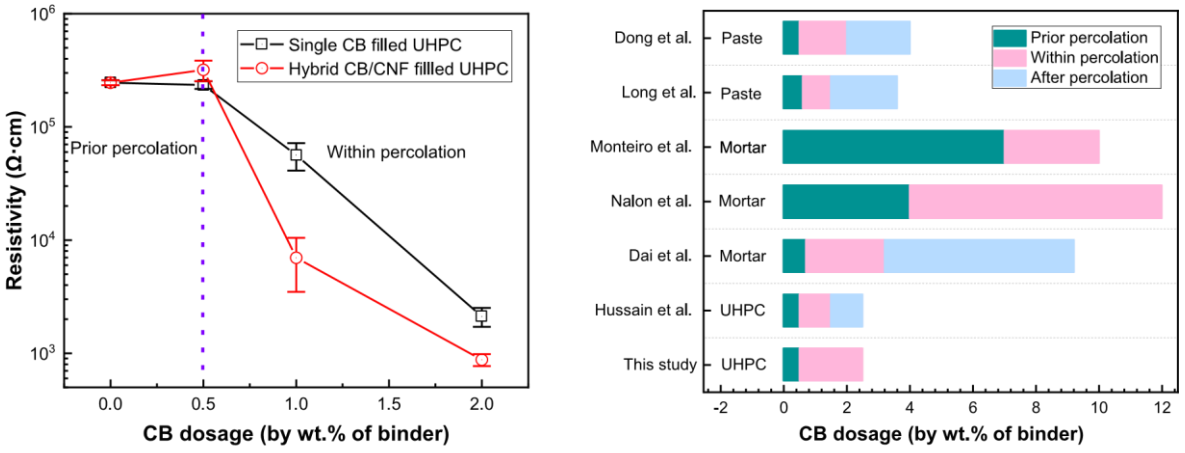

(a) Percolation zone (b) Comparative analysis

Fig2. 10 Comparing the percolation zone of single and hybrid filled UHPC specimens with findings from other research (Li , et al., 2024).

(Qi, et al., 2023) The samples' resistivity dramatically dropped when the rGO dose rose from 0.01 weight percent to 0.07 weight percent. Regarding the GNPs, a similar pattern was seen: when the dose of GNPs rose from 0.08 wt% to 0.20 wt%, the resistivity dramatically dropped. The resistivity remained low at high doses of GNPs (0.20 % wt%) and rGO (0.07 % wt%). The resistivity of rGO-LO dropped to 15.672 kΩ·cm at 0.03 wt% and to 14.083 kΩ·cm at 0.05 wt%. At 15.323 and 13.475 kΩ·cm, respectively, rGO-HO was measured. For 0.12 wt% and 0.20 wt% GNP-S, the resistivity decreases to 15.393 kΩ·cm and 12.847 kΩ·cm, respectively. rGO-HO is 11.658 kΩ·cm and 14.420 kΩ·cm, in that order. At a GNP <1%, the initial resistance was measured to be 311.637 kΩ. The resistance dropped to 19.325

kΩ at 1.0 %. Because the graphene kinds and test techniques differ, it is not possible to directly compare the resistance findings. In line with our findings, cement-based materials' resistivity may still be considerably decreased by adding graphene.

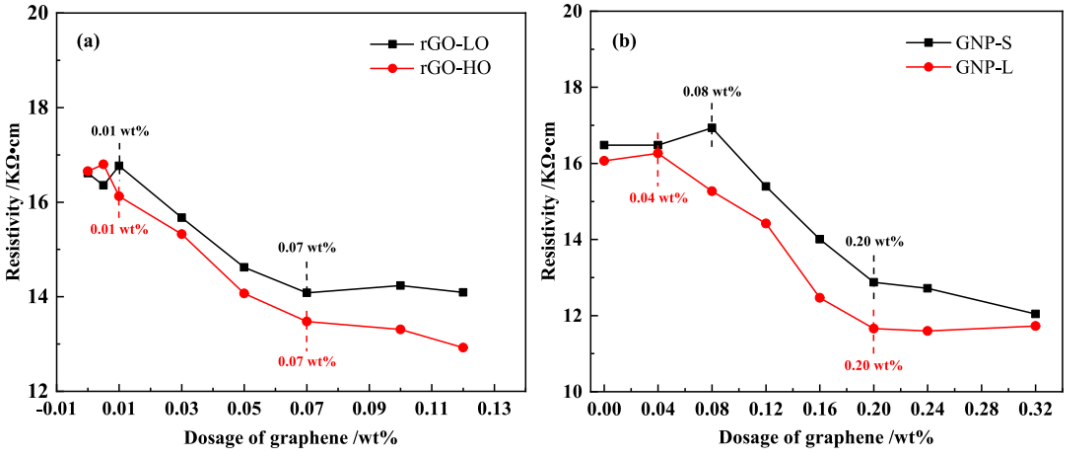

Fig2. 11 Effect of rGO/GNPs on the electrical conductivity (Qi, et al., 2023)

(wang, et al., 2018) The study shows the conductive behavior of cement-based materials at different concentrations of CNF and its impact on resistivity. The resistance of CNF-RPC, CNFM, and CNFP decreased slowly as the CNF dosages ranged from 0 to 0.5%, 1.5%, and 1.5%, respectively. Given that the principal mode of electric conduction involves the movement of electrolyte ions, the variation in dosages did not have a substantial impact on conductivity. Advanced carbon nanofibers established an electrically conductive pathway that connected to a contiguous conductive pathway. A more efficient network of conductive pathways was formed due to the fillers being brought closer together. CNF-RPC was used to estimate the optimal conductivity in various cement-based materials. because to its superior conductive network, CNF-RPC exhibits reduced porosity compared to CNFM, mostly because to its lower water-to-cement ratio (w/c). Silica fume and quartz sand were shown to be advantageous for dispersing CNFs and improving the conductive network in CNF-RPC. Overall, the conductivity decreased in the following sequence: CNF-RPC > CNFM > CNFP.

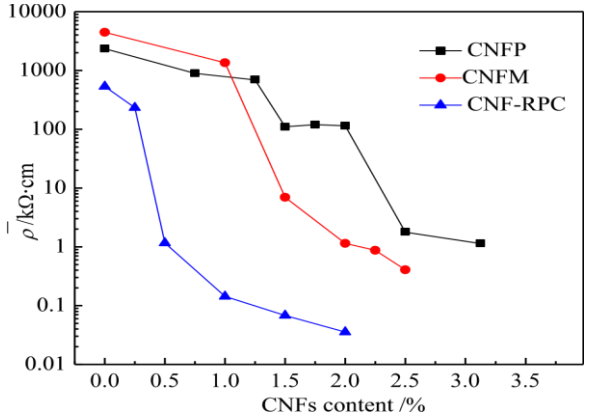

Fig2. 12 Electrical resistivity of the CNFs cement-based composites (wang, et al., 2018)

(wang & zhang, 2022) Both M0 and M6 exhibit increased DC electrical resistance when the curing periods are increased. Upon increasing the curing age from 3 days to 56 days, M0 and M6 exhibit an approximately 233.8% and 144.2% increase in DC electrical resistivity, respectively. M0 exhibits a single order of magnitude AC electrical resistivity, whereas M6 demonstrates two orders of magnitude AC electrical resistivity. The M0 and M6 drop as the frequency increases from 100Hz to 100KHz. The polarization phenomena may be reduced by alternating current (AC), and this effect becomes stronger with increasing frequency. This study examines the effects of GNPs and CNTs on cementitious composites' electrical conductivity. Whereas the tunnelling effect and contact conduction caused by GNPs/CNTs are the main drivers of M6's electrical conductivity, the conduction of electrolyte ions primarily controls M0's electrical conductivity.

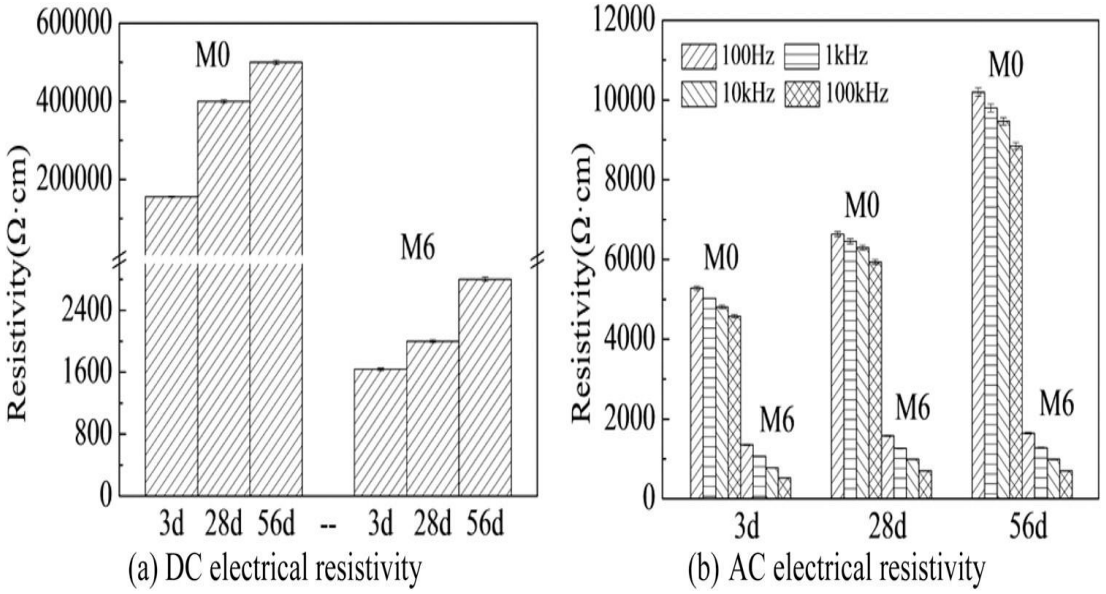

Fig2. 13 GNP-containing cementitious composite's electrical resistivity (wang & zhang, 2022)

(Monteiro, et al., 2017) Piezoresistive behavior was observed in two samples, CB7 and CB10, under cyclic compressive pressure. Reversible association between resistivity and deformation was shown by the FCR fluctuations, and both samples exhibited strong global linearity and repeatability. Despite having a lower gage factor and sensitivity value, CB10 demonstrated superior accuracy because of its linearity and reduced dispersion distribution. According to the findings, CB0, CB1, and CB4 exhibited comparatively high resistance. This might have been brought on by the inclusion of superplasticizer or by a reduced concentration of CB in combination with subpar filler dispersion. On the other hand, CB7 and CB10 demonstrated reduced resistivity, which made piezoresistivity measurement possible. This finding points to a maximum resistivity threshold that these composites cannot be taken into account for PCSS. The research also discovered that CB may be added to cement in even smaller quantities as a conductive addition. The kind of CB that was utilized might be one factor in this disparity. The primary attributes that set them apart are the particle

size, the particular region, and the "structure." Piezoresistivity may be achieved with lower CB fractions due to the greater conductivity of CB particles with larger surface area, bigger size, and higher structure. the sensitivity levels found for the CB7 specimen were around 50% lower. The CB7 demonstrated high levels of linearity and reproducibility even with 53% less CB filler.

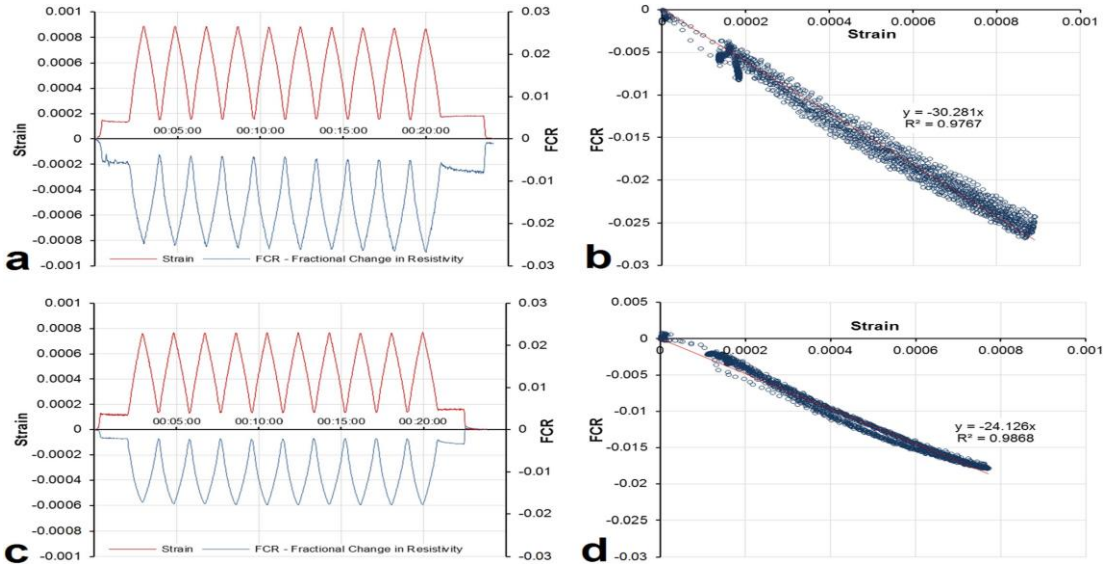

Fig2. 14 Cycle loading results for samples CB7 and CB10. FCR and strain vs time (a) (CB7); FCR and strain versus time (b); FCR and strain versus time (CB7); c) FCR and strain vs time (CB10); d) FCR and strain versus time (CB10)(Monteiro, et al., 2017)

(Tian, et al., 2023) To obtain a reversible resistance response, an elastic condition is used for the piezoresistive test. By tracking the resistance of carbon fiber reinforced hydraulic concrete specimens in the axially compressed elastic phase cyclic loading test, the change law of each specimen's resistivity fraction with increasing loading duration under equal and unequal amplitude cyclic loading was investigated. For carbon fiber doping of 0.05 vol%, 0.08 vol%, and 0.1 vol% and carbon fiber lengths of 3 mm, 6 mm, and 9 mm at each doping level, the resistivity fraction variation laws under the elastic loading stress of 20% ultimate load of each specimen are as follows.

Under unequal loading, the specimens' stress and resistivity fractions change over time for different volume doping concentrations (0.05 vol%, 0.08 vol%, 0.1 vol%) with a carbon fib er length of 12 mm.

The FCR is given as an absolute value in the research that follows. Whether under conditions of equal amplitude cyclic loading or unequal amplitude cyclic loading, specimens of carbon fiber reinforced hydraulic concrete that are uniaxially compressed show a good correlation between the FCR and stress in each loading cycle, and each specimen displays compressive resistivity. In other words, as compressive stress increases during loading and decreases during unloading, the specimen's FCR decreases. Because of the specimen matrix's relative compaction during compression, the carbon fiber insertion is more likely to create a

conductive channel and decrease in resistance. The resistivity increases when the pores open and the fibers are pulled out of the matrix when it is unloaded. At the conclusion of each cycle of loading and unloading to a load of 0, the resistivity of the specimens recovered less than the initial value at the loading, and the resistivity increased slightly, with the resistivity change fraction of all specimens exhibiting an increasing trend. Since cementitious materials are brittle and may sustain some degree of damage from irreversible microstructural changes even in the elastic phase, the irreversible phenomena emerged even though the specimens were loaded in the elastic phase.

The FCR of the specimen under each loading cycle is analyzed instead of taking the first curve from the beginning of the test loading to the stress amplitude in the first cycle because the specimen resistivity is not yet stable when it is first loaded. gives, given the volume content of carbon fiber, the maximum amplitude of the stress loading amplitude and the FCR of the specimen under constant amplitude cyclic loading. It is evident that the specimen's stress loading amplitude reduces with increasing carbon fiber length. Consequently, as carbon fiber length increases, it is harder for the fiber to disperse uniformly throughout the cement matrix, which has an increasing impact on the matrix's microstructure. In the (d) plot of carbon fiber lengths of 3 mm, 6 mm, and 9 mm, the resistivity change fraction had the highest values of 0.176%, 0.359%, and 0.329% for carbon fiber doping of 0.05 vol%, respectively. With a 0.08 vol% carbon fiber doping, the resistivity change fraction was 0.477%, 0.333%, and 0.396% for carbon fiber lengths of 3 mm, 6 mm, and 9 mm, respectively. The resistivity variation percentage for carbon fiber lengths of 3 mm, 6 mm, and 9 mm was 0.641%, 0.363%, and 0.608%, respectively, for carbon fiber doping of 0.1 vol%. The effect of increasing carbon fiber length on the resistivity change % of specimens doped with a certain amount of carbon fiber does not follow a regular pattern. Specimen CF005-3C-2 has a much smaller resistivity change part amplitude than the other specimens, suggesting that carbon fiber length should not be excessively shortened when doping levels are low.

Under uneven amplitude cyclic loading, the specimen CF04-12C-3 exhibits a resistivity change fraction with a maximum amplitude of 0.149% during the last two cycles, and a maximum amplitude of 0.086% over the first four cycles. The specimen CF06-12C-3 exhibits a resistivity change fraction with a maximum amplitude of 0.141% during the last two cycles, and a maximum amplitude of 0.087% over the first four cycles. For specimen CF010-12C-3, the FCR has a maximum amplitude of 0.325% during the last two cycles, and a maximum amplitude of 0.189% during the first four cycles. As the stress amplitude increases by two times, the maximum amplitude of the resistivity change % of the three groups of specimens increases by 1.733 times, 1.621 times, and 1.72 times. The results show that the rise in the resistivity change percentage of the carbon fiber reinforced hydraulic concrete specimen is approximately correlated with the increase in stress amplitude for each group of carbon fiber content.

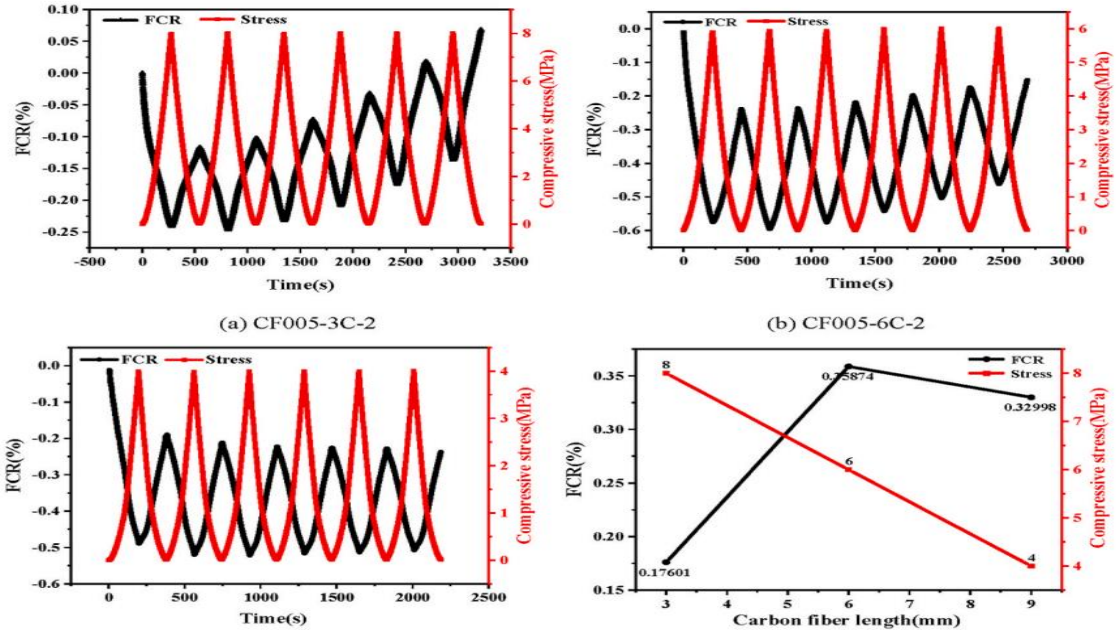

Fig2. 15 (a), (b) and (c) are the stress and FCR with time for 0.05% of carbon fiber volume doping; (d) is the maximum magnitude of loading amplitude and FCR for 0.05% of carbon fiber volume doping (Tian, et al., 2023)

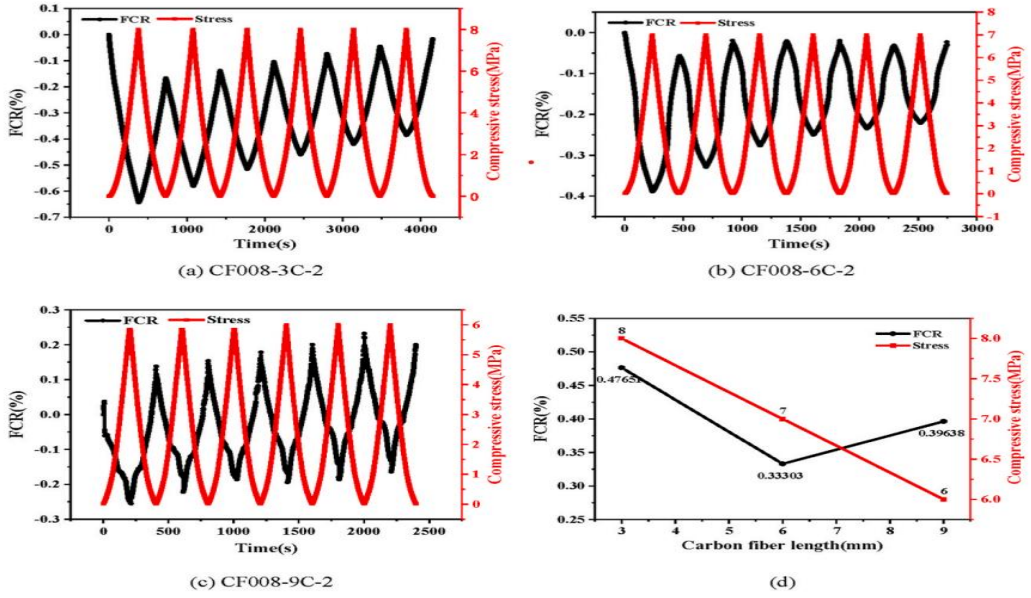

Fig2. 16(a), (b) and (c) are the stress and FCR with time for 0.08% carbon fiber volume doping; (d) is the maximum values of loading amplitude and FCR for 0.08% carbon fiber volume doping (Tian, et al., 2023)

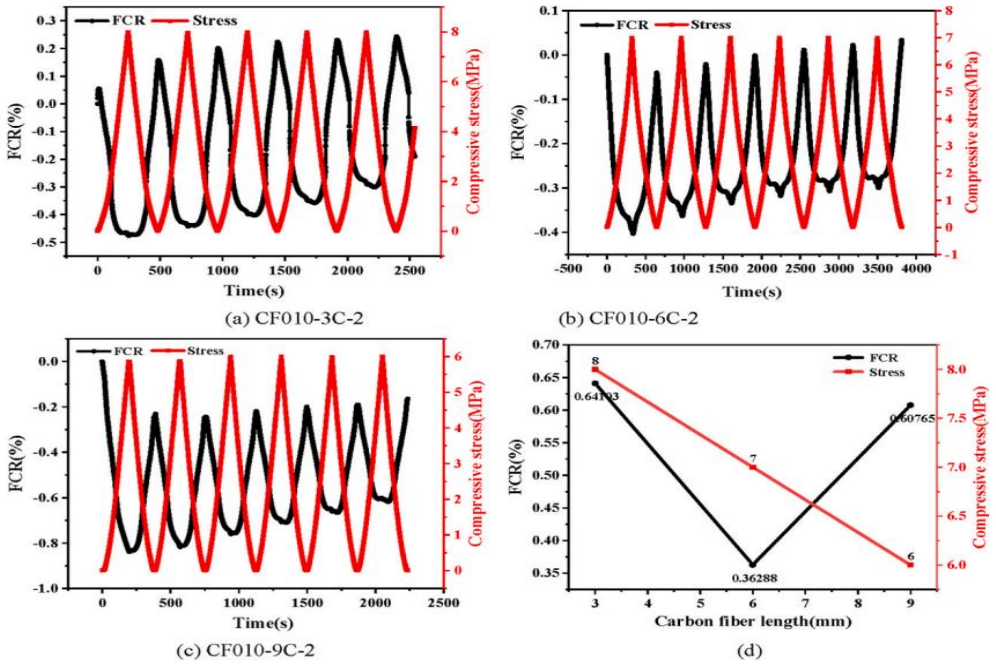

Fig2. 17(a), (b) and (c) are the stress and FCR with time for 0.10% carbon fiber volume doping; (d) is the maximum values of loading amplitude and FCR for 0.10% carbon fiber volume doping (Tian, et al., 2023)

(wang & zhang, 2022) shows the relationships over time between the FCR and the stress/strain of M6 at different loading rates (0.2, 0.4, and 0.6 mm/min) and a cyclic compressive stress amplitude of 20 MPa. demonstrates how, at different loading rates, cyclic compressive stress/strain increases cause FCR to drop, and vice versa. The absolute maximum FCR of the M6 stays almost constant under different loading rates. As a result, loading rates have no effect on the piezoresistivity of M6, and the material's stress and strain sensitivities remain consistent at varied loading rates of 0.2, 0.4, and 0.6 mm/min.

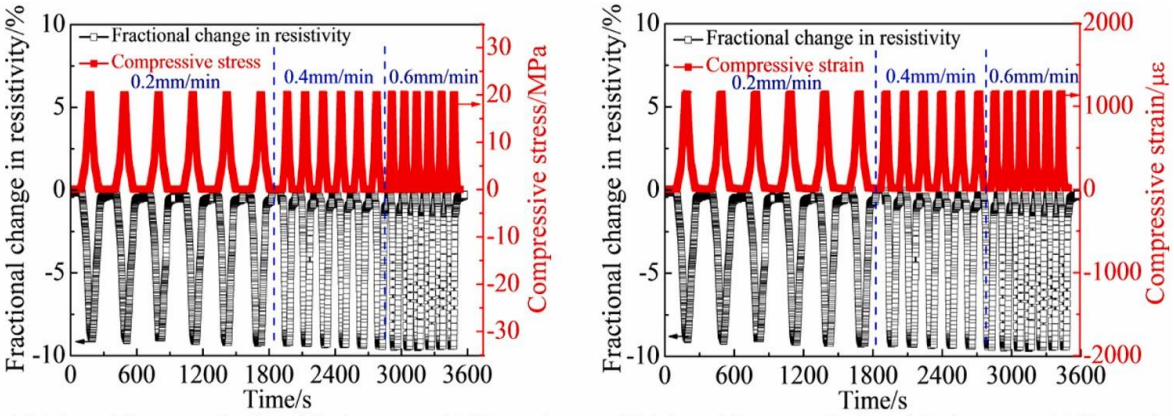

(a) Time history relationship between FCR and compressive stress with different loading rates

(b) Time history relationship between FCR and compressive strain with different loading rates

Fig2. 18 Relationships over time between M6's stress/strain and FCR during cyclic compression at various loading rates (wang & zhang, 2022)

The time history relationships between M6's stress/strain and FCR during cyclic compression are shown in Figure 2.19 for different stress amplitudes of 10, 15, and 20 MPa. The loading rate is 0.4 mm per minute. Figure 2.19 shows that during cyclic compression at different stress amplitudes of 10, 15, and 20 MPa, the FCR decreases with increasing stress/strain and increases with decreasing stress/strain. Moreover, the absolute maximum FCR rises in parallel with the stress amplitude. The absolute maximum FCRs of 5.63%, 7.09%, and 8.72%, respectively, are correlated with the stress amplitudes of 10, 15, and 20 MPa. Under higher stress amplitude, more conduction channels and networks occur when there is a wider separation between GNPs and GNPs, CNTs and CNTs, and GNPs and CNTs. As a consequence, the absolute maximum FCR increases as stress amplitude grows.

For stress and strain of 10 MPa/540 με, 15 MPa/850 με, and 20 MPa/1150 με, respectively, M6's sensitivity values are (0.56%/MPa)/104.26, (0.47%/MPa)/83.41, and (0.44%/MPa)/75.83. It is clear that M6's sensitivity decreases as stress/strain amplitude rises. These are a few theories on the mechanics behind this occurrence. The average separation between adjacent GNPs and GNPs, CNTs and CNTs, and GNPs and CNTs tends to shrink under compressive stress. Consequently, the tunneling effect and contact conduction are improved. A portion of the space between functional fillers may reach the electronic transition distance when stress/strain reaches a critical threshold. Many conductive, stable networks and pathways are formed. Consequently, sensitivity decreases as stress amplitude rises.

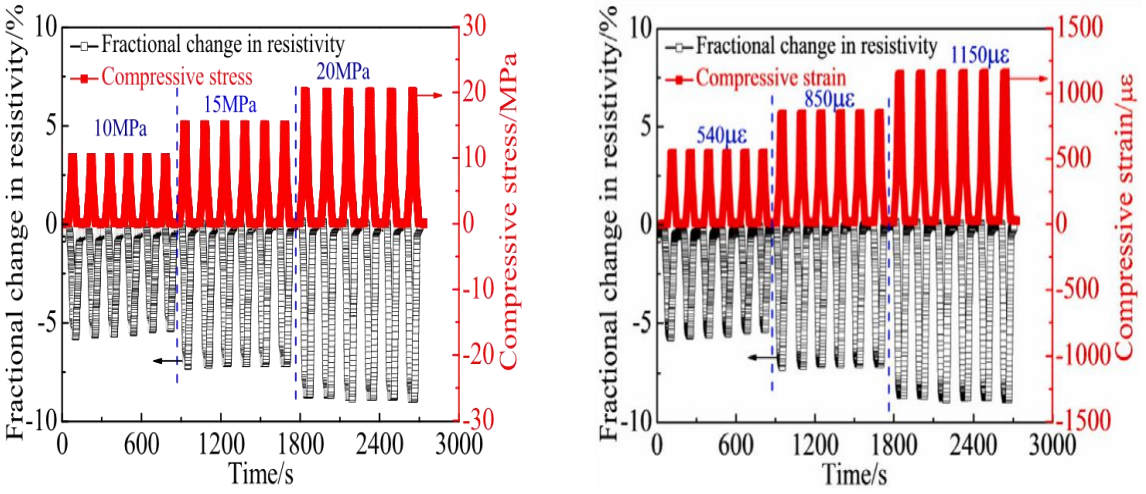

(a) Time history relationship between FCR and compressive stress with different stress amplitudes

(b) Time history relationship between FCR and compressive strain with different stress amplitudes

Fig2. 19 Relationships in time history between M6's stress/strain and FCR under cyclic compression at varying stress amplitudes (wang & zhang, 2022)**.**

Fig. 2.20 displays the time history connections between the FCR of M0 and M6 and the compressive stress/strain during monotonic compression from loading to failure. Fig. 19 shows that when compressive stress/strain increases, the FCR of M6 and M0 decreases.

When stress reaches its maximum amount, the specimen fails and the FCR rises abruptly. As a result, these traits may be used to assess the stress states of specimens. M0 and M6 have absolute maximum FCRs of 9.28% and 12.79%, respectively. In contrast to M0, which has

maximum stress and strain sensitivity of 0.09 MPa/% and 20.75, respectively, M6 has maximum stress and strain sensitivities of 0.19 MPa/% and 25.08.

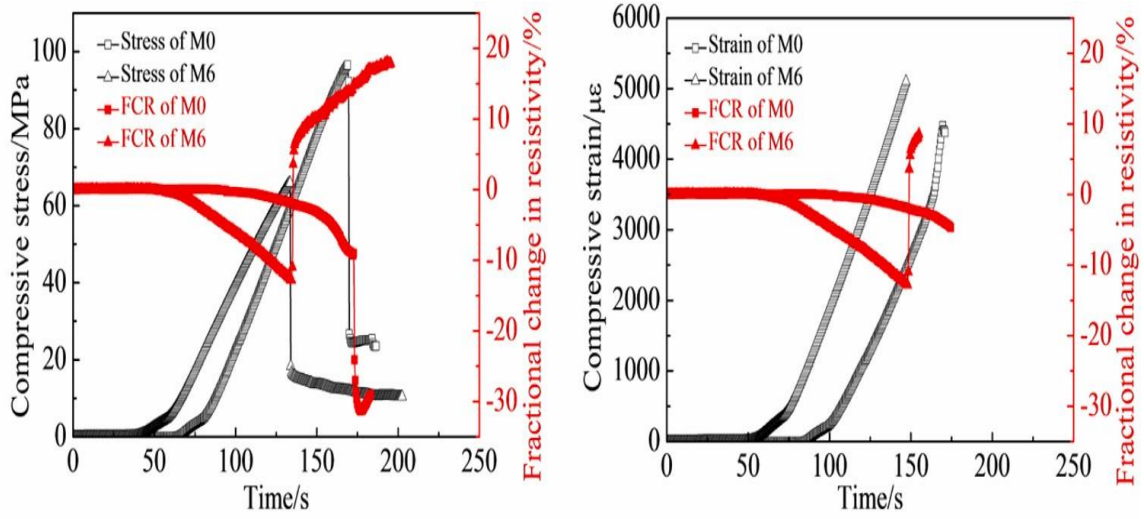

(a) Time history relationships between compressive stress and FCR of M0 and M6 from loading to failure

(b) Time history relationships between compressive strain and FCR of M0 and M6 from loading to failure

Fig2. 20 Compressive stress/strain time histories and FCR of M0 and M6 from loading to failure (wang & zhang, 2022)**.**

(Dong, et al., 2021) The electrical resistivity of cementitious composites without conductive GNP was as high as plain cement paste, but only cementitious composites filled with GNP were tested for piezoresistivity. The change in electrical resistivity and compressive strain of a cementitious composite exposed to compressive stress, with the goal of determining piezoresistive behavior under varied loading rates and magnitudes. The fractional variations in resistivity and strain increased/decreased as the amount of the loading increased/decreased. Their values at the stress peaks were linearly fit, and the square deviation of fitting curves was shown, with R12 and R22 reflecting the fractional change in resistivity and compressive strain, respectively. Because the loading rates and magnitudes of the compressive cycles varied, the square deviations of 0.999 and 0.992 suggest that these resistivity change figures had an outstanding linear connection to the compressive stress, independent of their loading rates and magnitudes. Furthermore, it was discovered that the compressive strain of the specimen had comparable linearity to the compressive stress. However, the linearity of fractional variations in resistivity is weaker, with deviation values of 0.991 and 0.970, respectively. The accumulated microdefects in the cementitious composite with each compression might explain the nonlinearity. Table 1 displays the square deviation of the cementitious composites under different stress magnitudes based on linear regression to explicitly demonstrate the influence of stress magnitude. It was discovered that fractional changes in resistivity and compressive strain had worse linearity at small stress magnitudes than under big stress magnitudes. This might be related to cementitious composites' unstable porous architectures and microstructures, which alter conductive pathways and electrical resistance.

The changed electrical resistivity is minimal under low stress circumstances, and the fractional changes of resistivity (FCR) are readily affected by resistivity changes caused by unstable structures. Large FCR values, on the other hand, are significantly more stable and devoid of interferences from unstable resistivity changes under high-stress circumstances. It follows that the cementitious composite is more suited for measuring compressive stress/strain under high external forces. Nonlinearity-induced deviation on cement-based sensors may develop in a low-stress setting and decrease accuracy.

Table 2. 1 Square deviation of cementitious composite under stress magnitudes (Dong, et al., 2021)

Group	Square deviation	Ranges of stress magnitudes		
		$0 \leq \sigma \leq 5$ MPa	$5 \leq \sigma \leq 10$ MPa	$0 \leq \sigma \leq 10$ MPa
1% GNP and 2% SHP	R_1^{2*}	0.998	0.999	0.999
	R_2^{2*}	0.989	0.998	0.991
2% GNP and 2% SHP	R_1^2	0.993	0.994	0.992
	R_2^2	0.966	0.999	0.970

Note*: R_1^2 means the square deviation of the FCR; R_2^2 represents the square deviation of compressive strain.

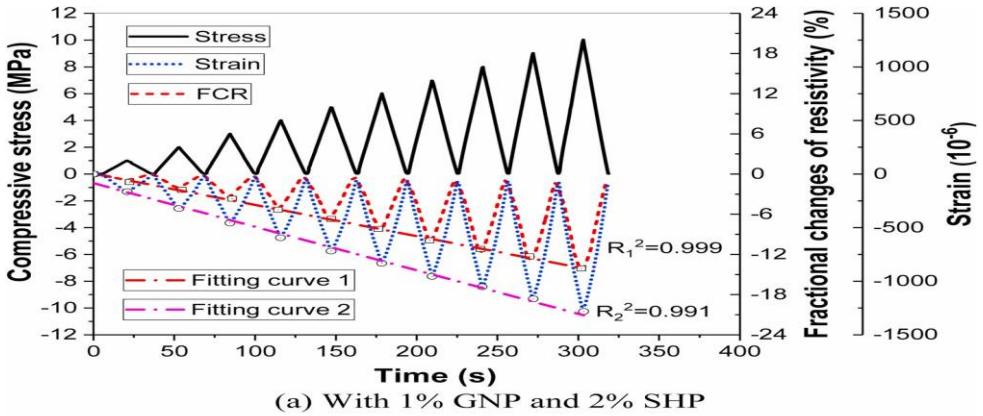

(a) With 1% GNP and 2% SHP

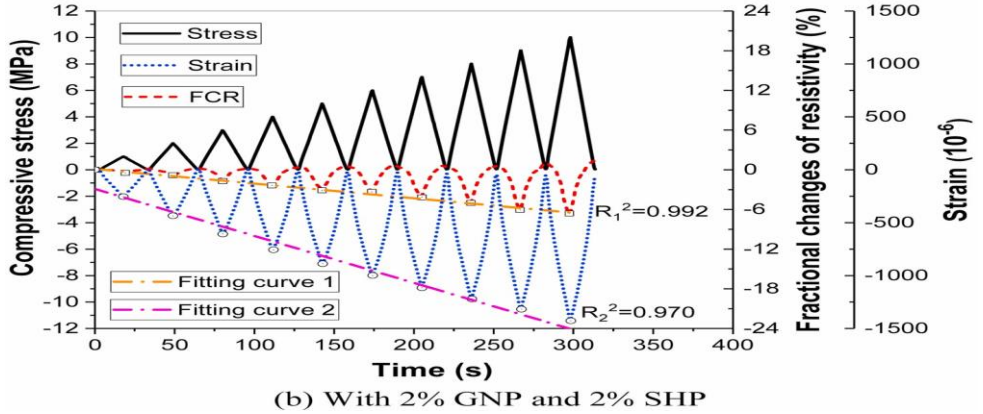

(b) With 2% GNP and 2% SHP

Fig2. 21 FCR as a function of compressive stress and strain of cementitious composite with 2% SHP (Dong, et al., 2021)

(Tao, et al., 2019) demonstrates the relative (fractional) variations in electric resistivity with time for all five mixtures under the predesigned loading schemes. In general, the relative electric resistivity follows a serrated path, wherein it reaches its maximum value at the lowest load and decreases with half phase difference along the loading path. This is reasonably acceptable, given that, under a certain burden, the conductible paths either lengthen or increase. Within this overarching regime, an increase in load should lead to a decrease in electric resistivity; consequently, the load-induced variations in electric resistivity have a negative sign. Additionally, upon closer inspection, the figure may unveil some significant attributes that are potentially intricately linked to the materials and the experiments. To begin with, it should be noted that the magnitude of piezoresistive reactions does not invariably increase with the concentration of GNPs. The electric resistivity changes in M2 and M3 are the most substantial, as illustrated in Figure 2.2.8, whereas M4 exhibits the least substantial change. Second, as the level of applied force does not invariably result in an augmentation of the extent of piezoresistive reactions. As an illustration, the piezoresistive reaction extents for M3 remain comparable over time, provided that the applied load level does not fall below 12 kN (refer to Fig. 2.2.8(d)). This phenomenon could potentially be correlated with the rate at which the GNP-modified cement compounds undergo piezoresistive reactions under strain . Furthermore, the electric resistivity signals of pure cement mortar devoid of GNPs exhibit dispersion and irregular fluctuations, particularly when subjected to modest loading levels (see Figure 12(a)). The incoherent nature of the electric resistivity to external load signals could potentially be attributed to two factors: (i) the imperfect contact between the load-bearing machine heads and the surface ends of the specimens, and (ii) the redistribution of conductible media, such as ions in pore solution, which are confined within a microspace that is complex and heterogeneous. Undoubtedly, the intricate microstructure of CBMs can be assembled in the form of fractal patterns, also known as self-similarity patterns .Nevertheless, M0 still exhibits piezoresistive reactions, which contradicts the findings reported elsewhere , which found no piezoresistive reactions in specimens with and without nanoadditions at low concentrations. Furthermore, it has been observed that the magnitude of the electric resistivity 'chaos' to external load diminishes with increasing GNP content . This indicates that piezoresistive responses become more apparent, despite the fact that their external load sensitivity is considerably more complex.

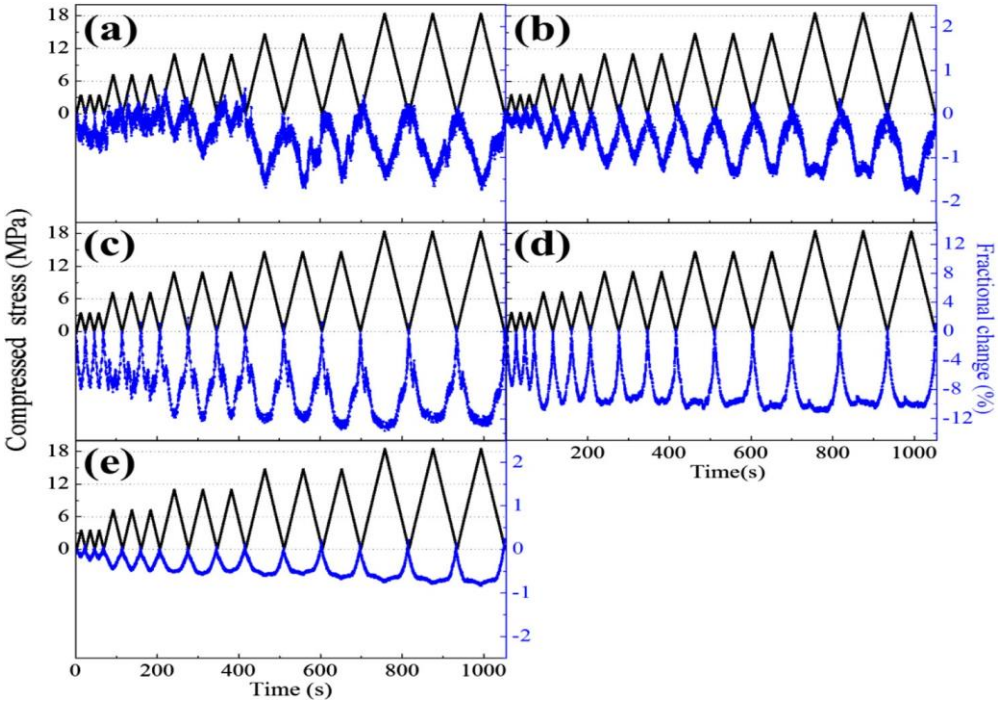

Fig2. 22 Relative (fractional) changes in electric resistivity with time for the GNP-modified cement mortars: (a) M0, (b) M1, (c) M2, (d) M3, and (e) M4 (Tao, et al., 2019)

(Rehman , et al., 2018) The fraction change in resistance was calculated using electrical resistivity measurements. The capacity of the control specimen and cement mortar containing nano Fe2O3 to self-monitor is being studied. and it was discovered that the nano-Fe2O3 cement mortar was more sensitive to monitor tension than the control specimen, which was shown to be inefficient at monitoring its own stress. Rather than resistivity per se, they found that the secret to self-sensing is a fractional change in resistance. The FCR for the control cement mix was very low. 15% carbon black and 3% nano FE203 were added, which increased the FCR, or strain sensing properties. The scientists came to the conclusion that as the quantity of graphene nanoplatelets increases, so do the piezoresistivity properties.

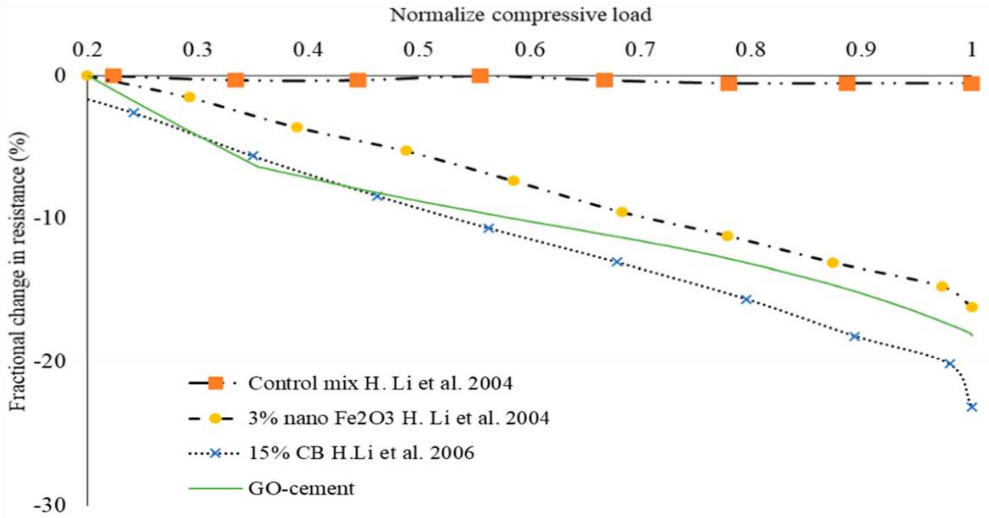

Fig2. 23 Fractional change in resistance against normalized compression load for various samples (Rehman , et al., 2018)**.**

(Tian, et al., 2019) Rx is the resistance during loading, where R0 is the starting resistance. The FCR value under cyclic compressive stress in the literature is listed in Table 2. It generally rises when tension does, and it behaves reversibly within the elastic zone. Cement paste containing carbon nanotubes showed a strong correlation with the external cyclic compression force. When the load peaks at 90 kN, for example, the maximum FRC is 33%, and it shows complete reversibility when the load is less than 50 kN. There was then residual resistance as the load increased, indicating that some of the resistance was irreversible. When the load reached between 50 and 60 percent of its highest value, microcracks may have developed within the matrix, leading to this outcome. Nanocomposites with comparatively less filler showed a superior piezoresistive effect than composites with more filler. This might have happened because there was more tunneling barrier to alter during cyclic loading, but a high filler content could have created more conductive pathways, which would have prevented the network from growing further. Therefore, a filler content that is either too high or too low will not result in piezoresistive performance.

Formula for FCR

$$FCR = \frac{\Delta R}{R_0} = \frac{R_x - R_0}{R_0}$$

Table 2. 2 Statistic of Fractional change in resistance under cyclic compressive loading(Tian, et al., 2019)**.**

References	Matrix	Filler	Filler concentration	Loading amplitude	Samples Type (mm)	FCR
[53]	Concrete	CF	2.0 wt%	3 Mpa	Concrete cubes: 51 X 51 X 51	1%
				6 Mpa		3%
				10 Mpa		4%
[46]	Paste	CF	15 vol%	15 Mpa	Cement cylindrical: 50.8 X 100	24%
[73]	Paste	CNT	2.0 wt%	6 Mpa	Cement cubes: 51 X 51 X 51	70%
			0.5 wt%			40%
			0.1 wt%			30%
[36]	Paste	CNF	0.1 wt%	4 Mpa	Cement cuboid: 20 X 20 X 80	5.40%
			0.3 wt%			2.00%
		CNT	0.1 wt%			4.10%
			0.3 wt%			1.40%
[117]	Mortar	CNT	0.6 wt%	1.25 Mpa	Mortar cuboid: 40 X 40 X 160	1.80%
[118]	Paste	CNT	1.0 wt%	0.8 Mpa	Cement cubes: 51 X 51 X 51	1%
[103]	Mortar	GNP	4.0 wt%	Strain = 80	Mortar cuboid: 40 X 40 X 160	2.20%
		CF	0.2 vol%			4.90%
[52]	Mortar	CF	3.0 wt%	20 Mpa	Mortar cuboid: 40 X 40 X 160	10%
[62]	Paste	CNT	1.0 wt%	32 Mpa	Cement cubes: 51 X 51 X 51	33%

2.4 APPLICATION METHODS FOR SELF-SENSING BEHAVIOUR OF CEMENTITIOUS COMPOSITE

2.4.1 BULK FORM

(Sarwary, et al., 2019) High electrical conductivity concrete materials need to demonstrate damage self-sensing from the moment a load is applied. Increased self-sensing capabilities

are shown by visible electrical property changes in the concrete material with applied stress. Large-scale reinforced mortar beams' capacity for self-sensing was investigated in terms of fractional changes in electrical resistivity (FCER). It is anticipated that specimens with improved self-sensing capabilities would have higher FCER values. In Figure 2.24. To evaluate the effectiveness of self-sensing at low damage levels, specimens with CF and CNT up to 5 mm (0.197 in.) displacement had their FCER data compared to four-point bending loads. Figure 2.24 shows that applied flexural loads on CF-bearing reinforced beams increased FCER significantly for CNT-Beam-1, whereas CNT-Beam-2 and CNT-Beam-3 showed only marginal increases. CF-bearing beams' FCER was 600%, 800%, and 1300% at 5 mm midspan displacement, respectively. The first beam containing CNT broke more quickly than the others, with a maximum midspan displacement value of 0.177 in. (4.5 mm). The FCER result for CNT-Beam-1 reached a maximum of 1400% at a midspan displacement of 2 mm (0.079 in.). The AC device's impedance exceeded its maximum limit at this point, reaching 1000 kΩ. Increased impedance or FCER did not follow from additional mechanical loading. Even while the FCER values increased by less than 100% after continuous loading, the second and third CNT-based beams did not exhibit a comparable trend. The FCER results revealed different increments with loads because of flexural straining that resulted in cracks on the tensile sides of the beam members with different characteristics. It is well known that traditional concrete has poor electrical conductivity. Depending on fracture factors like quantity, width, and depth, cracking won't have a major impact on electrical resistance measurements if the concrete is non-conductive.

According to a recent research, specimens doped with CF and CNT exhibited much higher self-sensing capabilities than reference specimens devoid of carbon-based compounds. To compare FCER changes with those containing carbon-based materials, reference specimens devoid of carbon-based materials were not produced for this experiment. The resistivity meter's capacity to detect cracks was enhanced in the presence of conductive fillers (CF and CNT), indicating the important influence of these fillers on self-sensing abilities. In comparison to beams with CNT, those with CF demonstrated a higher degree of self-sensing of flexural damage following loading. Up to 5 mm (0.197 in.), the FCER values of CF-based beams were superior to those of CNT-based beams. displacement, with the exception of CNT-Beam-1, suggesting higher large-scale component resilience to flexural damage. The authors investigated the self-sensing properties of steel reinforcing bar-free, CF- and CNT-based short beams under cyclic four-point bending loads in both plastic and elastic areas.43 Even with low damage intensity, the study showed that CF-based beams were susceptible to moderate damage within the elastic range. No comparable results were found when using beams based on CNTs. For both CF- and CNT-based beams, self-sensing behaviours were similar as damage intensity increased within the plastic range where cracking occurred. Because CF particles have larger electrical charges than CNT particles, which results in higher FCER values, CF-based beams may resist minimal damage during cyclic flexural stress without breaking. The probability of individual carbon-based materials coming into touch with one another was shown to be correlated with the capacity of CF-doped large-scale beams to detect damage up to 5 mm (0.197 in.). This increases the outcomes of FCER by

making established electrical contact more susceptible to even minor damages. Comparing CF-based beams to steel reinforcement, there may be a significant correlation between electrode movement and overall failure types, especially at higher displacement levels, when it comes to FCER values. According to earlier studies, CF-bearing specimens show ductile behaviour by producing flexural cracks on the tensile face of beams and limiting slanted shear fractures. This is probably because of the specimens' higher matrix dispersion and tensile straining capability. Because they can tolerate larger flexural displacements, electrodes positioned in the tension zone of CF-based beams may move closer to the tensile reinforcement of the beams. Current intended for two electrodes positioned opposite each other may diverge and pierce tensile reinforcement due to variations in the electrical characteristics of steel, brass, and cementitious systems with various carbon-based compounds. This might result in further FCER measures. It is crucial to remember that the assumption might alter depending on the quantity, details, conductivity, and other characteristics of the steel reinforcement. It is beyond the purview of this work to compare specimens with and without steel reinforcement in order to get a deeper understanding. Eventually, the implanted electrodes may partially detach from the mortar material due to further flexural strain and crack widening. When large bending capacity beams, such CF-based beams, are involved, FCER values may rise noticeably in the vicinity of final failure zones. Conclusively, CFs may function as efficient carbon-based electrically conductive materials for self-sensing monitoring of infrastructure degradation provided that the loading is not high enough to result in fiber breaking and if notable enhancements in fundamental mechanical characteristics are required. For self-sensing purposes, it is advised to include CNTs into cementitious materials. In FCER data, CF-bearing beam specimens shown superior self-sensing behavior, even under early loads without breaking. Overall, the study discovered that self-sensing and continuous damage monitoring could be accomplished using mortar mixes that included both CF and CNT.

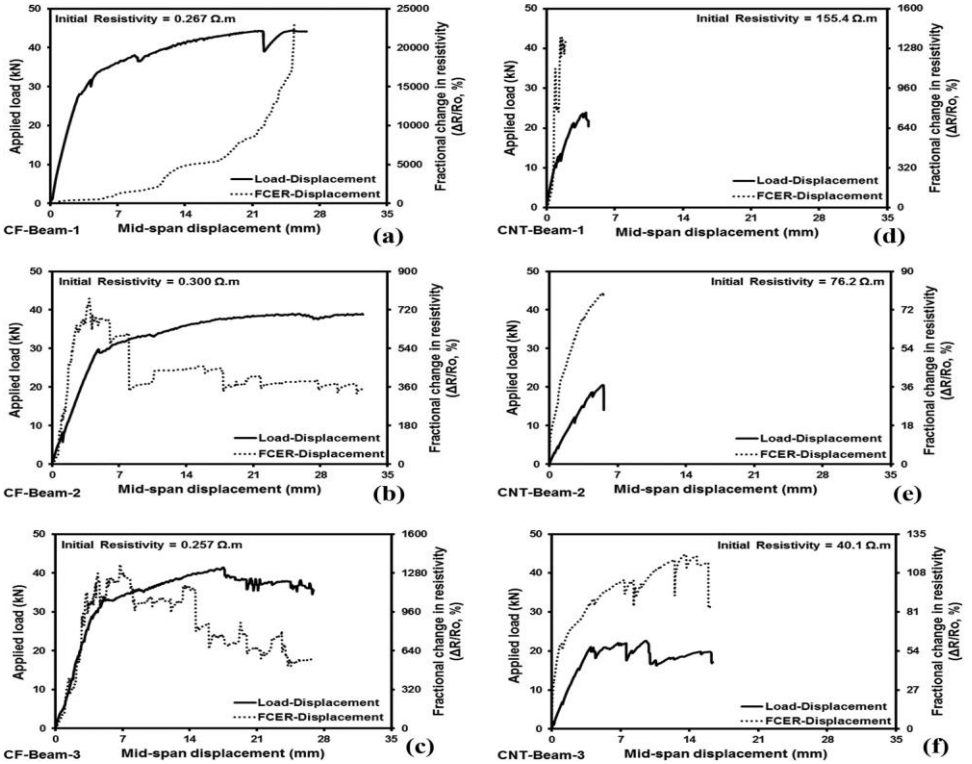

Fig2. 24 Self-sensing behaviour of CF specimen (a to c) and CNT specimen (d to f) (Sarwary, et al., 2019)

2.4.2 COATING FORM

(Qiu, et al., 2024)displays the distribution of fractures in concrete beams under a constant flexural force. FCR data for T1, T3, C1, C3, and M1 or M2 are only shown for more severe diagonal fractures or the ultimate destructive side of concrete beams due to symmetry. Under a monotonic flexural stress, the FCR in CNCF-coated self-sensing cement mortar corresponds with the degradation of concrete beams. Beam crack growth under flexural pressure showed the following features: Positive stress in the pure bending portion of the concrete beams was the first source of microcracks in the tension zone at 20%–40% of peak load. The pure bending zone produced two or three vertical microcracks before the fractures stopped expanding and gently climbed down the neutral axis. As the load rose, oblique fractures developed in the bending-shear region, which experiences both shear and positive stresses. Underweight, oblique fractures grow and spread. Oblique fractures widened and extended toward the major loading point due to increased flexural stress. As shown in Figure 6, there are no fractures because the self-sensing cement mortar covering FCR variations in the compression and tension zones of the concrete beam is mild at low loads.FCR climbed to 60.6%, 55.9%, and 19.8% in CCN5, CCN6, and CCN7 in T2, as load increased. Given that FCR responds swiftly in T2, it seems that early-stage damage, such as vertical fractures at the pure bending span of concrete beams, might affect it. With the same mid-span deflection, these concrete beams' FCR amplitudes were lower in the compression zone (14.6%, 31.3%, and 13.1% for CCN5, CCN6, and CCN7) than they were in the tension zone. The interfacial resistance between CNCFs and cement matrix varies under tensile stress, producing the FCR more vulnerable to microcracks. Flexural fracture initiation

loads/deflections for CCN5, CCN6, and CCN7 are 2.74, 2.00, and 1.36 kN per mm, in that order. CCN5, CCN6, and CCN7 showed load/deflections of 3.42, 3.33, and 2.26 kN/sq mm at the beginning of the shear fracture. Because diagonal fractures spread swiftly and in an acute, flat, and continually rising manner, FCR changes in T1, M1, and C1 are often coordinated. At the point of final destruction, FCR variations in the compression zone's C1 and C2, as well as the tension zone's T1 and T2 of CCN5, CCN6, and CCN7, indicated conflicting trends, with pure bending span abruptly declining and bending-shear span dramatically rising. Concrete beams are destroyed by shear failure caused by diagonal fissures. Concrete beams suffering diagonal fractures in T1 and C1 saw a sharp rise in FCR and a loss of load-bearing capacity as a result of the elimination of effective conductive channels. At pure bending span, the T2 and C2 resistivity decreased due to the rapid closure of vertical fractures.

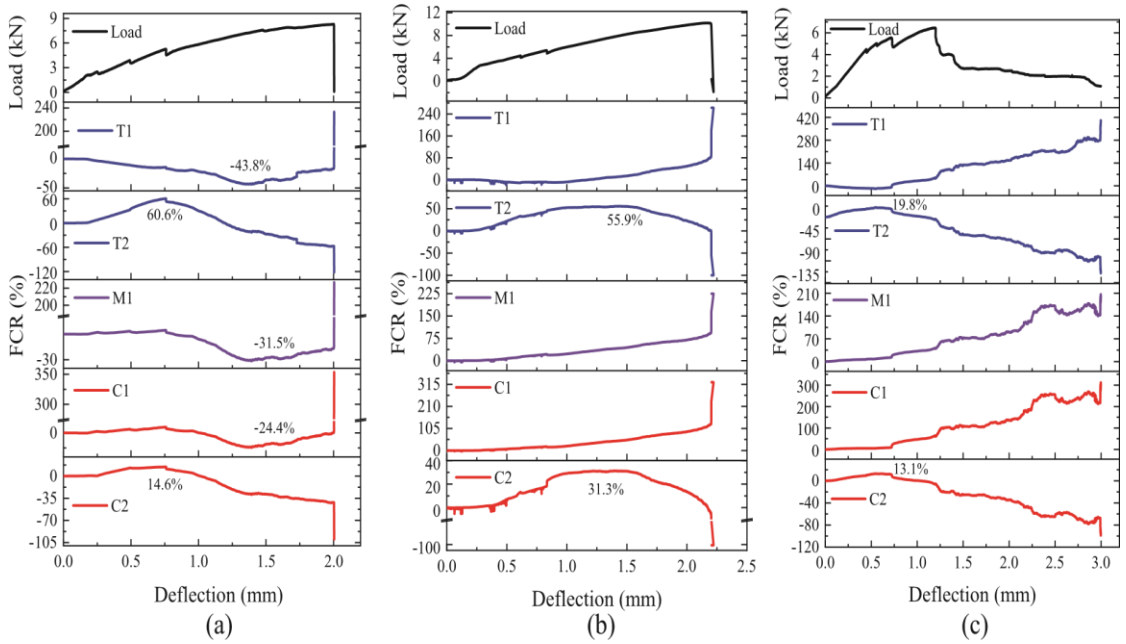

Fig2. 25 shows the load, FCR, and mid-span deflection of compression and tension zones of CCN5, CCN6, and CCN7: (a) CCN5, (b) CCN6, and (c) CCN7 (Qiu, et al., 2024)

2.4.3 SENSOR FORM

(L. Castañeda-Saldarriaga, et al., 2021) This section determines the relationship between strain and the change in the CBM/CNT material's electrical resistance during a compression test. Because there was not enough BDC equipment available to measure the composite electrical resistance, the DC-based approach was employed to analysis the piezoresistive behaviour. The bespoke nature of this BDC equipment makes it difficult to adopt on an industrial scale and raises the cost of instrumentation. Samples without an electrical polarization effect were the only ones used for piezoresistive characterization. This was due to the fact that, particularly when obtaining SHM applications, it would be impracticable to wait for the electrical resistance in samples that showed electrical polarization to stabilize. For the sample containing 0.8%wt, only the piezoresistive behavior was characterized. Figure 2.26 displays the experimental results for the sample with a weight percentage of

0.8%. This image illustrates the repeatable and reversible piezoresistive behavior of the CBM/CNT. This is so that the load exerted does not exceed the CBM/CNT's elastic limit. Unless damage develops, issues like hysteresis or alteration of the electrical response may be avoided by avoiding repeated load application. There exists a noteworthy link between electrical resistance and the compression-induced load. The reduction in the spacing between the CNTs is the cause of the negative slope seen in the CBM/CNT electric response under compression stresses.

$$\lambda = \frac{\Delta R}{\epsilon R}, \qquad (1)$$

Using Equation 1 on all eight of the repetitions shown in Figure 10, we were able to calculate the standard deviation (17.47ε−1) and average gauge factor value (972.87ε−1). This study demonstrates the repeatability of the CBM/CNT material with a weight percentage of 0.8%. Moreover, it has been shown that CBM/CNT's electric resistance changes as soon as a load is applied, making it possible to assess even very small strain levels. It may be deduced from Figure 2.26 observation that the CBM/CNT material can withstand stresses of up to -100 μwithout sacrificing the sample's structural integrity. This is due to the fact that any instances of microcracking or plastic deformation would change the material's overall electric resistance as well as its piezoresistive behaviour. This result is consistent with the mechanical characterization of CBM/CNT performed in accordance with ACI 318-14 and ASTM C109/C109M-16a standards. It was determined that the Young's modulus was 20 GPa and the compressive strength was 30 MPa.

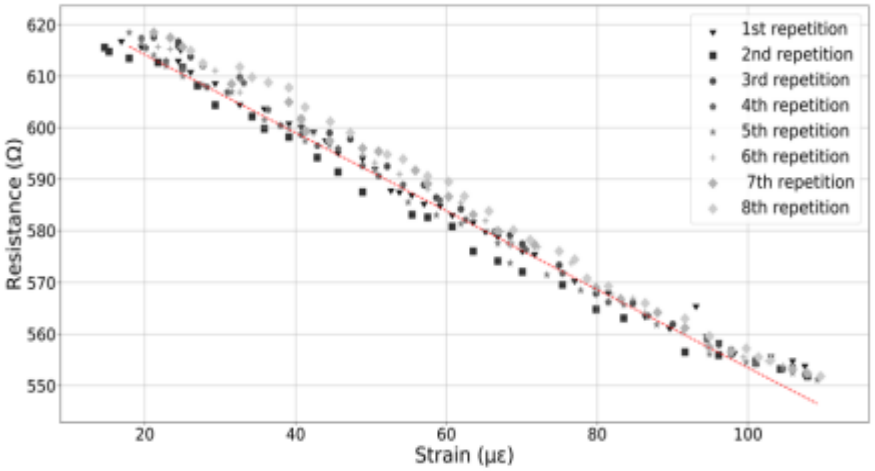

Fig2. 26 Characterization of the piezoresistive phenomena in a sample containing 0.8% weight of carbon nanotubes (CNTs) (L. Castañeda-Saldarriaga, et al., 2021)

2.5 SUMMARY

According to a review of many papers on electrical properties like piezo-resistivity, electrical resistivity, and stress sensitivity, researchers are still a long way from being able to identify the sensing properties of CB cement-based examples. This thesis has experimental self-sensing tests that were done on different amounts of CB cement-based examples.

2.6 RESEARCH GAPS

- There was limited research done on using carbon black (CB) to make concrete self-sensing.
- The study of the piezoresistive ability of cement containing CB is still uncommon, despite the publishing of a few research on its electrical characteristics.
- All the work is done only in bulk for in the beam for SSC not in the sensor form.
- The impact of environmental factors, such as temperature, carbon dioxide levels, chloride content, and humidity, on the sensing capabilities of SSC has not been investigated yet.
- The construction sector has yet to explore the potential uses of SSC in areas such as corrosion monitoring and fracture identification.

CHAPTER 3 EXPERIMENTAL DESIGN AND METHODOLOGY

3.1 GENERAL

The primary aim of the experimental investigation is to examine the characteristics of cement mortar with various proportions of Carbon Black (CB). An analysis was conducted on the self-sensing characteristics, which includes electrical resistivity and piezo-resistivity and further on its mechanical and microstructural parameters of the specimens. This chapter covers the essential assessments of cement mortars.

3.2 MATERIALS USED

3.2.1 ORDINARY PORTLAND CEMENT GRADE 43 (OPC- 43)

Ordinary Portland Cement of Grade 43 (OPC-43), which complied to the code IS:8112-1989 of BIS (Reaffirmed 2005) has been utilized in each of the experiment. The cement originated from the same batch. The manufacturer provides the specifications of OPC-43, which are shown in Table 3.1 below:

Table 3. 1 Physical characteristics of OPC-43 used.

PHYSICAL CHARACTERISTICS	VALUES AS PER IS:8112-1989
Initial Setting time (minutes)	Not less than 30
Final setting time (minutes)	Not less than 600
Fineness (%)	10 max.
Specific Gravity	3.15 max.

3.2.2 STANDARD SAND

The investigation used Indian Standard sand of three different classes, namely Grade 1, Grade 2, and Grade 3. Standard sand was obtained from Ambala, Haryana. The vendor has submitted specifications that are stated in Table 3.2. These requirements align with the rules outlined in IS:650-199

Table 3. 2 Particle size specifications of Standard Sand

GRADE	PARTICLE SIZE SPECIFICATION OF STANDARD SAND (MM)	% USED AS PER CASTING.
I	1-2	33
II	0.5-1	33
III	0.09-0.5	34

3.2.3 WATER

Given that regular tap water contains charged particles from the environment, pipes, and other sources. Generally, deionized water is used for scientific and research purposes by using nanofillers. All experimental mixing was done using deionized water, with the exception of the curing step, which utilized regular tap water.

3.2.4 SUPERPLASTICIZER (SP)

Superplasticizers are concrete additives that enhance workability while maintaining strength. Superplasticizers, when administered in the appropriate dose, may enhance the fluidity of concrete mixes, facilitating the process of placing and compacting the material. However, above the prescribed dose of superplasticizer might lead to various adverse consequences. The superplasticizer utilized in the combination was MasterGlenium51. MasterGlenium51 is a state-of-the-art admixture that utilizes a modified poly-carboxylic ether as its main component. Addition of nano-materials to cementitious composites decreases workability. Thus, SP was used to desired flow for all the mixes.

3.2.5 COPPER PLATES

Copper plates were used for testing of electrical and piezo-resistive properties. The plates acted as electrodes in the sensor for supply of current and measuring voltage. These plates were installed in the samples during the casting process (**Figure. 3.1**). The specifications of the plates used can be seen below

Table 3. 3 Specifications details of Copper plates.

Specimen type	Size of plates (mm)	Number of plates in each specimen	Spacing(mm)
Cube	70 × 20	4	10
Prism	70 × 20	4	20

Fig3. 1 Copper plates embedment in cube samples

3.2.6 CARBON BLACK :- The specific surface area of CBN was 80 m^2/g and particle size of 46nm. The total mass of 85% in CBN is carbon. X-ray diffraction (XRD) analysis (Fig. 3.3) showed the presence of broader and more intense peaks at $2\theta=25^0$.

Fig3. 2 Carbon black (Alshammari, et al., 2023)

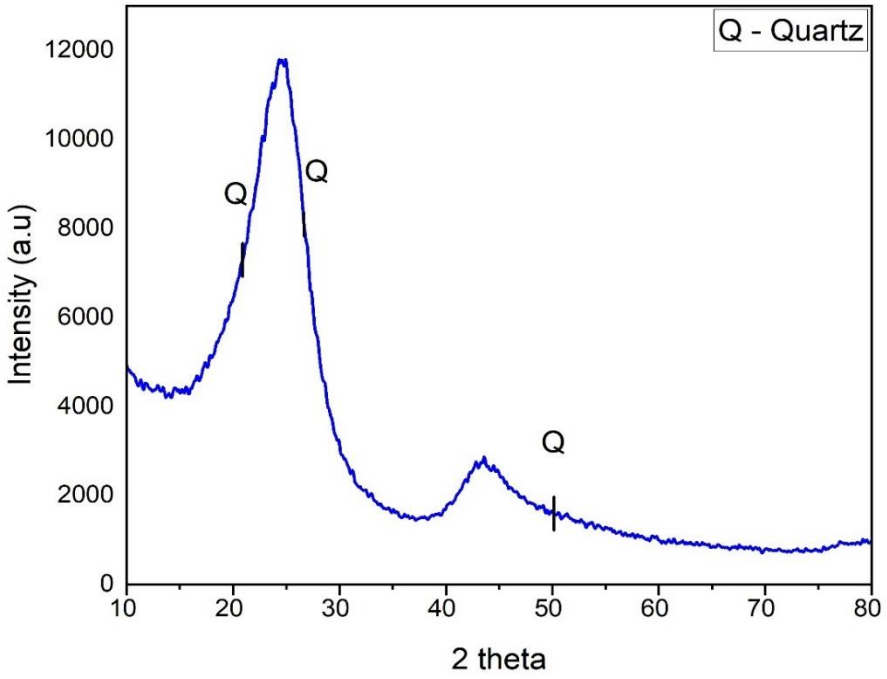

Fig3. 3 XRD of Carbon Black

The result of the XRD of carbon black are presented in Fig3.3. The layout included a broad peak width and a very high baseline. The diffraction angle (2θ) of the peak of crystalline Quartz is known to be 26.64^0, but the peak in this figure was located near 25^0. This indicated that its micro-crystallites differ from those of Quartz. This suggested that the structure's layers of carbon atoms were not fully stacked.

3.3 BATCHING, MIXING AND CASTING OF SPECIMENS

3.3.1 FLOWABILITY

The flowability of the mix was assessed following the prescribed method as per ASTM C1437,which involved carrying out a flow table test. A representative sample was placed on circular,flat-flow table equipment mounted on a tripod stand. The test sequence included placing a sample into the flow mold in the shape of a truncated cone which has a base diameter of 70 mm, upper diameter of 60 mm and a height of 40 mm, in three equal layers and compacting each layer with 25 tamping rod strokes. After levelling the specimen, the mold was verticallylifted after 1 minute, followed by 25 blows onto the table. The flow was subsequently measuredthrough a scale. The standard specifies a flow ranging from 105% to 115%.

Fig3. 4 Measurement of flow using scale.

The percentage increase in the average diameter of the spreading concrete over the basediameter of the mould is called the flow of concrete. It is given as:

$$\text{Flow \%} = (\text{Spread diameter in mm} - 70 / 70 \times 100)$$

3.3.2 CEMENT MORTAR SAMPLES WITH CB

Samples of mortar were created with a 1:2.75 cement-to-sand ratio in accordance with ASTM C-109 guidelines. CB was mixed into the cement matrix after being initially ultrasonically mixed in deionized water. Three distinct mortar cube specimens constructed of CB cement were named CB-1%, CB-2%, and CB-3%, in that order Table 3.4.

Table 3. 4 Mix proportions of cementitious cube specimens with CB.

Sample Id	Cement:Sand	Water:Cement	SP % (by weight of cement)	CB % (by weight of cement)
Control	1:2.75	0.42	0.8	0
CB1%	1:2.75	0.42	0.8	1
CB2%	1:2.75	0.42	0.8	2
CB3%	1:2.75	0.42	0.8	2.5

3.3.3 DISPERSION OF CB

Before casting, it is important to spread carbon black effectively in order to create a cement-based self-sensing nanocomposite. In order to reduce the resistivity of the non-conducting matrix and create an effective network, it is necessary to evenly distribute the carbon black throughout the cement matrix. Various methods have been developed to effectively distribute nanoparticles inside a cement matrix. There are two sorts of techniques available: physical and chemical treatments. Sonication, ball grinding, and mechanical stirring are physical techniques, while chemical approaches include the use of dispersing agents to disperse nanoparticles.

Sonication breaks clusters by providing energy to oppose Van der Waals forces. voltage changes into pressure waves, which generate a field of cavitation and tiny bubbles. This will cause the fibers to break away from one other. In the present study, the same technique was used to distribute carbon black throughout the cementitious composite. The solution underwent sonication using an ultrasonicator for a duration of 30 minutes in order to produce the aqueous solution for the mortar mixes. Following the process of ultrasonication, carbon black is prepared for utilization in the casting mixture. SP also added to the solution to enhance the workability. SP chemically breaks the bonds while sonication mechanically.

3.3.4 CASTING OF SPECIMENS

Before casting, the moulds were greased and well cleaned. The screws were exactly tightened to the proper measurements before casting. The beakers were carefully cleaned with acetone before measuring CB. Weighing the appropriate component amounts for the design combination helped us to 50x50x50 mm moulds were used for compressive strength along with piezo resistivity specimens. Using 40x40x160mm moulds following (IS:4031-Part 6), samples for flexural strength and electrical resistivity

Casting involves the following process:

• Standard sand of three grades was exactly weighed beside cement.

• Only clean tools were used in mixing.

•In a mortar mixer machine at low rpm, dry combined cement and sand well for 60 seconds.

Fig3. 5 Digi mixer for preparing the mix

•To create a homogeneous composition, water, superplasticizer and CB were dispersed in liquid form in a mortar mixer.

• Finally, the mortar mixer was set to run for yet another 120 seconds at high rpm. The components of every batch were handled independently **(Figure 3.5).**

• Minimum three samples must be prepared for the testing at each specified curing age i.e., 28days and 56 days.

Fig3. 6 Cube & Prism specimens after casting

3.3.5 CASTING OF BEAM

Beam is the most important part of the structure and very weak in the flexural reason. The main motive was to cast a self-sensing flexural beam which can sense the stress/strain with respective to the FCR. The beam was casted as a sensor form. The sensor was made with 2.5% of carbon black nanomaterial and copper plates were inserted in the sensor as shown in figure. The wires were attached to the copper plates and connected to the data logger to detect and record the FCR and changes in strain and stress.

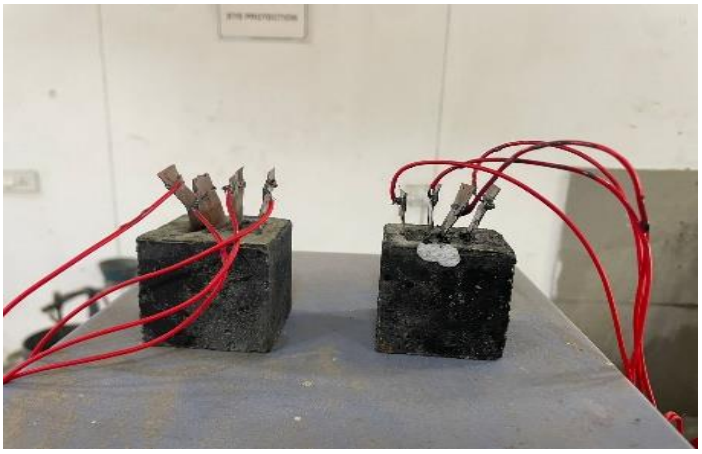

Fig3. 7 Sensors of size 50*50*50mm

The sensors were placed in the tension zone. The sensors were attached to the main reinforcement bar with steel wires. The main reinforcement used in the casting of a beam for compression and tension zone were of 12mm diameter. And 8mm diameter stirrups were used with the spacing of 90mm shown in the Fig3.8. A beam with dimensions of 700 x 150 x 150mm was casted.

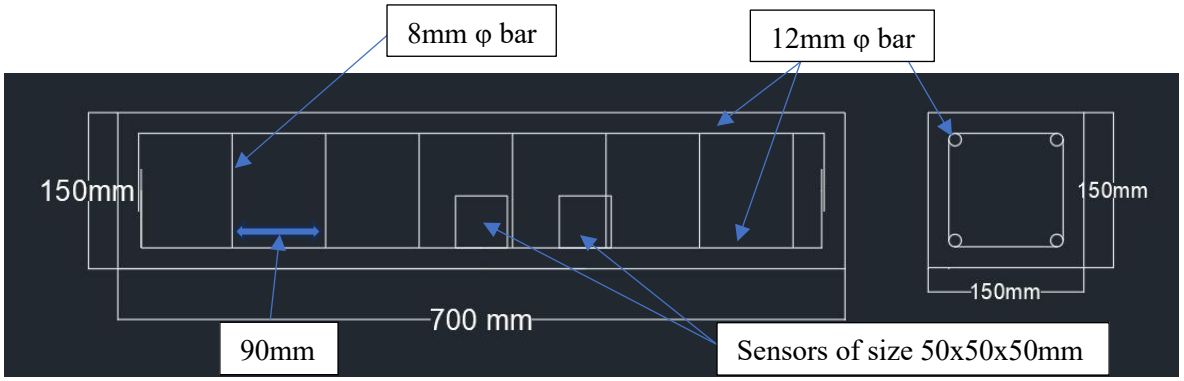

Fig3. 8 Detailing of beam

Fig3. 9 Sensor attached to the reinforcement

The beam specimen was casted using M25 concrete mix according to the IS:456 specification. For casting the flexural beam, the OPC 43 cement grade, river sand (grade 2) and coarse aggregate were used.

Before casting, the moulds were greased and well cleaned. The screws were tightened to the proper measurements before casting. Weighing the appropriate component amounts for the design combination helped us to 700x150x150 mm moulds. Drum mixer was used for the mixing process, the drum mixer was run almost 4 to 5 minutes. The concrete mix was poured in the mould in 3 to 4 layers. With the help of the manual vibrator the concrete mix was dispersed in the mould properly. This process was used in order to eliminate any voids of air from the recently poured concrete and for uniform and even surface. The de-moulding process was completed after 24 hours and the specimen was prepared for curing in water tank. For specimens to reach their maximum strength, it was cured for 28 days.

Fig3. 10 Beam after casting.

3.4 EXPERIMENTAL METHODS

Figure 3.11 presents the test matrix and technique illustrating different doses of CB along with the many parameters tested throughout the operation.

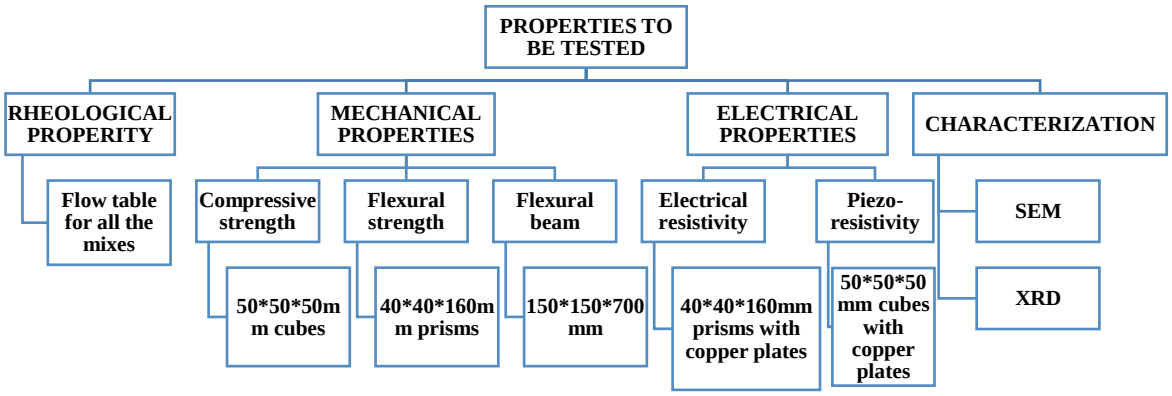

Fig3. 11 Schematic of research methodology

3.4.1 FLEXURAL STRENGTH TEST (ASTM 348-21)

At many curing ages, flexural strength was evaluated using a flexure strength test on mortar prisms. Here 3 point bending method was used for the testing of the specimens. The test was carried out for three prisms for 28 and 56 days, the average value should be recorded as the test result. The loading rate was set at 0.03kN/min while the highest capacity of the flexibility testing equipment was 100kN.

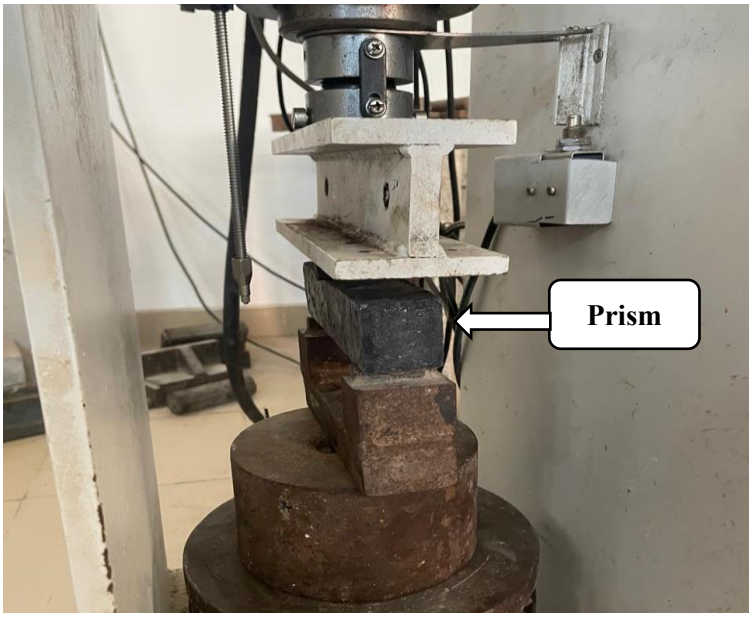

Fig3. 12 Flexural testing of prism

3.4.2 COMPRESSION STRENGTH TEST (ASTM C 109:1988)

Compression testing CB samples at varying curing ages of 28 and 56 days let one ascertain the compressive strength of mortar cubes. Samples were taken from the curing tank during testing and allowed to air dry for five to ten minutes. The samples were assessed using a compressive testing machine (CTM) using a 0.1kN/s loading rate. CTM's highest capacity is 5000kN.

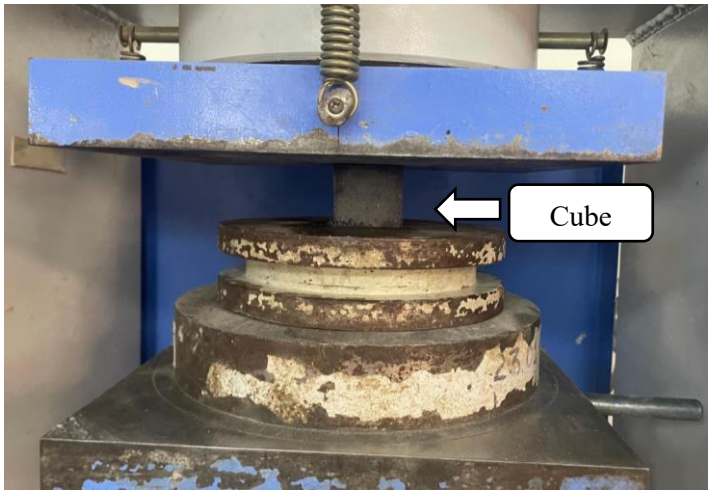

Fig3. 13 Compression testing of cube

3.4.3 ELECTRICAL RESISTIVITY TEST

Four probe method was used for the electrical resistivity test. The specimens were dried at 80°C for 24hours to remove the water (rodrigues, et al., 2021). All the connection are in series. One end of the wire was connected to the positive terminal of the power supply and another end was connected to the rheostat. Another end of the rheostat was connected to the outer plate of the specimen. And the negative terminal of the power supply was connected to the 2nd outer plate of the specimen. This was the complete circuit. A power supply (DPS-305CF) delivered a constant direct voltage (U) of 10 V to the two probes; a digital multi-meter coupled to the monitored the current differential (I). Figure 3.14

Using Ohm's law, Equation 3.1, one computed the sample's electrical resistance (R).

$$R = V/I. \qquad 3.1$$

All specimens were first thoroughly dried until weights were constant, then polarize the samples for 20 to 30 mins. The outer two probes were connected to a reference resistor (R1 ohms) in series powered by a direct current source with the constant value of 10V. Two voltage measurements were recorded i.e. one across resistor (V1) and one between inner probes (V2) using high impedance multimeter. Equation 3.2 computed electrical resistivity.

$$\rho = \frac{RA}{L} = \frac{\frac{(V2xR1)A}{V1}}{L} \qquad 3.2$$

where, ρ = Electrical resistivity, R = Resistance of the sample, L = Distance b/w two internal electrodes of the sample and A= Cross sectional area within electrodes.

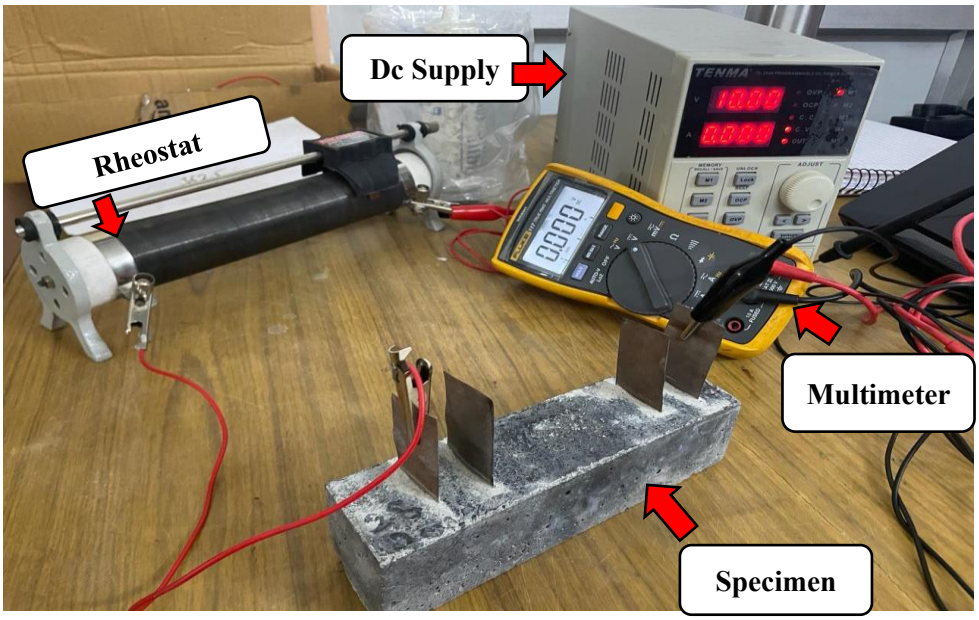

Fig3. 14 Setup for Electrical resistivity test

3.4.4 PIEZO RESISTIVITY TEST

The Fraction change in the electrical resistivity of a specimen when mechanical stress/strain is applied. The specimens were dried at 80°C for 24hours to remove the water (rodrigues, et al., 2021). The deformation and electrical resistance of the composites were simultaneously measured while monotonic compressive load was applied to analyse their piezo-resistivity (Figure 3.15). FCR is typically calculated in percentages. FCR was computed using Equation 3.3 (wang & zhang, 2022)

$$FCR\ (\%) = \frac{\rho 1 - \rho 0}{\rho 0}\ X\ 100 = \frac{\Delta \rho}{\rho 0}\ X\ 100 \qquad 3.3$$

Where, Δρ represents the change in resistivity in ohms per meter, "ρ1" represents the resistivity following the application of stress or strain, while "ρ0" represents the initial resistivity, ΔR is the change in electrical resistance in ohms, R represents the initial electrical resistance in ohms.

The experimental procedure for piezo-resistivity measurement was as follows: -

- The computer was initially connected to the CTM, and all of the initial testing parameters (loading rate, specimen type, curing age, and specimen dimensions) were assigned.
- The subsequent phase involved the wire-connection configuration, which consisted of a resistor, a data recorder, a DC supply unit, and plate connectors (Figure 3.12).
- The piezo-resistivity measurement was conducted using a four-point electrode setup. A data recorder was used to measure the current difference (I) between the inner and

outer copper plates, and a constant direct voltage (U) of 10 V was applied to the outer two copper plates by a power supply (DPS-305CF).

- The computer then issued a command, which triggered the compression loading process.
- The recording function on the data recorder was activated prior to the commencement of the test in order to accumulate all the essential data required for the electrical resistivity recording.
- In addition to the data logger, a computer was recording a Force-time graph of the applied compressive stress until the specimen failed.
- The recording function on the data was deactivated following the test, and all wired connections were removed in preparation for the subsequent specimen.
- After calculating resistivity, FCR was finally calculated using **Equation 3.3.**
- The resistivity was calculated by utilizing a variety of parameters, including the area, length, current, and voltage output of the inner and outer plates (Figure 3.15).

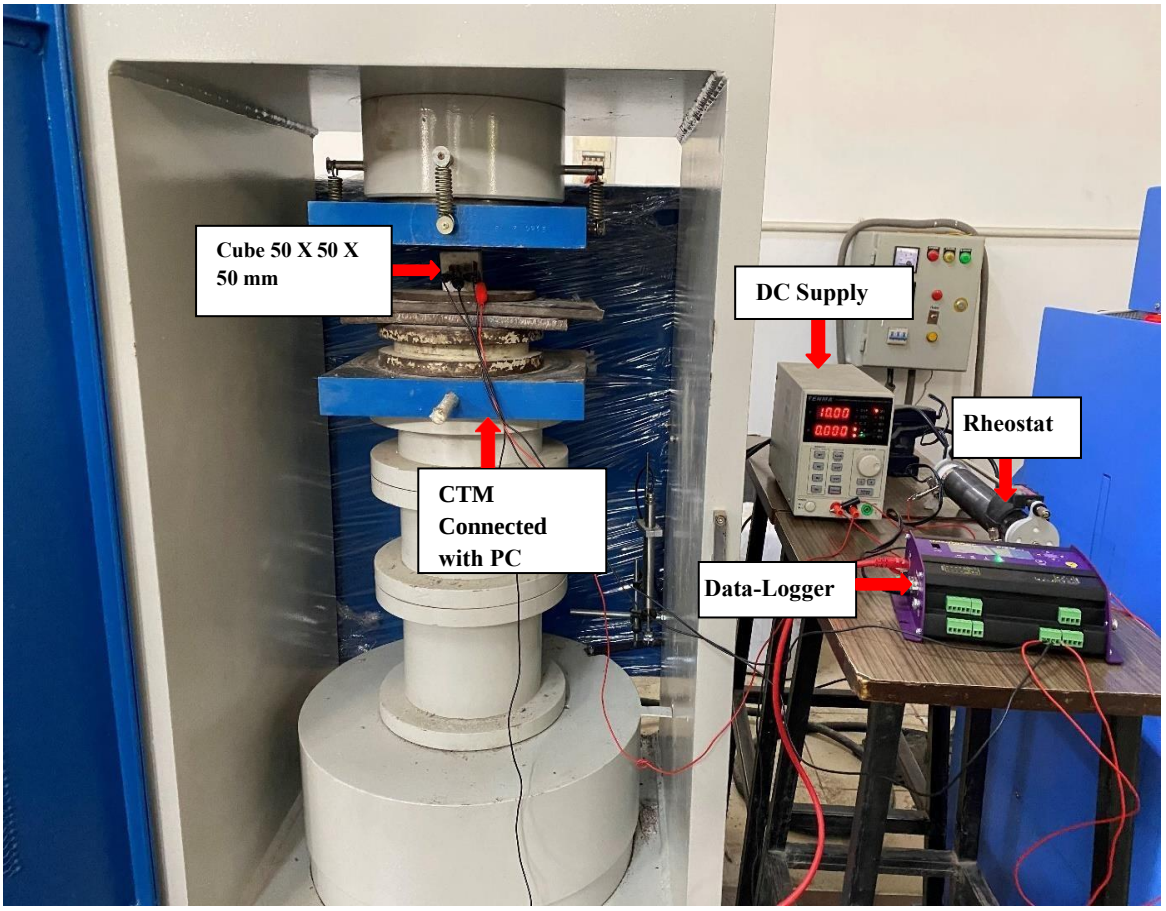

Fig3. 15 Piezo resistivity test for cubes

3.4.5 TESTING OF THE SELF SENSING CEMENTITIOUS SENSOR IN THE FLEXURAL BEAM

The experimental procedure for beam was as follows: -

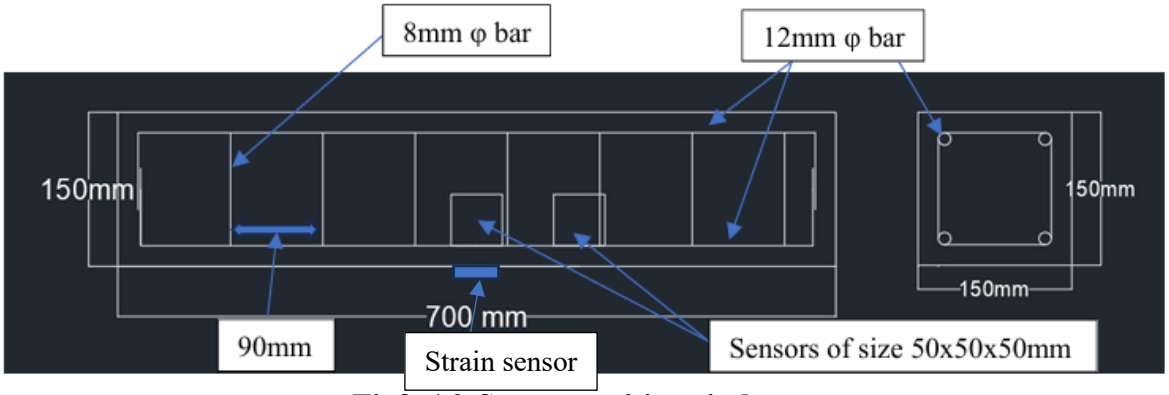

Fig3. 16 Sensor positions in beam

- In order to test the beam, the four point bending technique and the universal testing machine were used.
- The computer was initially connected to the UTM, and all of the initial testing parameters (loading rate, specimen type, curing age, and specimen dimensions) were assigned.
- The subsequent phase involved the wire-connection configuration, which consisted of a resistor, a data recorder, a DC supply unit, and plate connectors (Figure 3.17).
- In order to determine the value of the strain, the strain gauge was mounted in the tension zone shown in Fig.3.16. With the help of wires, the strain gauge was connected to the data logger, and the strain is immediately recorded in the data logger.
- The piezo-resistivity measurement was conducted using a four-point electrode setup. A data recorder was used to measure the current difference (I) between the inner and outer copper plates, and a constant direct voltage (U) of 10 V was applied to the outer two copper plates by a power supply (DPS-305CF).
- The computer then issued a command, which triggered the compression loading process.
- The recording function on the data recorder was activated prior to the commencement of the test in order to accumulate all the essential data required for the electrical resistivity recording. Strain vs time value also recorded in the data logger. In addition to the data logger, a computer was recording a Force-time graph of the applied compressive stress until the specimen failed.
- The recording function on the data was deactivated following the test, and all wired connections were removed in preparation for the subsequent specimen.
- After calculating resistivity, FCR was finally calculated using **Equation 3.4** (wang & zhang, 2022)

$$FCR\ (\%) = \frac{\rho 1 - \rho 0}{\rho 0}\ X\ 100 = \frac{\Delta \rho}{\rho 0}\ X\ 100 \qquad 3.4$$

- The resistivity was calculated by utilizing a variety of parameters, including the area, length, current, and voltage output of the inner and outer plates.

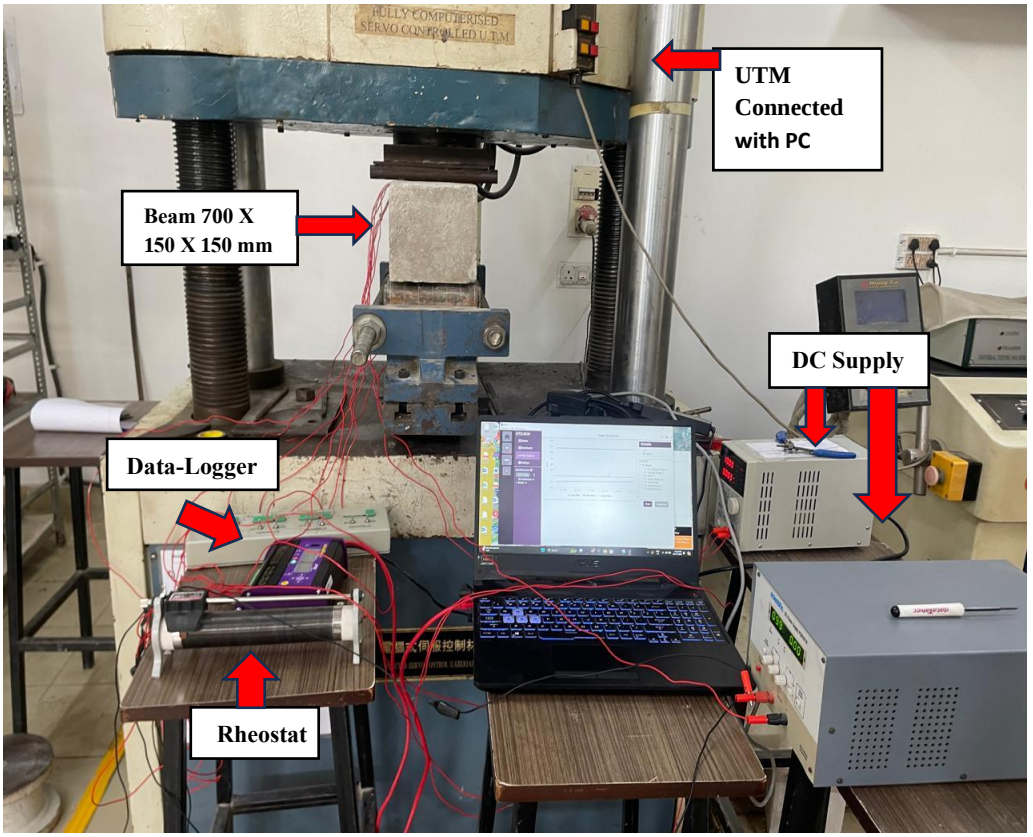

Fig3. 17 Setup for Beam testing

3.5 MICROSTRUCTURAL ANALYSIS

3.5.1 XRD

Cu- radiation was employed to conduct X-ray diffractometer (XRD) analysis to examine the chemical properties of the specimens. In addition, diffraction intensities ranging from 0° to 90° were achieved by applying 30kV and 40mV voltages. Examining the structure of material at the atomic or molecular scale. Classifying materials by analysing their diffraction pattern. Characterizing unidentified crystalline material, such as minerals and organic compounds. In our study, we use carbon black nanomaterial in powder form for XRD.

3.5.2 SEM

The microstructure of cementitious samples was examined using Scanning Electron Microscopy (SEM) to identify changes in the microstructure as a result of the addition of CB, which resulted in an increase in the composite's piezo-resistivity. Scanning electron microscopy (SEM) enables us to see the surface of the sample at a high level of magnification. In our mortar samples, this indicates we are able to visually analyse the arrangement of cementitious materials, aggregates, and pores.

3.6 SUMMARY

This chapter detailed the experimental experiments that were conducted. Materials and sample preparation details were disclosed. The mechanical and electrical properties of cement-based CB specimens were assessed in the experimental program, which was divided into two sections. Compressive and flexural strength evaluations are among the mechanical properties that are assessed. Concurrently, electrical properties encompass assessments of piezo-resistivity and electrical resistivity.

CHAPTER 4 RESULTS AND DISSCUSSION

4.1 GENERAL

This chapter presents the results of the experimental investigation. This chapter examines the ability of carbon black (CB) as self-sensing materials for reinforced concrete (RC) constructions. This chapter provides a comprehensive presentation of the acquired findings and thoroughly analyzes the influence of CB.

4.2 FLOWABILITY

It was observed that the flow values and hence, the flow % decreases with the increase in the concentration of the filler material, which can be attributed to the thickening of the cement paste when more filler is added. Initially 1-3%CB were selected for the casting of the specimens but due to the sudden drop in the flow of 3% shown in Fig4.1, 2.5% was included in the study and the 3% was not considered for the further testing. With the same w/c ratio and same percentage of the SP.

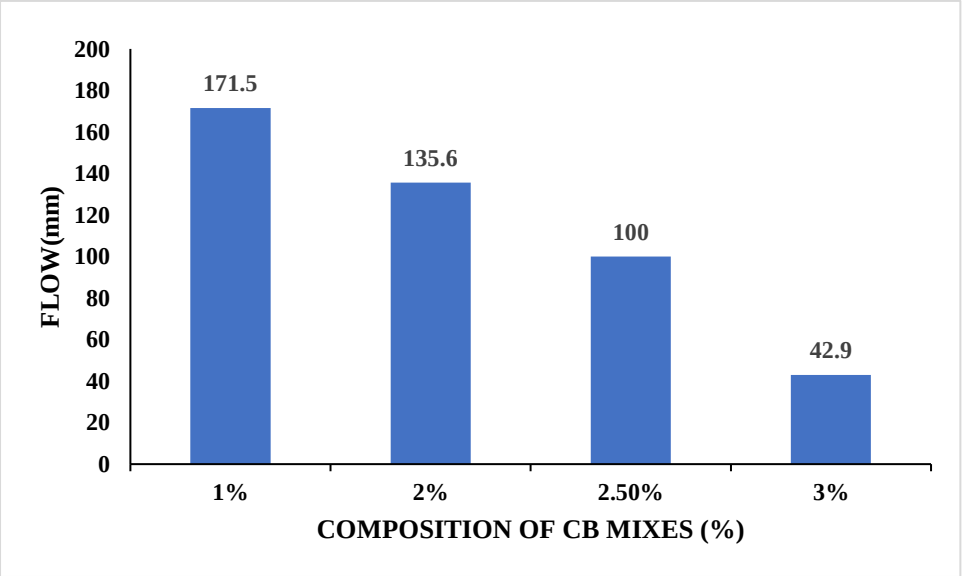

Fig4. 1 Flow characteristics of CB (%)

4.3 FLEXURAL STRENGTH

The change in the flexural strength for the different dosages of CB at different curing ages can be seen in the **Figure 4.2**. The increased percentage of CB, increased the flexural strength. The maximum strength was achieved by the 2.5%CB, it shown a 11.19% improvement in flexural strength at 28 days and a 6.36% improvement at 56 days when compared to the control mix. The decrease in the strength is due to the excess water absorption, the formation of voids and the presence of superplasticizer also shown in section 4.8. The increase in the Flexural Strength was due to the filling impact of CB and reducing the voids (Li , et al., 2024). For specimens made with CB cement, maximum flexural strength in the tested CB range was at 2.5%CB.

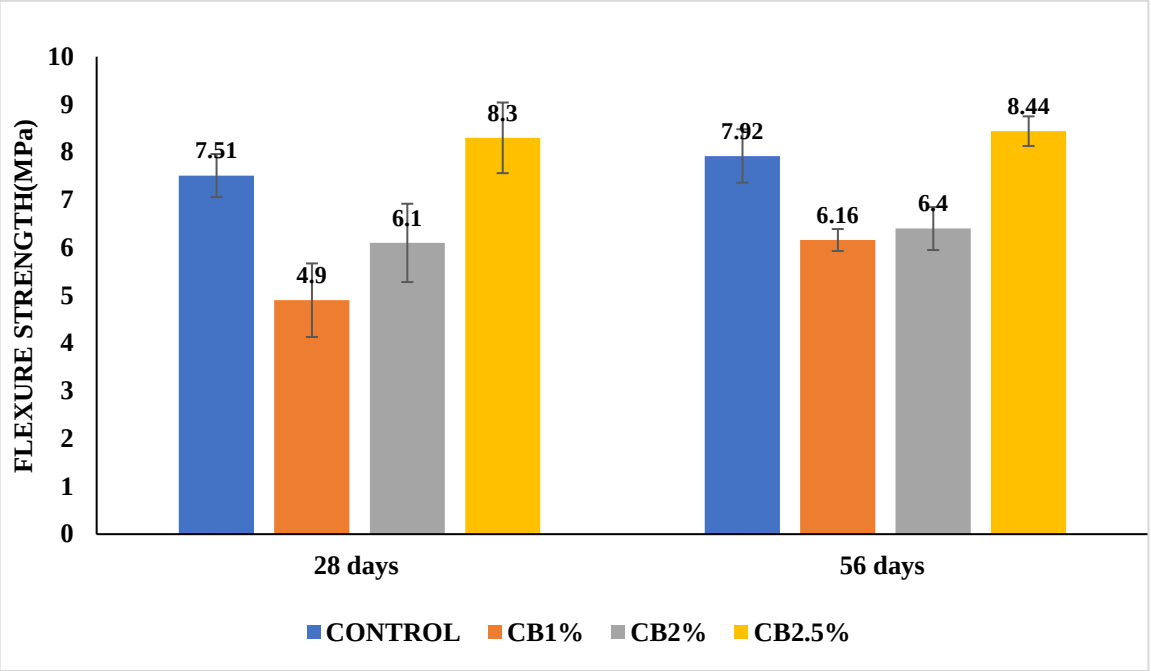

Fig4. 2 Flexural Strength results of CB based specimen.

4.4 COMPRESSIVE STRENGTH

The compressive strength of the cementitious mix changes as a result of the addition of varying concentrations of CB at various curing ages, as shown in **Figure 4.3**. The significant decrease (i.e. CB1%) in compressive strength may be attributed mostly to the absorption of excess water, more voids and the formation of agglomerates of CB particles, and the presence of superplasticizer as we can see in the section 4.8. These factors negatively affect the hydration and fluidity of the cement, thereby impacting the distribution of particle sizes and the resulting compressive strength. Furthermore, research suggests that CB has a negative impact on the binding force between hydration products. Furthermore, the decrease in compressive strength was likely due to the dilution effect, where the decrease in cement content hinders the development of strength. When the percentage of carbon black increases the mortar paste gets more denser, the increase in compressive strength is mostly due to the filling impact of CB and the lowering effect of harmful pores (Li , et al., 2024).. The highest strength was achieved by the 2.5%CB for both 28 and 56 days.

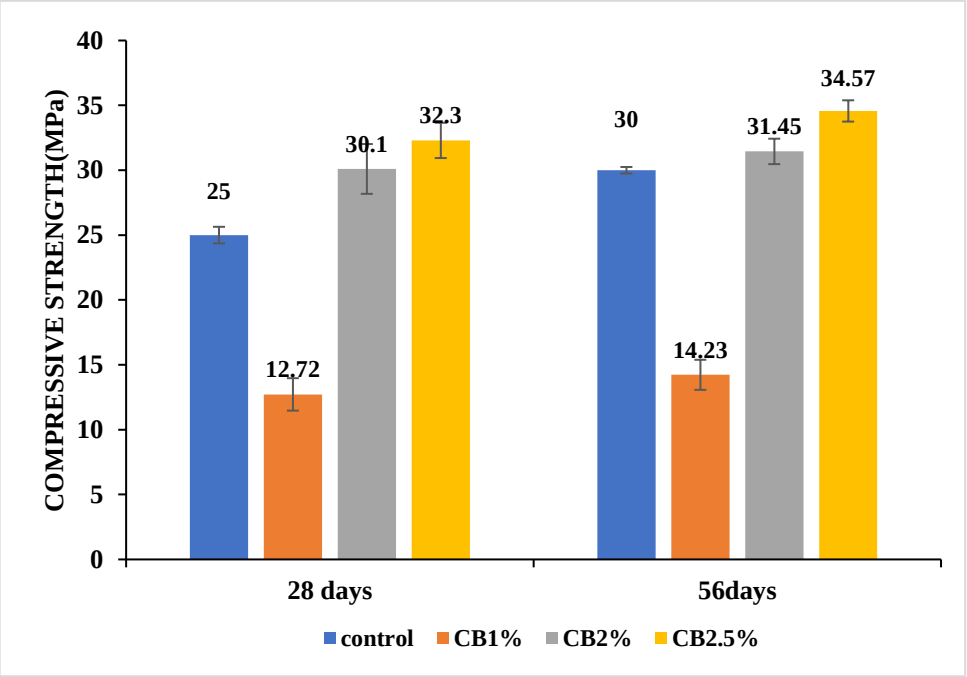

Fig4. 3 Compressive Strength results of CB based specimen.

4.5 ELECTRICAL RESISTIVITY

Electrical resistivity was continuously measured for 4 types of specimens– the control specimen and the specimen that contained 1%CB, 2%CB and 2.5%CB by weight of cement. The results are presented below in table4.1. It can be seen in table4.1 that electrical resistivity of the control samples as well as the samples containing CB increased with an increase in the testing duration. This could be attributed to the gradual rise in temperature of the environment the samples have been subjected to after their preparation. The conditions (e.g., moisture, temperature, humidity) during the testing period could affect the development electrical properties in the cement mortar samples. After 28 days the value of electrical resistivity for control sample is 412 KΩ-cm but if we compared it with the 1%,2% and 2.5% CB samples the values of electrical resistivity is 18.9 KΩ-cm, 12.1 KΩ-cm, 10 KΩ-cm. The control sample was non-conductive in nature so the values are high i.e. 182.5% if we compared it with the CB samples. With the increase in the CB% the void ratio is decreasing due to the filling effect of the CB and the formation of the conductive networks increasing. But at 56days there is a sudden jump in the electrical resistivity for 2.5%CB sample shown in table 4.1. This was due to the high temperature the specimens are getting to much dry. So, again all the specimen was cured for 28 days just to check the values of electrical resistivity at same temperature. The value of ER for 1%,2% and 2.5%CB was 12.9 KΩ-cm,11.36 KΩ-cm and 9.2 KΩ-cm. The 2.5% of the CB was more conductive if we compared it with the others samples so 2.5%CB specimen was used as a sensor.

Table 4. 1 Values of Electrical resistivity at different days

No of samples	28 days	42days	56days
Control sample	412 KΩ-cm	597 KΩ-cm	618 KΩ-cm
CB 1%	18.9 KΩ-cm	23.3 KΩ-cm	25 KΩ-cm
CB 2%	12.1 KΩ-cm	18.8 KΩ-cm	22.8 KΩ-cm
Cb2.5%	10 KΩ-cm	45.2 KΩ-cm	216.4 KΩ-cm

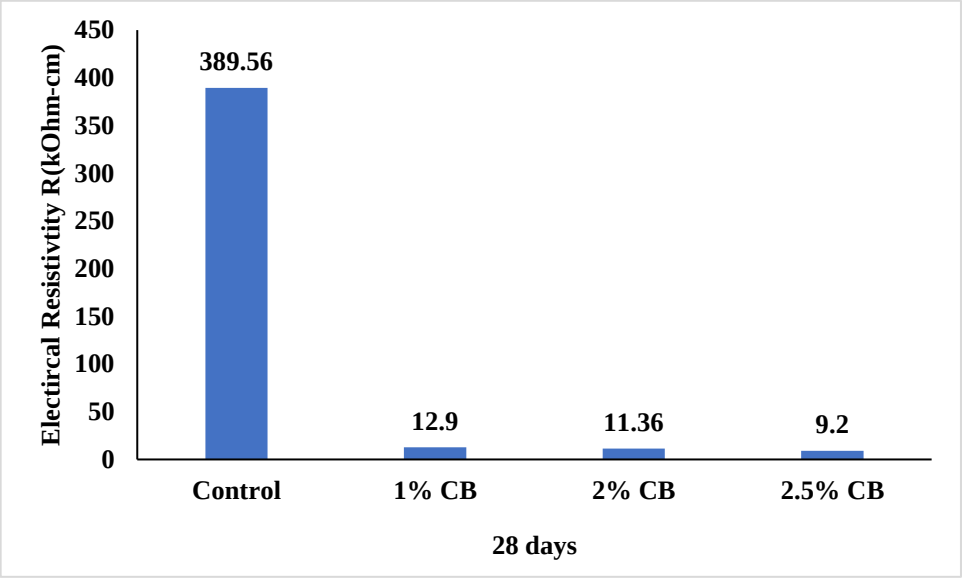

Fig4. 4 Electrical Resistivity of the specimen containing CB in different proportation.

4.6 PIEZORESISTIVITY

FOR CONTROL SAMPLE

Fig 4.5, Fig 4.6 displays the time history correlations between compressive stress and FCR of the control mix throughout 28 days and 56 days of curing under monotonic compression, respectively, starting with loading and continuing until failure. It was shown that the FCR of the specimen stays consistent as the compressive load increases. The control mix has an absolute maximum FCR of 0%. The control specimen didn't show any sensitivity to stress.

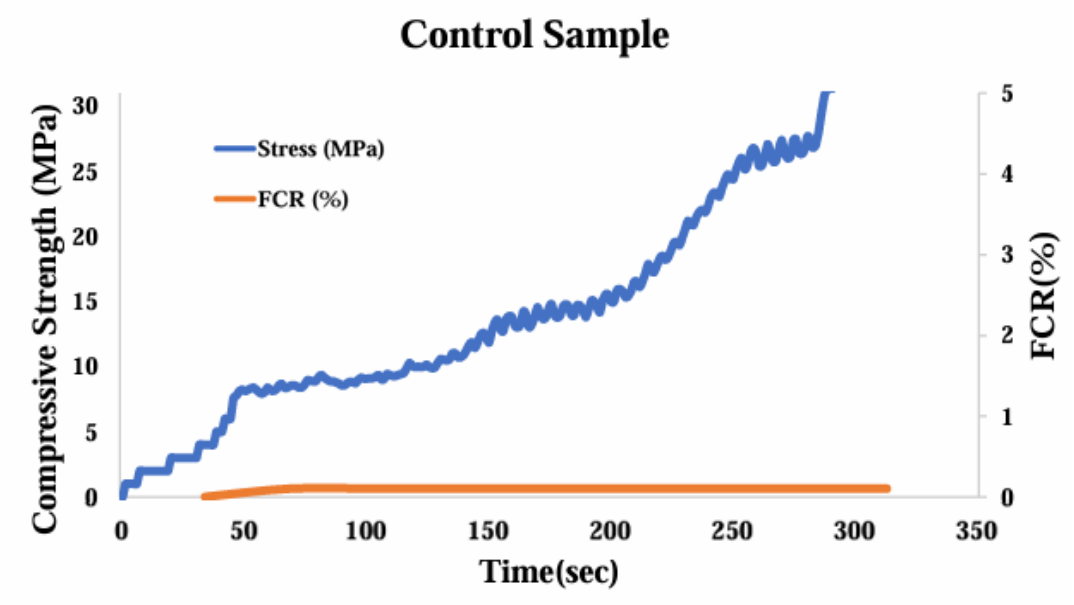

Fig4. 5 Compressive strength vs FCR for control specimen tested for 28 days.

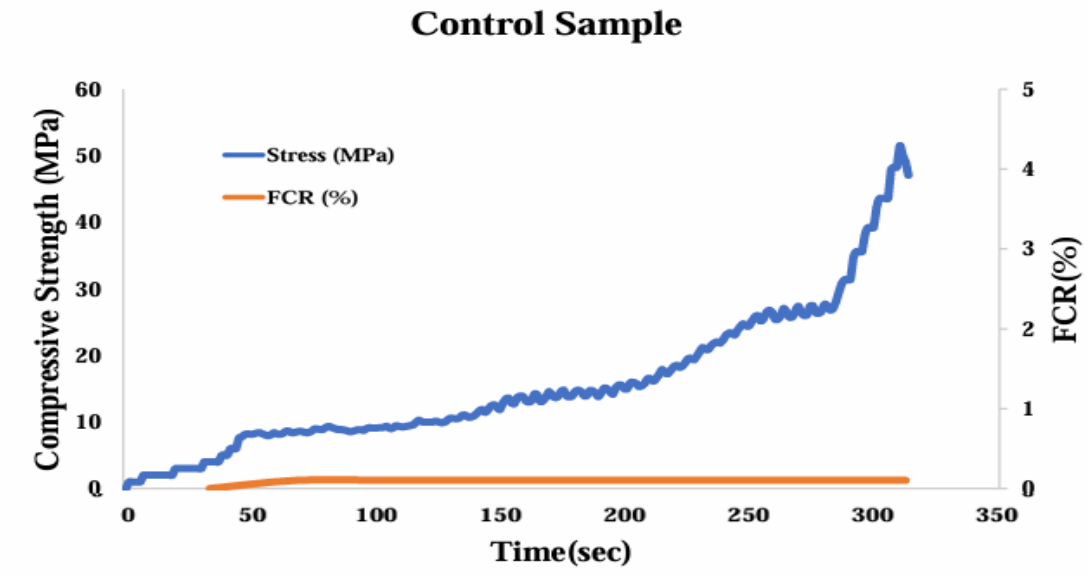

Fig4. 6 Compressive strength vs FCR for control specimen tested for 56 days.

FOR CARBON BLACK

The time history connections between the (FCR) and the monotonic compressive stress of CB-1, CB-2, and CB-2.5% at the curing age of 28 and 56 days are shown in **Figure4.7 to Figure 4.12**. A general trend can be observed between the FCR values and the compressive strength of the sample, for all the CB samples. As the compressive strength increases, the FCR values decreases but as the sample nears its yielding point, a sudden jump is noticed in the FCR values. A reasoning for this jump can be provided that as the load increases, the sample under compression sees more conductive filler particles coming together which

results in the formation of more conductive networks and explains the decrease in the FCR values. However, when the sample yields, these conductive networks are broken which results in an abrupt increase in the resistivity of the sample. This indicates that the specimen possesses a good sensing ability and can be used to monitor conductivity changes corresponding to increasing stress. The FCR pattern for the CB1% was very different so we neglect it for the sensor purpose.

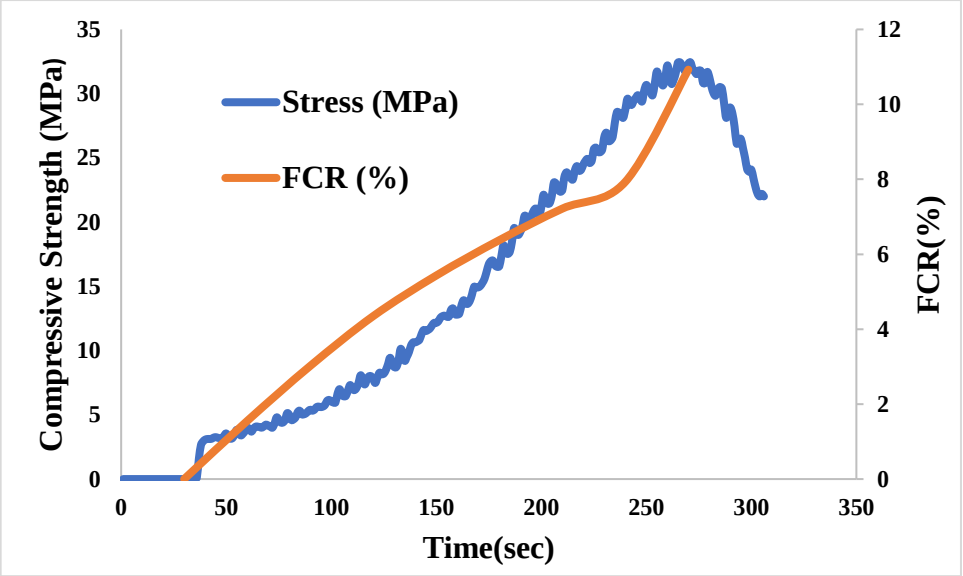

Fig4. 7 Compressive strength vs FCR for 1%CB tested for 28 days.

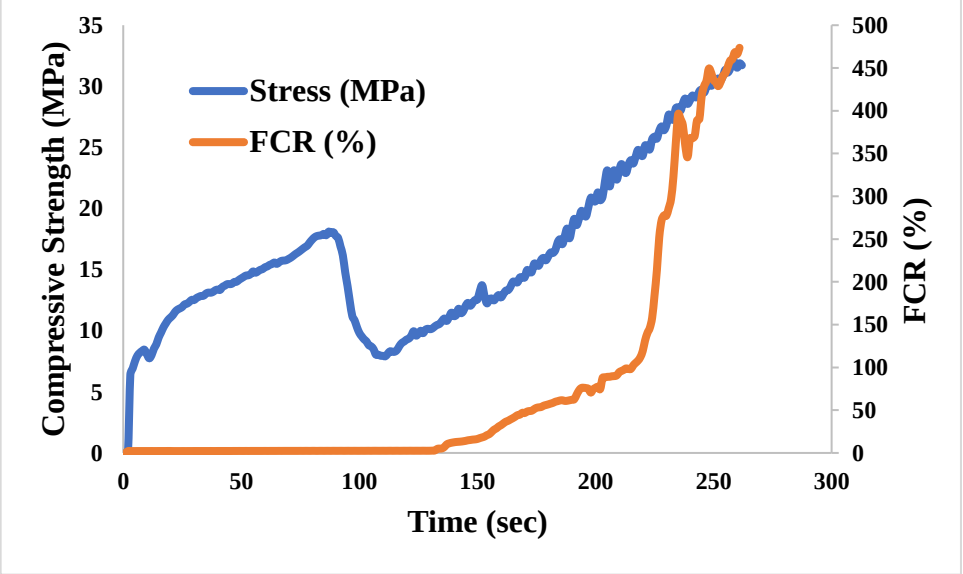

Fig4. 8 Compressive strength vs FCR for 1%CB tested for 56 days.

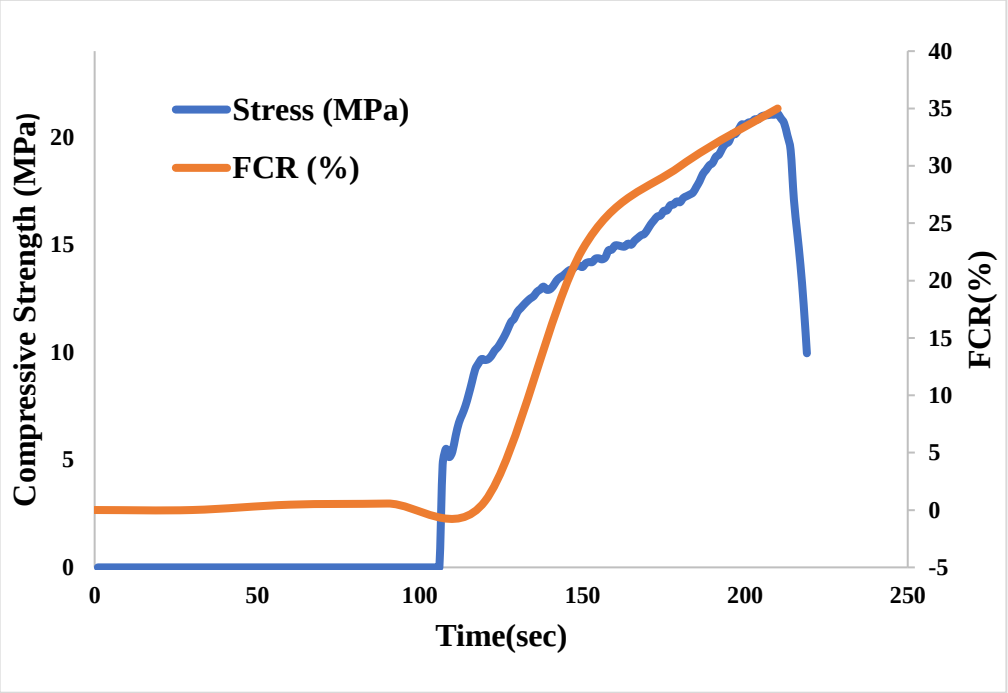

Fig4. 9 Compressive strength vs FCR for 2%CB tested for 28 days.

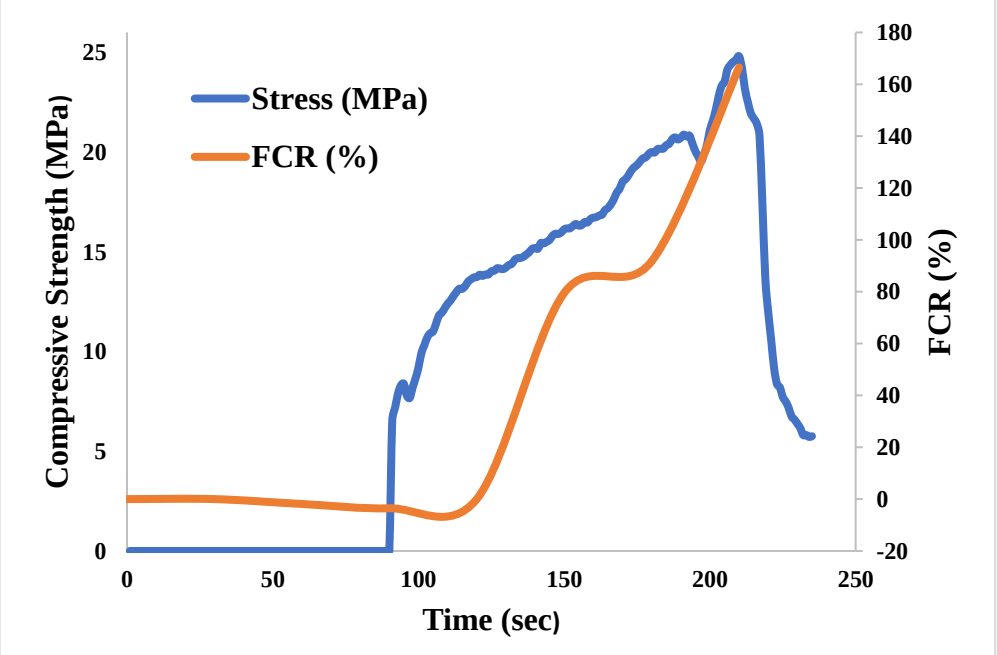

Fig4. 10 Compressive strength vs FCR for 2%CB tested for 56 days.

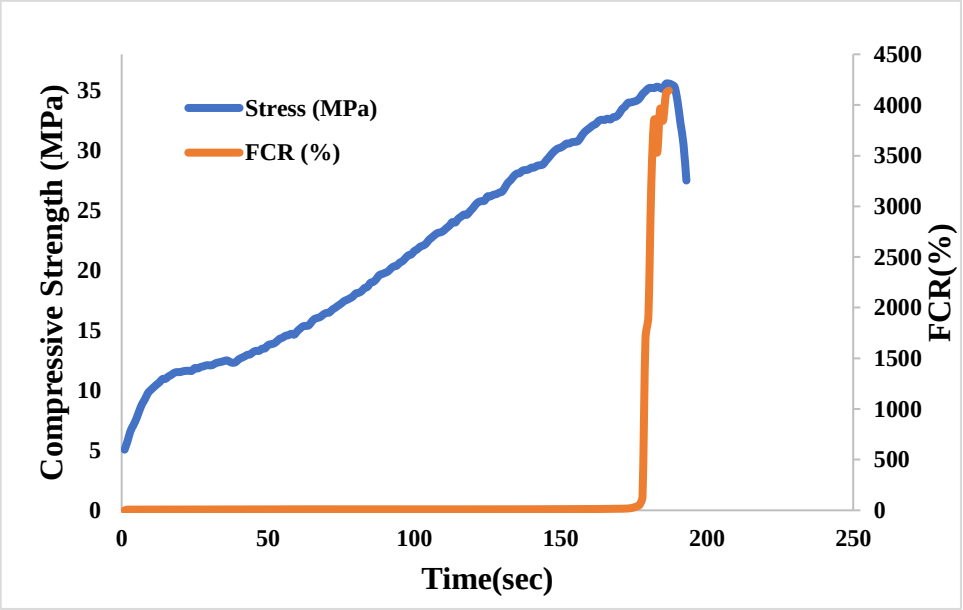

Fig4. 11 Compressive strength vs FCR for 2.5%CB tested for 28 days.

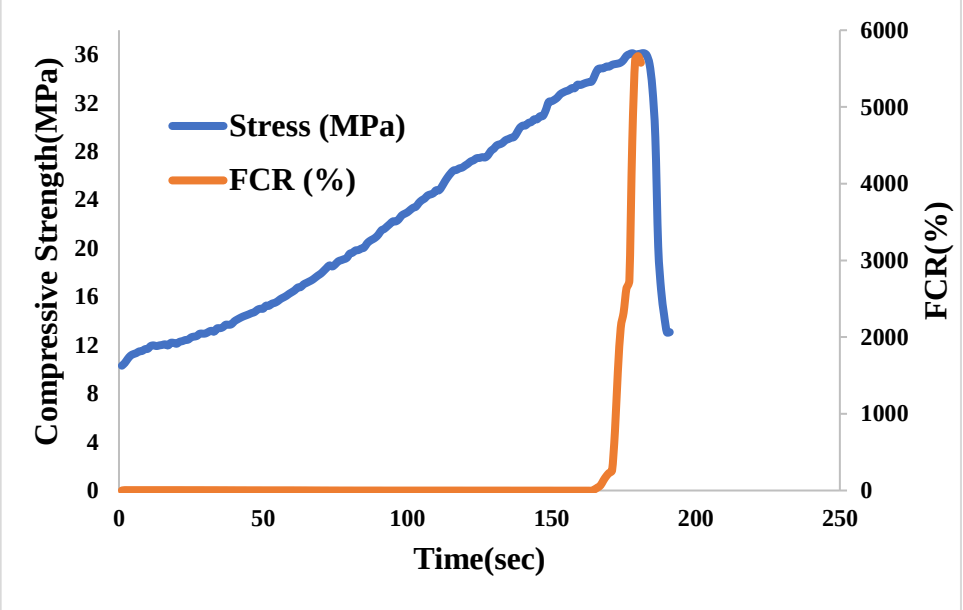

Fig4. 12 Compressive strength vs FCR for 2.5%CB tested for 56 days.

The value of FCR was very high, like for 2.5%CB the value of FCR is approximately 4500% for 28days specimen, similarly for the 56days specimen it is approximately 6000% due to the temperature or humidity effect. The specimen was very dry due to the high temperature which effects the conductive networks of the specimen also we can see these changes in the electrical resistivity test. When the 1%CB samples were tested the temperature was in a range of 20 to 25°C but when the 2.5%CB samples were tested the temperature was in a range of 42 to 46°C. So, there was a huge difference in the temperature. This the main reason for the high value of FCR and also for the high Electrical resistivity.

FITTING CURVE ANALYSIS

Samples with greater R-squared value will suggest that the composite possesses a good sensing capability. The result show high stability and uniformity. As can be seen from **Figures 4.13, 4.15 & 4.17** for 28 days and **Figure 4.14,4.16 & 4.18** for 56 days of specimen. For 28 days the fitness of FCR and stress for CB 1%,2% and 2.5% was found to be 0.9307, 0.9983 and 0.8228, respectively. For 56 days the fitness of FCR and stress for CB 1%,2% and 2.5% was found to be 0.9525,0.9158 and 0.9746.

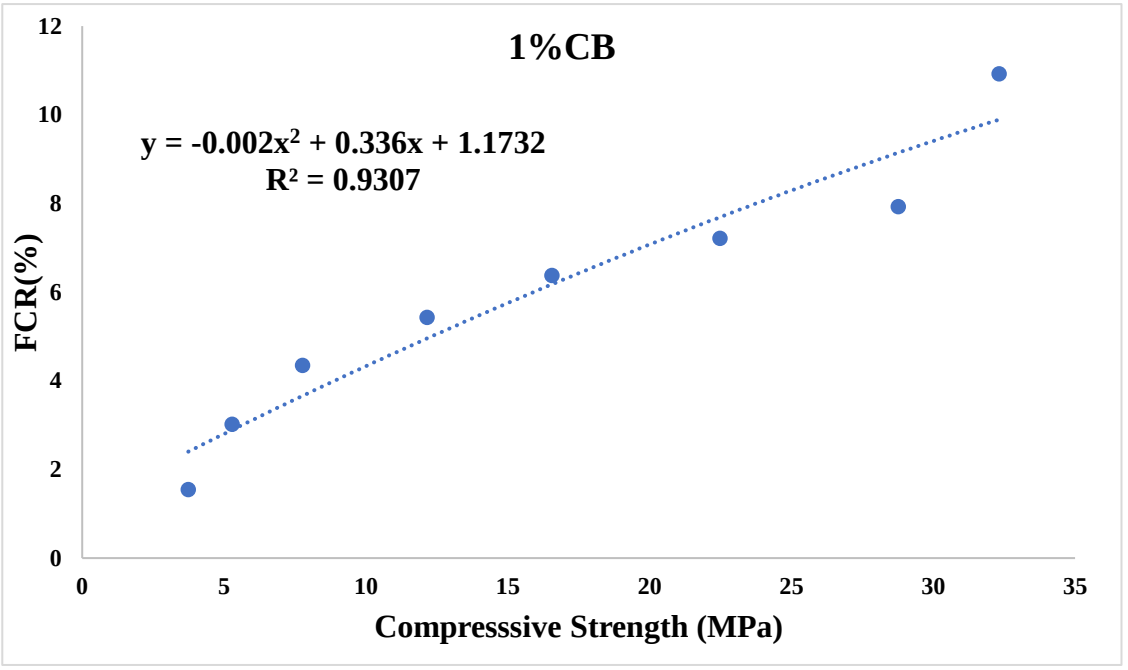

Fig4. 13Fitting curve between FCR and Compressive Strength of 1%CB for 28 days.

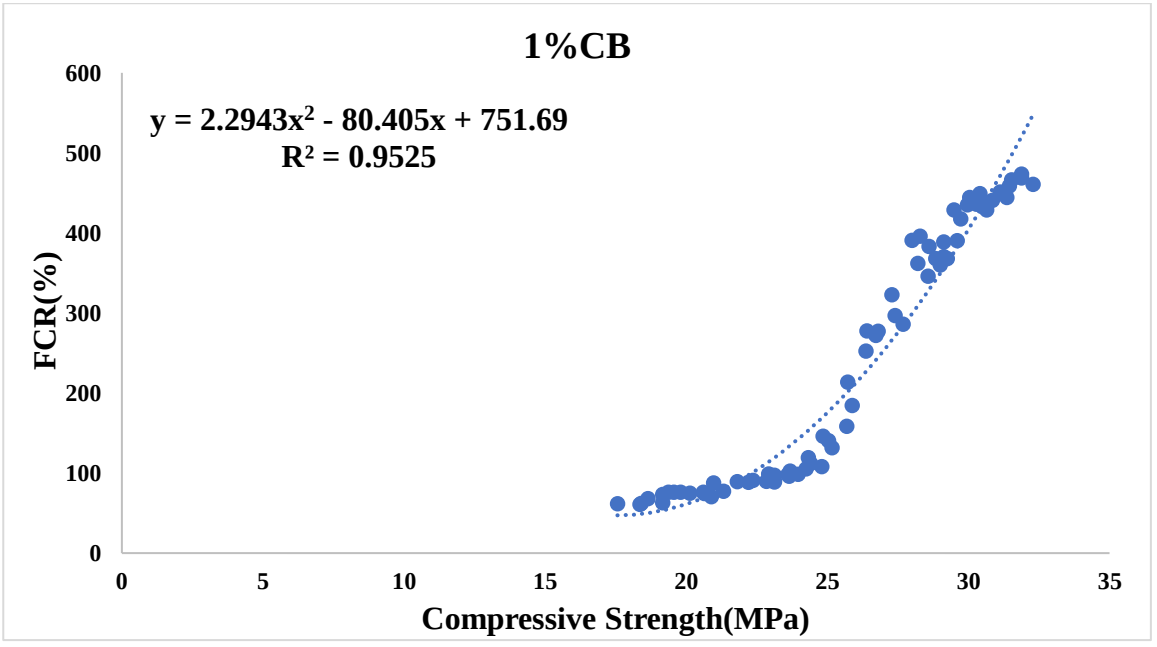

Fig4. 14 Fitting curve between FCR and Compressive Strength of 1%CB for 56 days.

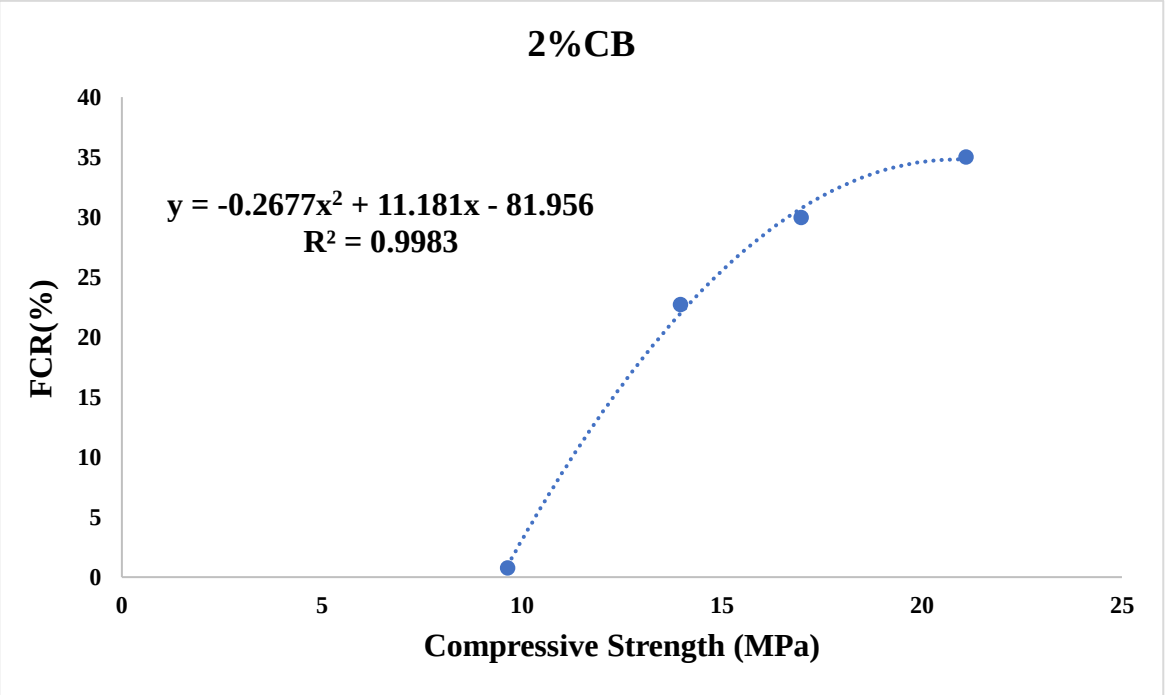

Fig4. 15 Fitting curve between FCR and Compressive Strength of 2%CB for 28 days.

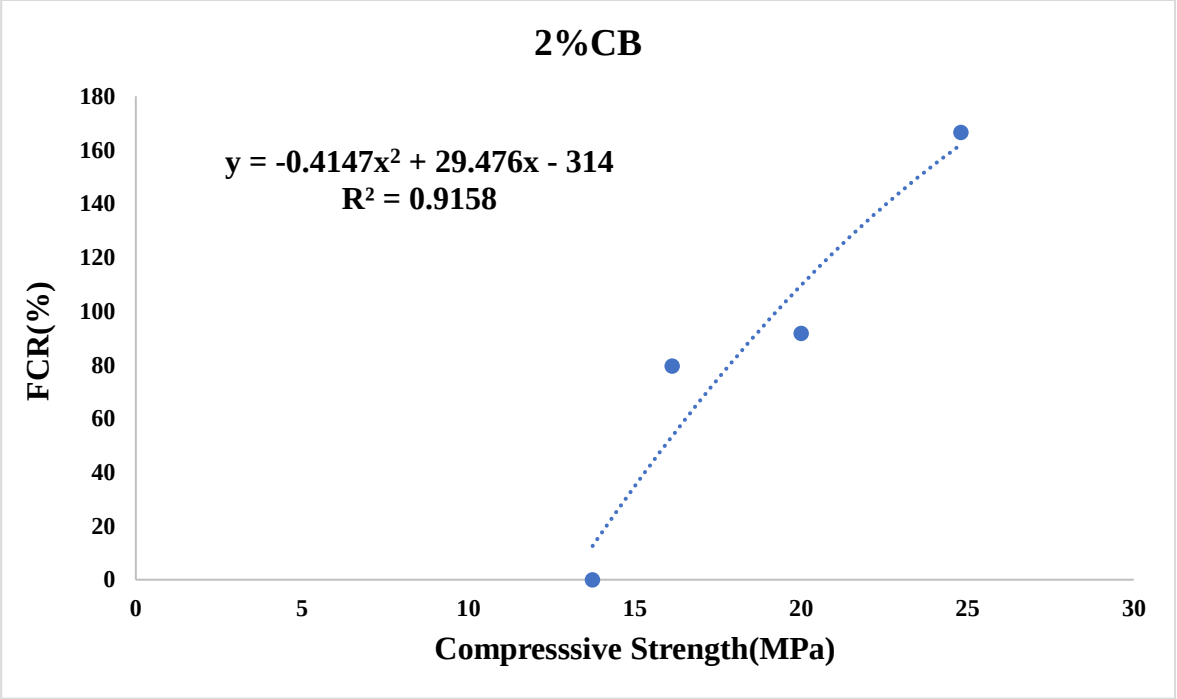

Fig4. 16 Fitting curve between FCR and Compressive Strength of 2%CB for 56 days.

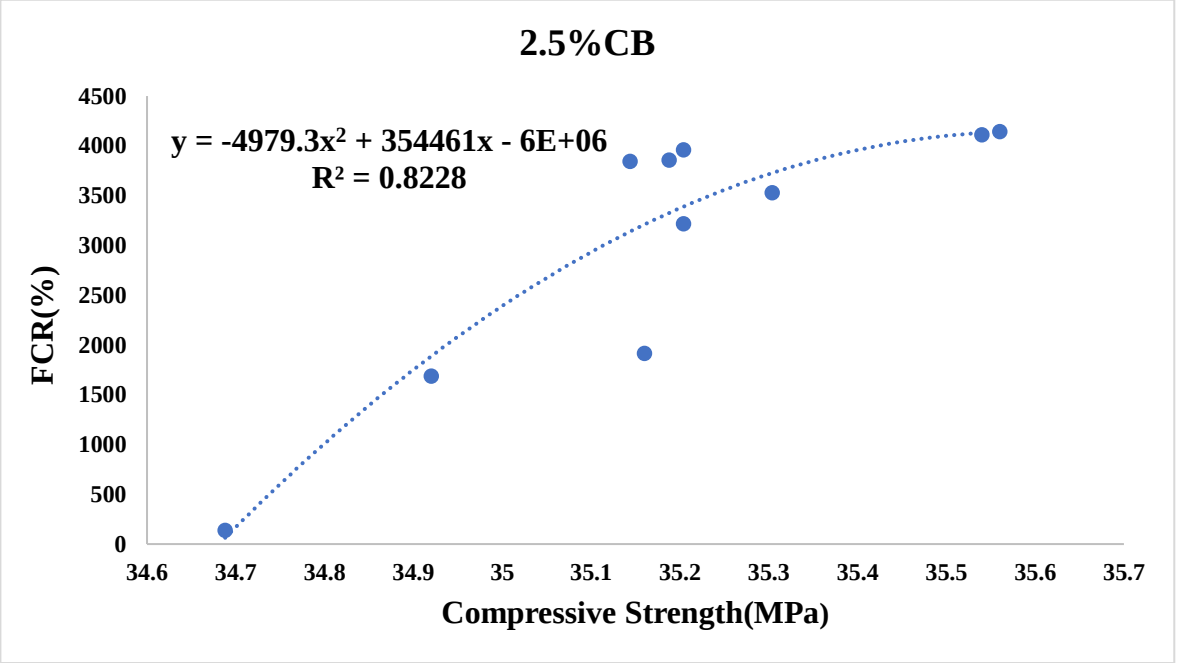

Fig4. 17 Fitting curve between FCR and Compressive Strength of 2.5%CB for 28 days

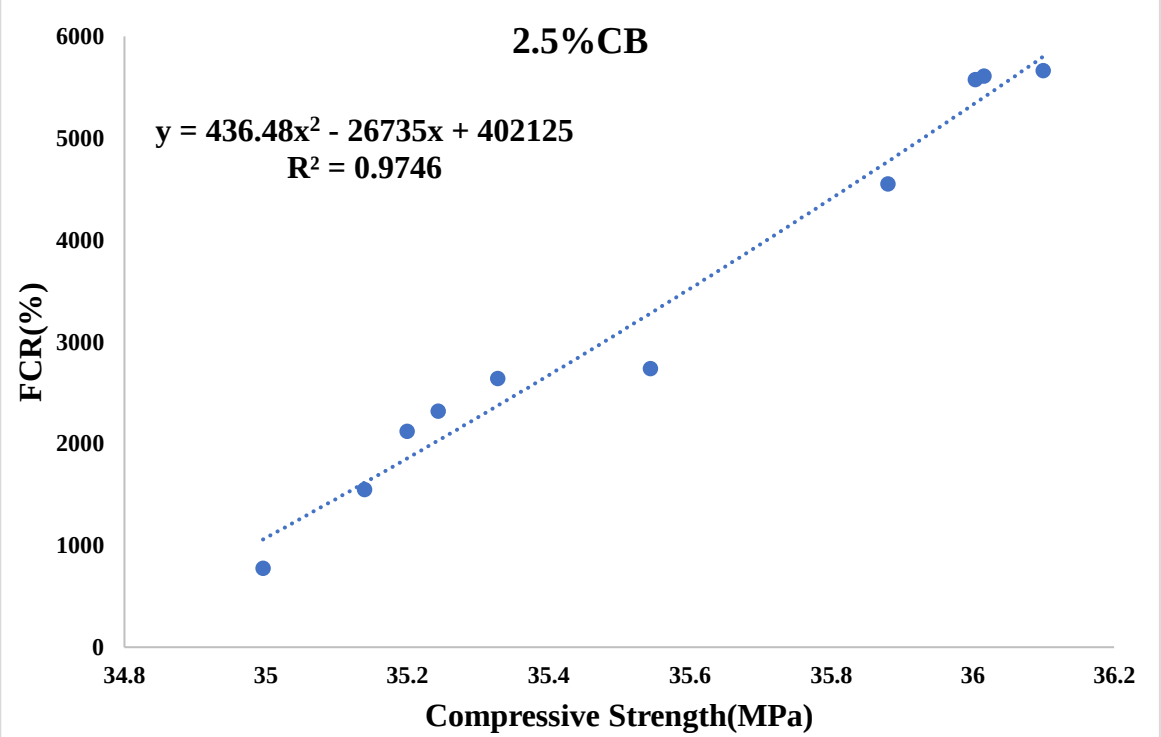

Fig4. 18 Fitting curve between FCR and Compressive Strength of 2.5%CB for 56 days.

STRAIN VS FCR ANALYSIS

Here we only discuss the 2.5%CB samples. Because the control sample didn't show any sensitivity to stress, the FCR of the sample remains constant. There is no change in the resistivity. And the value of electrical resistivity for both 1% is 61.6% high and 2% is 19.1%high. The 2.5%CB has less value of resistivity which means it is more conductive in nature, so we only opt 2.5%CB for strain sensing. As we can observe from the **Fig4.19.**and **Figure 4.20** for both the mixes, as the strain increases, the FCR values decrease or remain stable. A sudden increase, similar to FCR vs compressive strength curves is observed as the sample approaches its failure point. As we know that strain exhibits a behavior proportional to stress, on the basis of the behavior shown by the stress parameter, a comparable behavior shown by the stress parameter shows it is a good indicator that reinforces of the usability of the sample as a self-sensing tool. This shows that CB cementitious sensor can act as stress/strain monitoring.

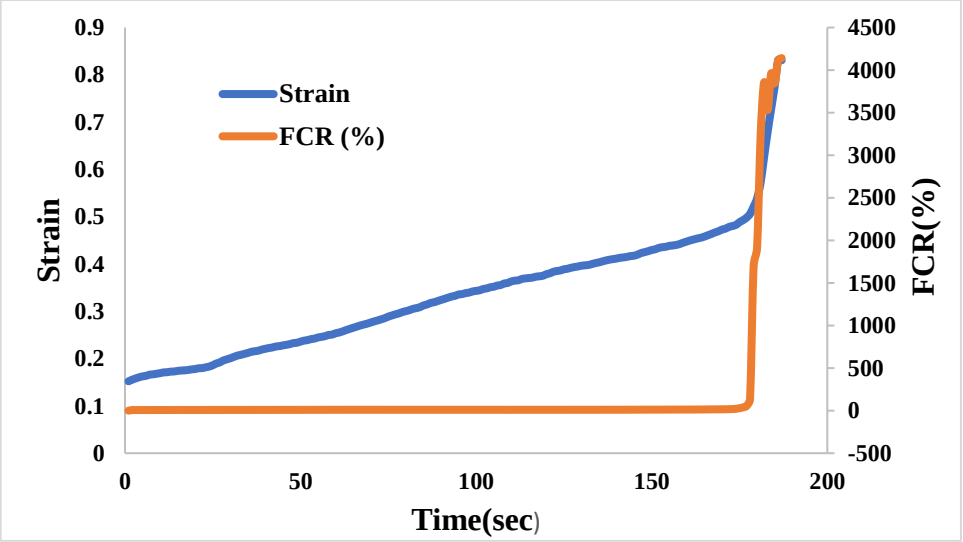

Fig4. 19 Strain vs FCR curve for 2.5% tested at 28 days.

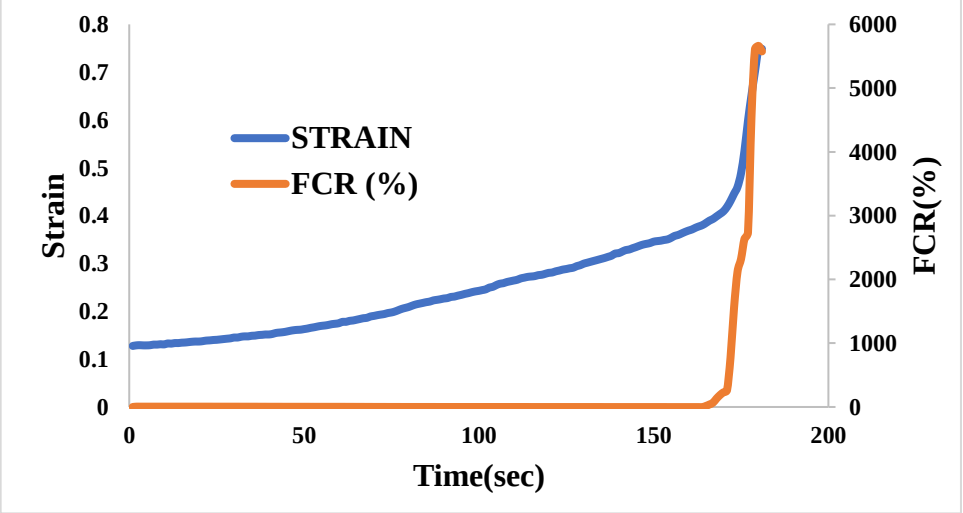

Fig4. 20 Strain vs FCR curve for 2.5% tested at 56 days

The fitness of FCR vs Strain for 2.5%CB for 28 days found to be 0.7212, for 56 days found to be 0.9457. Sample with greater R-squared value will suggest that the composite possesses a good sensing capability. The result shows high stability and uniformity.

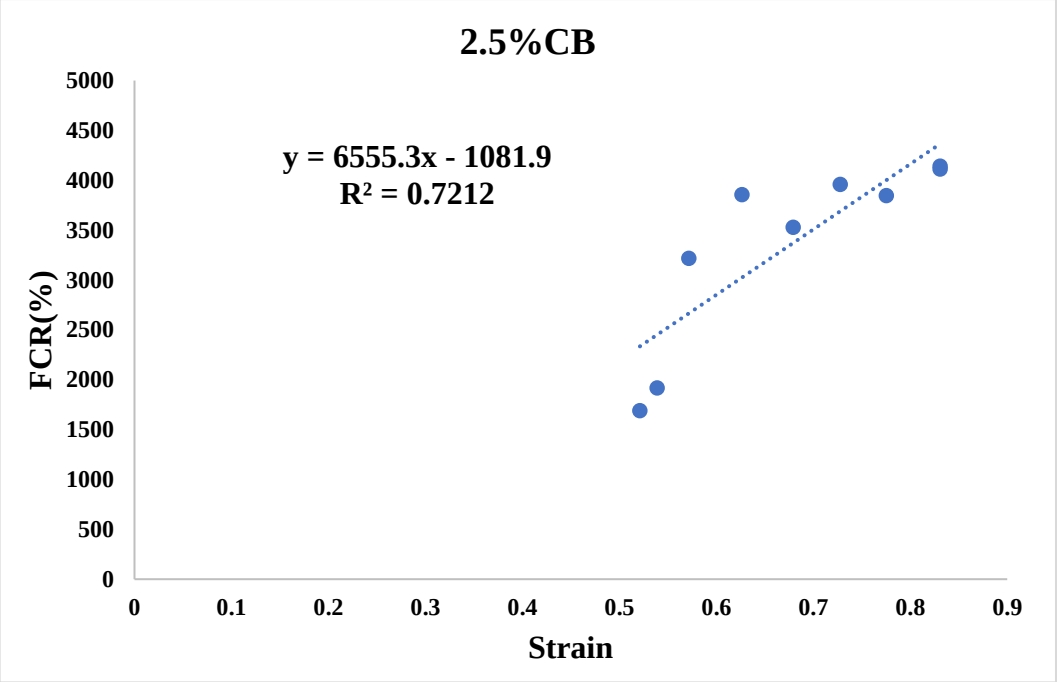

Fig4. 21 Fitting curve between FCR and Strain of 2.5%CB for 28 days.

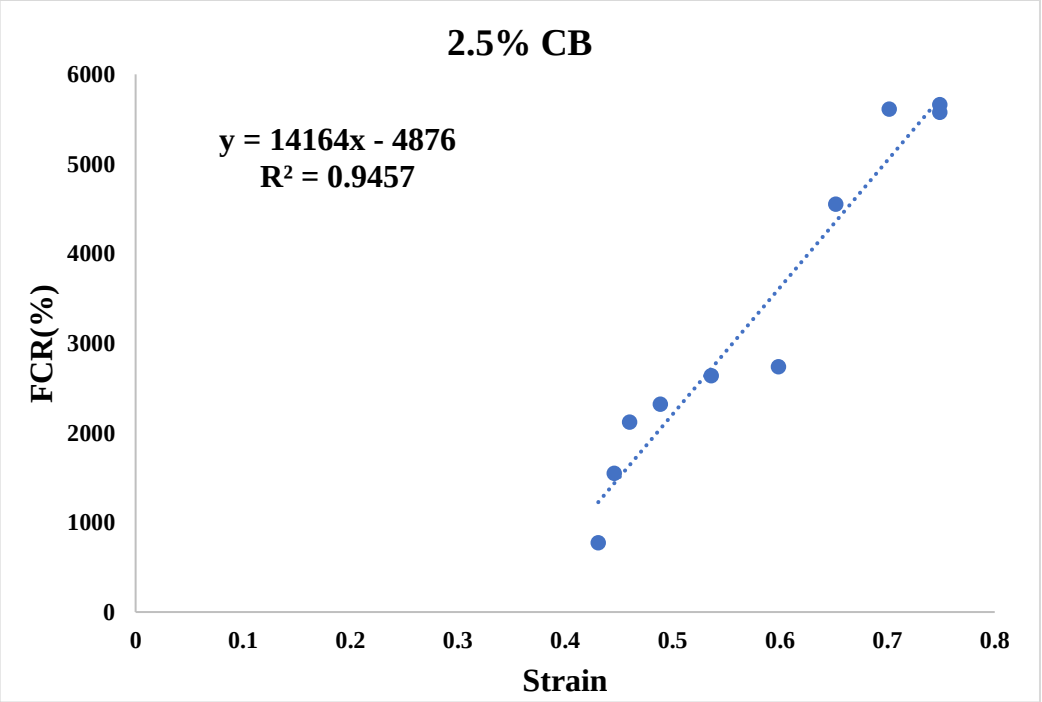

Fig4. 22 Fitting curve between FCR and Strain of 2.5%CB for 56 days

4.7 ANALYSIS OF SELF-SENSING CEMENTITOUS SENSOR IN FLEXURAL BEAM

Crack growth in the beam under flexural stress conditions showed the following characteristics: -

The variation in the FCR of CB material under the constant displacement speed of (0.5mm/min). In the beginning, tiny fractures formed in the tension zone of the pure bending section of concrete beams due to positive stress at 20%-40% of peak load. After a few vertical flexural cracks (usually 2–3) in the pure bending zone, the cracks stopped increasing and gradually shifted upwards along the neutral axis Shown in **Figure 4.31**. As the load increased, diagonal shear cracks appeared in the bending-shear portion, which experiences both positive and shear stresses. As the load rises, these diagonal shear cracks spread upwards and laterally. Increased flexural stress resulted in diagonal shear cracks extending towards the central loading point and increasing in width. Stress as well as strain both are measure. This stress/strain behaviour was monitored using the 1st SSC sensor located at the centre in the tension zone and second sensor which is located 10cm away from 1st sensor in the tension zone. Two sensors were installed because if one sensor was not working then we get the FCR value form the 2nd sensor. Same trend was followed Firstly, the FCR decreases when the load was increases because the conductive networks started coming together so the resistivity reduces but when peak load was applied to the beam the FCR Increases due to the sudden break of the specimen the conductive network breaks and the beam gets failed. This was so because shear failure under control by diagonal fractures dominated the ultimate damaging mode of concrete beams (Qui, et al., 2024). Two sensors were installed in the beam which gives different values of FCR Shown in **Figure 4.23 and 4.24.**

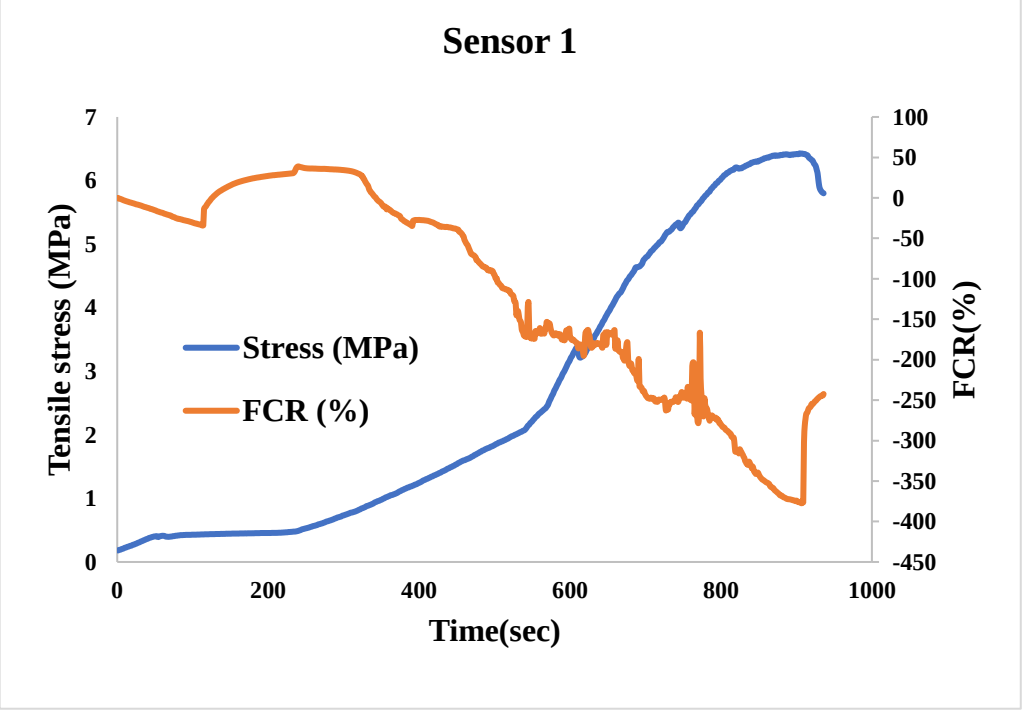

Fig4. 23 FCR vs Tensile Strength recorded by the sensor 1.

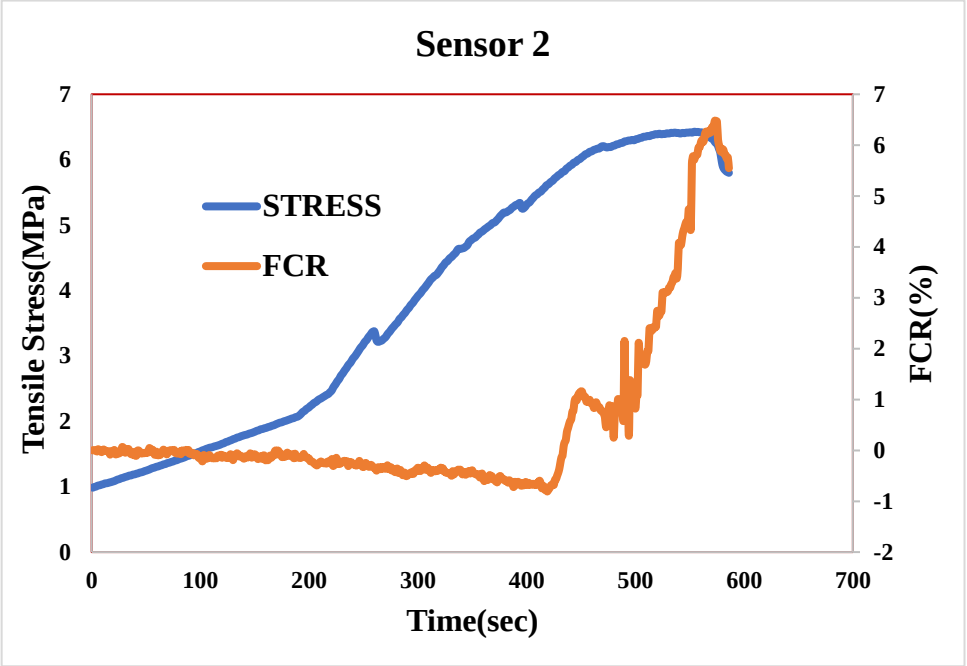

Fig4. 24 FCR vs Tensile Strength recorded by the sensor 2

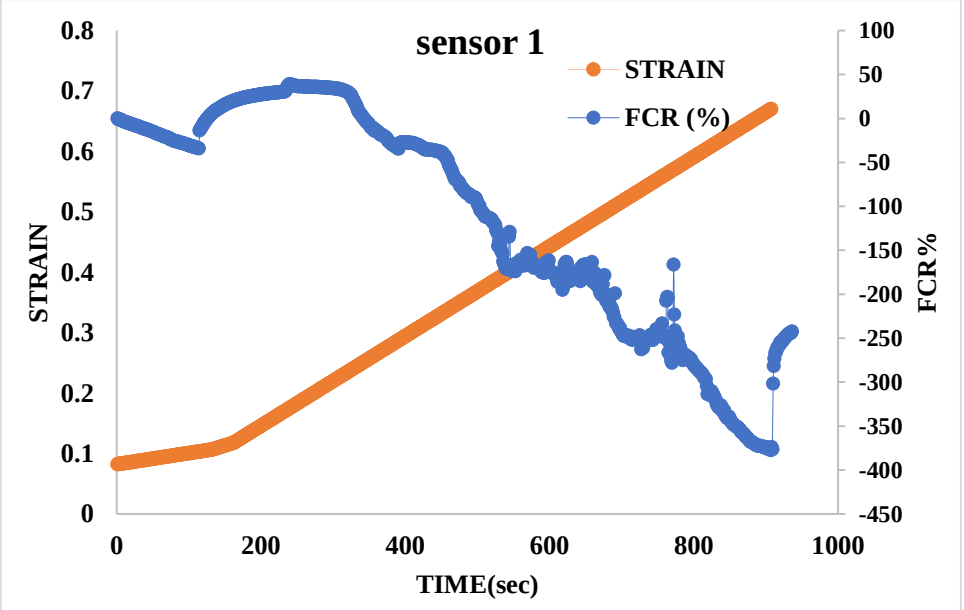

Fig4. 25 FCR vs Strain recorded by the sensor 1.

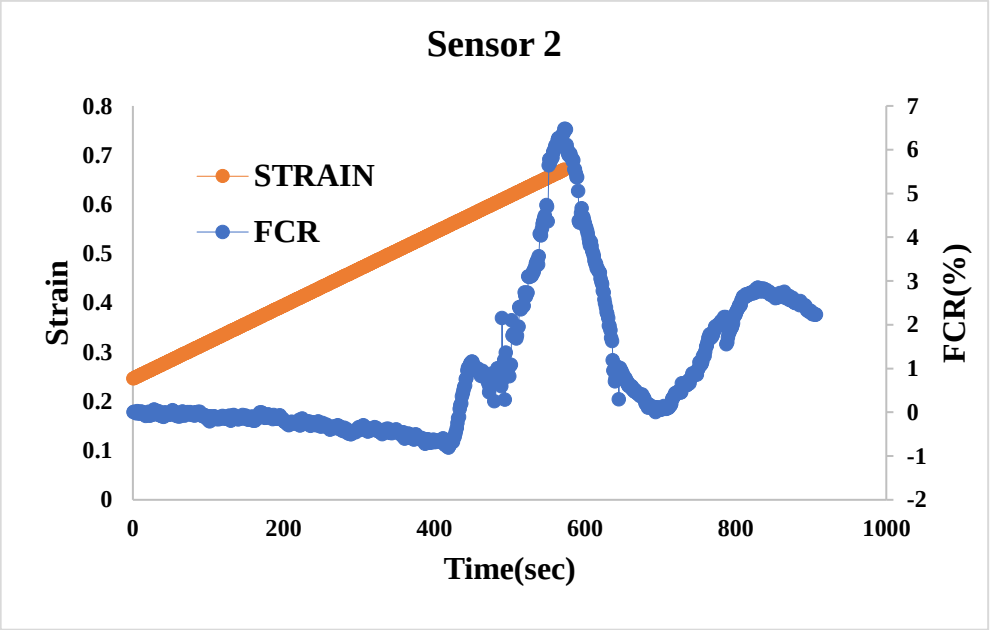

Fig4. 26 FCR vs Strain recorded by the sensor 2.

The fitness of FCR and Stress for 2.5% CB for sensor 1 was 0.9396 and for sensor 2 was 0.8477. Higher the value of R^2 means good sensing ability.

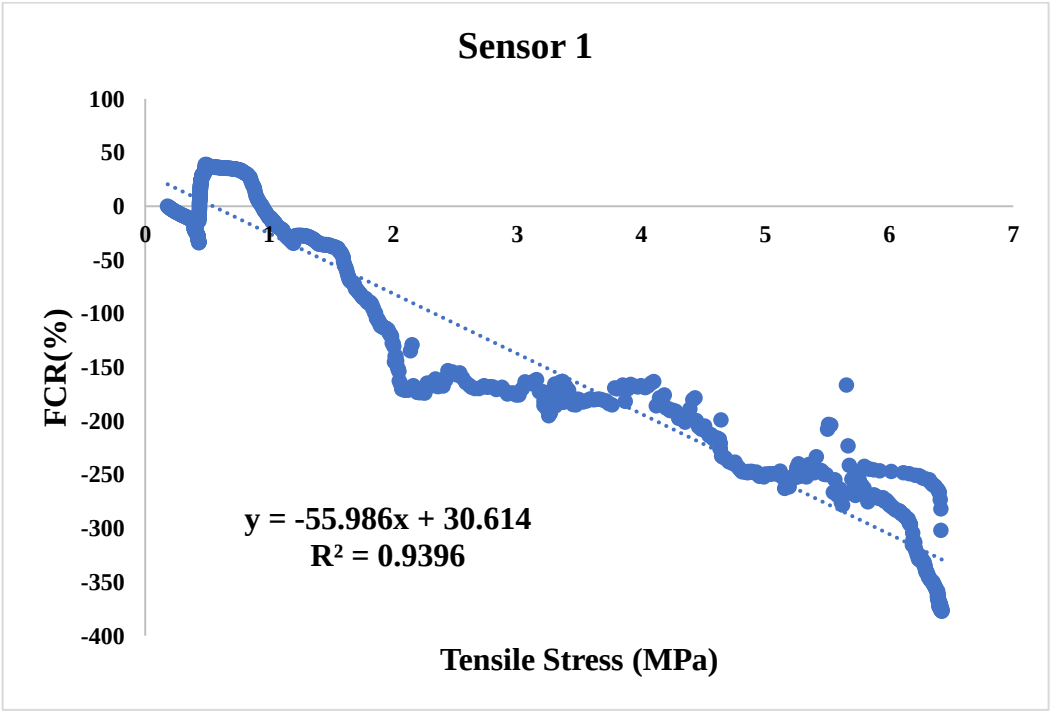

Fig4. 27Fitting curve between FCR and Flexural Strength (MPa) of 2.5%CB for sensor 1.

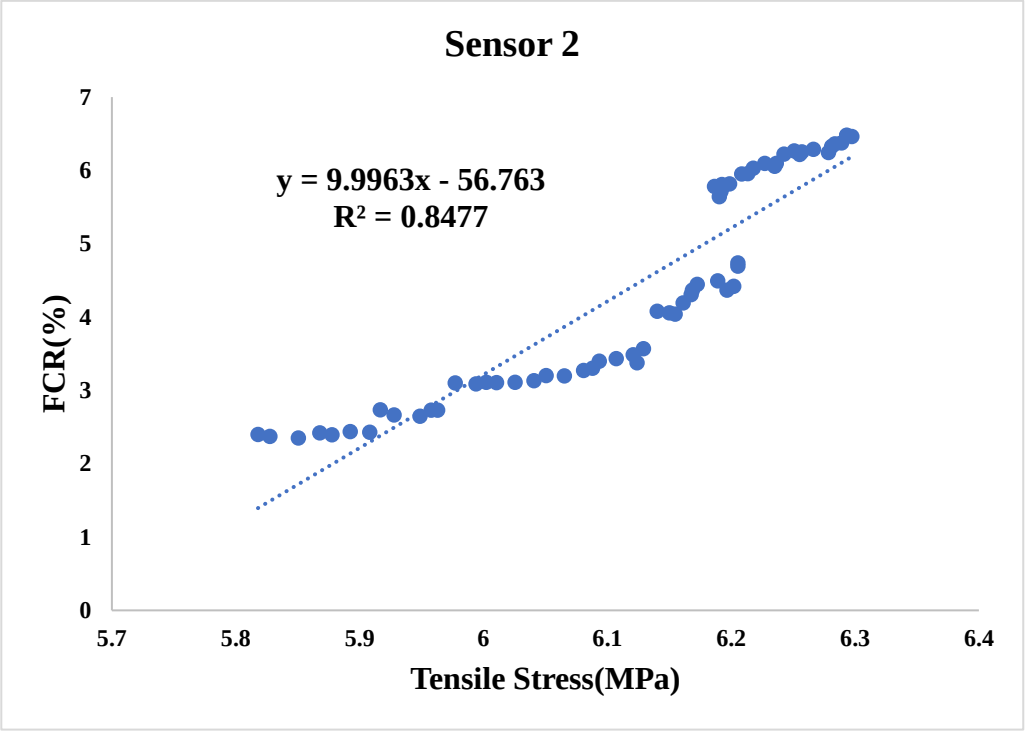

Fig4. 28 Fitting curve between FCR and Flexural Strength (MPa) of 2.5%CB for sensor 2.

The fitness of FCR and Strain for 2.5% CB for sensor 1 was 0.9472 and for sensor 2 was 0.8381. Higher value of R^2 means good sensing ability.

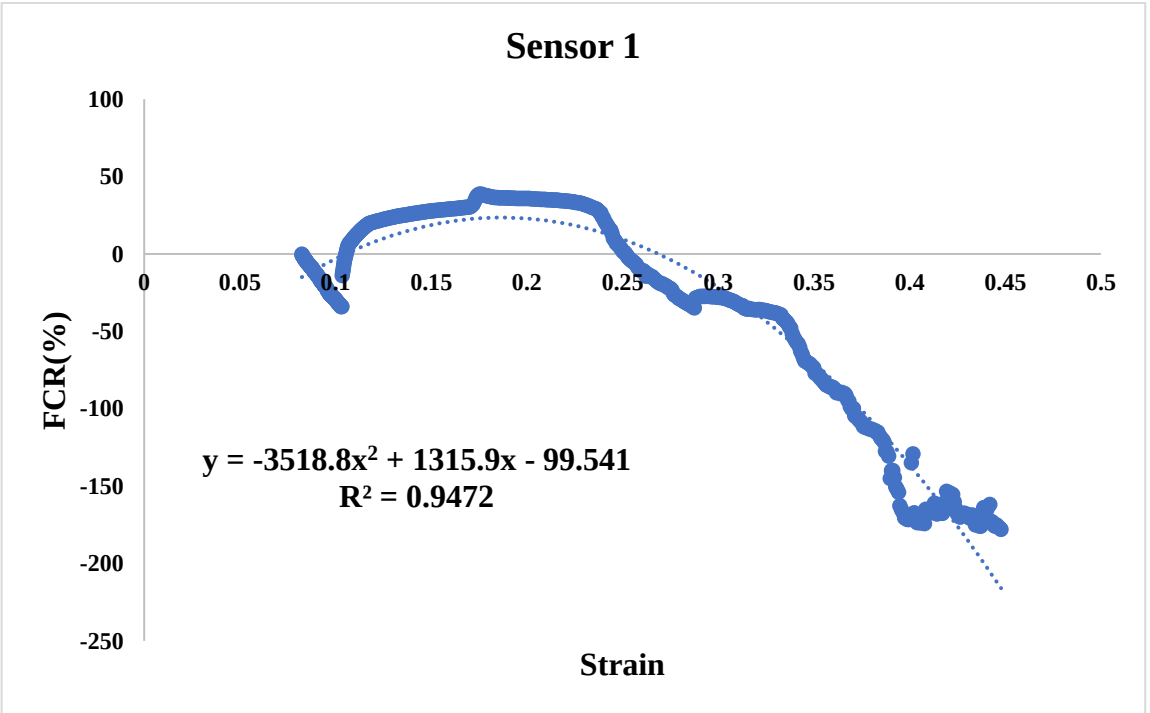

Fig4. 29 Fitting curve between FCR and Strain of 2.5%CB for sensor 1.

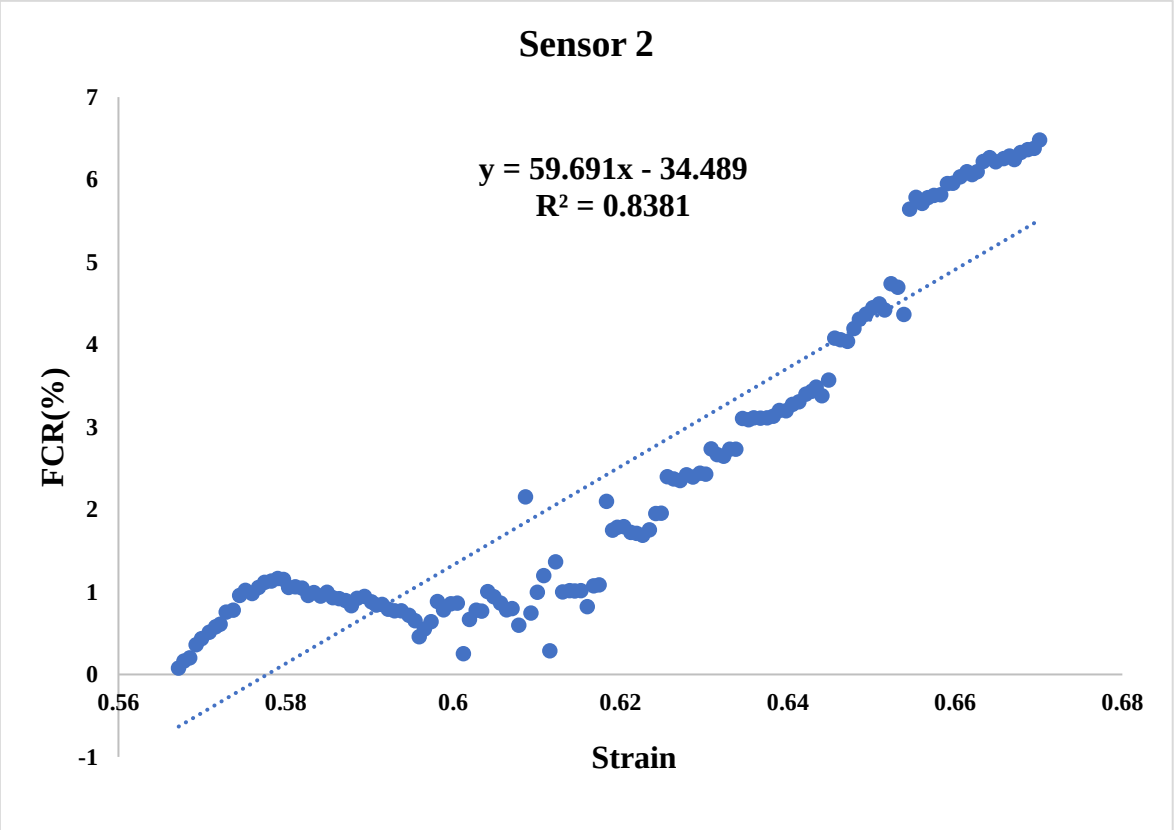

Fig4. 30 Fitting curve between FCR and Strain of 2.5%CB for sensor 1.

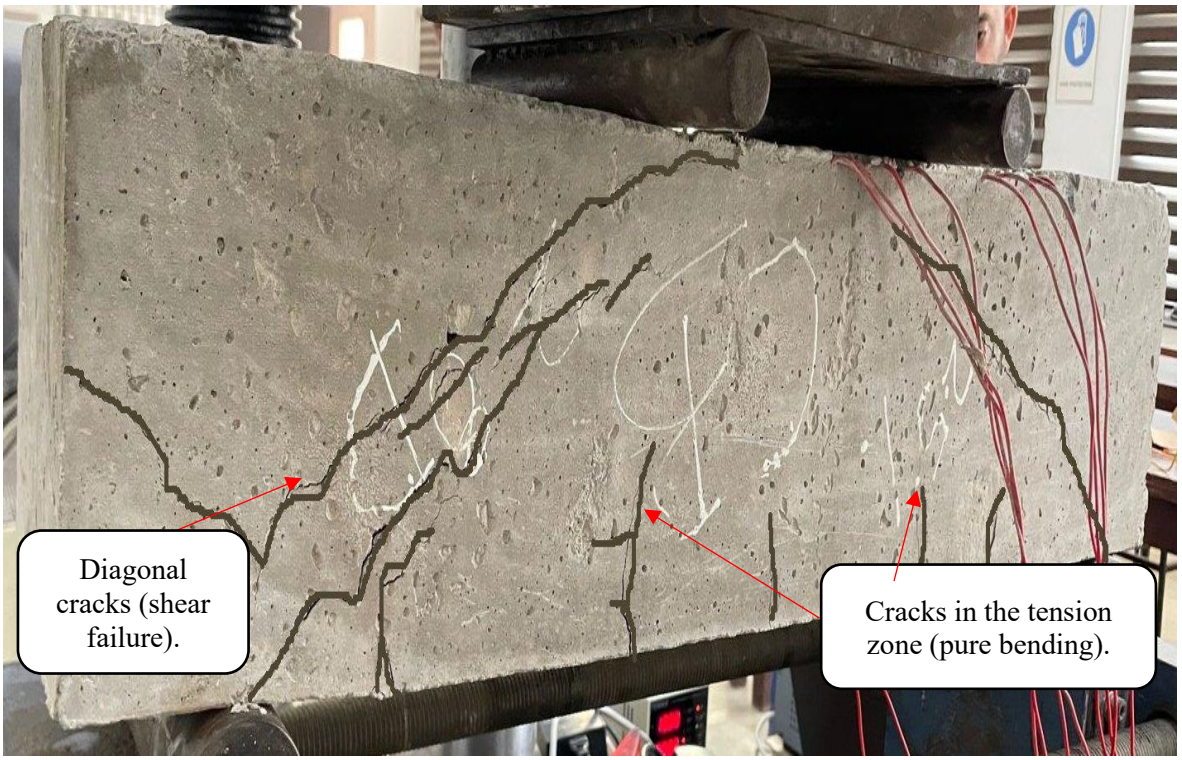

Fig4. 31 Shear failure of Beam.

4.8 MICROSTRUCTURAL IMAGE ANALYSIS (SEM)

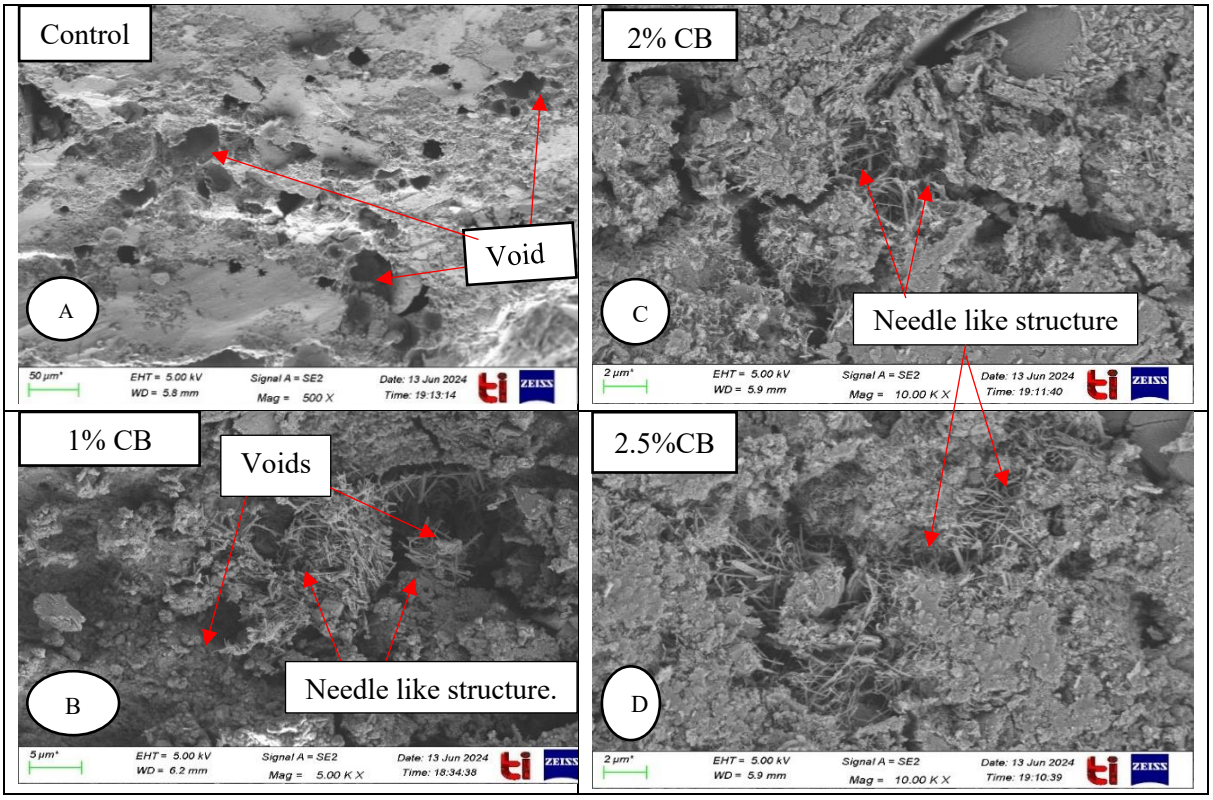

Fig4. 32 Shows Different SEM images of different percentage of CB

In Fig4.32(a). no needle-like structures(formation of conductive network) were seen in the control sample, but the voids are plainly visible. However, in Fig4.32(b, c, d), the nano structure of the concrete differed from the control mix. The number of voids was reduced, and a needle-like structure was visible. The needle like structure reduces porosity, leading to enhance the strength. The CB experienced a growth in the form of a needle-like shape. A higher concentration of CB resulted in a denser microstructure with reduced porosity. Very less voids are present in the CB specimens because of the filling effect of the nano material. And which indicated the great strength effect (R. Ashani, et al., 2018).

4.9 SUMMARY

After testing all the specimen, the best percentage of the CB was 2.5% as observed in the compressive strength results the higher strength also in the Flexural strength results higher value is obtained for the 2.5%CB and Electrical Resistivity results shows that the CB 2.5% is more conductive but with the duration of time the conductivity decreases due the temperature variation, but if the sensor is covered with some type of coating which reduce the environment effect i.e. temperature, humidity and moisture etc., then the sensor will not lose the conductivity. But there are some changes in the values of FCR. The value of FCR is high i.e. 4500% for 28days and 6000% for 56 days, as compared to the other samples because the specimen was dried due to higher Temperature and Humidity. The main objective is to develop a self-sensing flexural beam in a sensor form for stress/strain monitoring. Form both the sensors gives the values of Stress/Strain vs FCR values but, there was a shear failure in the beam but we get the value of FCR which is over main motive.

CHAPTER 5 CONCLUSIONS

5.1 GENERAL

The following conclusions may be gathered from the current study's findings about the addition of CB to cement-based composites for different mechanical and piezoresistive properties:

1. The addition of the CB resulted in an enhancement in the compressive strength of the cementitious mortar after 28 and 56 days except 1% of CB.

2. The compressive strength of the specimens with 2% and 2.5% addition of CB increased by 18.52% and 25.48% respectively at 28 days compared to the control specimen. At 56 days, the increase in compressive strength was 4.72% and 14.16% respectively.

3. The flexural strength of CB increased as the proportion of CB increased. The highest level of strength is attained with a 2.5%CB mixture, exhibiting a 11.19% enhancement in flexural strength compared to the control mixture after 28 days, and 6.36% improvement after 56 days.

4. The decrease in compressive strength for 1%CB is likely due to the dilution effect.

5. Electrical Resistivity results shows that the CB 2.5% is more conductive but with the duration of time the conductivity gets effected due the temperature variation, but if the sensor is covered with some type of coating which reduce the environment effect i.e. temperature, humidity and moisture etc., then the sensor will not lose the conductivity.

6. It was discovered that there was no significant alteration in FCR values for control specimens when the stress was increased, both at 28 days and 56 days.

7. The addition of CB resulted in the densification of the microstructure of cementitious mortar. This observation verified that the composites effectively filled the pores.

8. The piezoresistive behaviour of the CB composite is due to the reduction in distance between the CB particles and the formation of conductive channels when a compressive stress was applied. This results in increased conductivity and alteration in FCR.

9. The piezoresistive performance of cementitious composites containing carbon black (CB) shows their capacity to function as intrinsic sensors in cement-based materials.

10. For all the samples containing CB, there was a sudden increase in FCR value at the failure point due to breaking of conductive networks in the samples, indicating the reactivity of the enhanced samples to stress/strain applications. The FCR value for 2.5%CB specimen was 4500% and 6000% which was very high.

11. The self-sensing behaviour of the CB sensor, when it was inserted into a flexural beam, matches the response seen in the cubic samples used to study the piezoresistive effect. The sensor validates their use as stress/strain sensors.

5.2 FUTURE SCOPE

1. Further investigation is required to determine the impact of environmental factors, such as temperature, carbon dioxide levels, chloride concentration, and humidity, on the sensing capabilities of cementitious composites containing CB.

2. This research limits the piezoresistive performance to simply monotonic loading. However, in order to understand the repeatability of the produced SSC, it is necessary to investigate its performance under cyclic loading in real-life settings.

3. Further investigation is required to conduct a thorough examination of the microstructure in order to fully understand the fundamental mechanism responsible for the piezoresistive performance of carbon black-based (SSC).

4. Further research is required to explore other methods to make piezoresistive behaviour in sensors using carbon black (CB).

References

1. ASTM (2021) 'ASTM C348-21: Standard Test Method for Flexural Strength of Concrete'. American Society for Testing and Materials 1-6

2. ASTM (1988) 'ASTM C109: Standard Test Method for Compressive Strength of Hydraulic Cement Mortars', American Society for Testing and Materials 4031 (Part 6), 3-7

3. ASTM C1437 (2007) 'Standard Test Method for Flow of Hydraulic Cement Mortar'. C1437

4. Bureau of Indian Standard (2013) IS 8112: 2013, Ordinary Portland Cement, 43 Grade Specification. (March)

5. Bureau of Indian Standard (2000) IS 456: 2000, Plain and reinforced concrete - code of practice

6. L. Castañeda-Saldarriaga, D., Alvarez-Montoya, . J., Martínez-Tejada, . V. & Sierra-Pérez, . J., 2021. Toward Structural Health Monitoring of Civil Structures Based on Self-Sensing Concrete Nanocomposites: A Validation in a Reinforced-Concrete Beam.

7. Monteiro, A. O., Cachim, P. B. & Costa, P. M., 2017. Self-sensing piezoresistive cement composite loaded with carbon.

8. Qi, G. et al., 2023. Effect of rGO/GNP on the electrical conductivity and piezoresistance of cement-based composite subjected to dynamic loading.

9. Singh, S., Hasan, M., Sharma, P. & Narang, J., 2022. Graphene nanomaterials: The wondering material from synthesis to applications.

10. Alshammari, B. H. et al., 2023. Organic and inorganic nanomaterials: fabrication, properties and applications.

11. Azhari, F. & Banthia, N., 2012. Cement-based sensors with carbon fibers and carbon nanotubes.

12. Dong, W. et al., 2021. Multifunctional cementitious composites with integrated self-sensing and hydrophobic capacities toward smart structural health monitoring.

13. Han, . B., Ding, S. & Yu, X., 2015. Intrinsicself-sensingconcreteandstructures:Areview.

14. Li , W. et al., 2024. Development of self-sensing ultra-high-performance concrete using hybrid.

15. Qiu, L. et al., 2024. *Monitoring damage of concrete beams via self-sensing cement mortar coating with carbon nanotube-nano carbon black composite fillers*.

16. Qui, L. et al., 2024. Monitoring damage of concrete beams.

17. R. Ashani, H., Mehta, J. & Markna, J., 2018. SEM ANALYSIS OF NANO CARBON BLACK.

18. Rathinavel, S., Priyadharshini, K. & Panda , D., 2021. A review on carbon nanotube: An overview of synthesis, properties, functionalization, characterization, and the application.

19. Rehman , . S. K. U. et al., 2018. Influence of Graphene Nanosheets on Rheology,Microstructure, Strength Development andSelf-Sensing Properties of Cement Based Composites.

20. rodrigues, R. et al., 2021. Reinforced concrete structures: A review of corrosion mechanisms and advances in electrical methods for corrosion monitoring.

21. Sarwary, M. et al., 2019. Self-Sensing of Flexural Damage in Large-Scale.

22. Tao, J., Wang, X., Wang, Z. & Zeng, Q., 2019. Graphene nanoplates as an effective additive to tune the microstructure and piezoresistive properties of cement based composite.

23. Tian, X. et al., 2023. Self-sensing study of stress in low-doped carbon fiber reinforced.

24. Tian, Z., li, Y., Zheng, j. & wang, s., 2019. A state-of-the-art on self-sensing concrete: Materials, fabrication.

25. wang, h. et al., 2018. Multi-functional properties of carbon nanofiber reinforced reactive.

26. wang, Q. et al., 2015. Influence of graphene oxide additions on the microstructure and mechanical strength of cement.

27. wang, y. & zhang, l., 2022. development of self senisng cementitious composite in corportaing hybride graphene nanoplates and carbon nanotubes for structural health monitoring.

turnitin

Digital Receipt

This receipt acknowledges that Turnitin received your paper. Below you will find the receipt information regarding your submission.

The first page of your submissions is displayed below.

Submission author:	Arpit GOYAL
Assignment title:	Ashank Final ME Thesis
Submission title:	Ashank Final report.docx
File name:	Ashank_Final_report.docx
File size:	11.54M
Page count:	74
Word count:	16,718
Character count:	93,063
Submission date:	29-Aug-2024 02:35PM (UTC+0530)
Submission ID:	2440367851

CHAPTER 1 INTRODUCTION

1.1 GENERAL

Over time, there has been a growing focus on monitoring and analyzing concrete performance utilizing condition assessment methods and various materials. Structural Health Monitoring (SHM) is a novel technology that may identify performance issues in structures before they cause significant capacity loss. "SHM" is a technique that continuously monitors a structure's state to detect faults and prevent collapse or failure. By using an early damage monitoring method for load-bearing structural systems. Identifying vulnerabilities early on allows for early assessment and potential damage restoration. SHM analyzes a structure's functioning, monitors its performance, and provides real-time information on its current status. SHM can monitor several parameters, including corrosion, alkali reactions, humidity, ionic strength, loads, accelerations, strains, and fractures. Structural health monitoring uses a sensory method to accurately quantify the functioning of structures. Recently proposed cement-based sensors may detect stress/strain directly via electrical resistance analysis due to their piezoresistive properties. Smart sensors, also known as self-sensing structural composites, may be integrated into a structure to provide structural capabilities and respond to stress and damage (Azhari & Banthia, 2012).

In recent decades, there has been a growing interest in the ability of cementitious materials with conductive particles to feel themselves for SHM. Previous research suggests that many materials and sensors have emerged, but their practical usage remains limited due to the high cost of conductive materials. Nanoscale materials, such as carbon nanotubes (CNTs), may be difficult to disseminate in cementitious matrix.

Electric-resistivity strain gauges, piezo-resistivity detectors, and optic sensors are often used in construction to analyze and monitor conditions. However, their usage has considerable drawbacks, including limited sensitivity and low durability. Advancements in smart materials, such as cement-based sensors, may alleviate these worries (wang, et al., 2015).

1.1 SELF SENSING CONCRETE.

Self-sensing concrete (SSC) is a smart material that can detect and send real-time information on its own structural health and performance. It is a cutting-edge technology that blends concrete, sensors, and electronics to create a new generation of intelligent structures. SSC sensors are often inserted in the concrete matrix during the mixing process or affixed to the concrete's surface after it has hardened. Mechanical loads such as compression, tension, shear, and bending, as well as environmental parameters such as temperature, humidity, and moisture content, may be detected by the sensors (Han, et al., 2015).

Self-Sensing cementitious concrete (SSC) has been thoroughly studied because it might provide a realistic and cheap solution for civil infrastructure structural health monitoring. Concrete self-sensing is caused by the piezoresistive action of functional filler particles that generate a conductive connection throughout the composite phase. Thus, when concrete is pushed, the network and electrical resistance change. The structure of self-sensing concrete is complex. By detecting and monitoring them, self-sensing concrete may improve structural

1

Ashank Final report.docx

ORIGINALITY REPORT

19%	8%	17%	1%
SIMILARITY INDEX	INTERNET SOURCES	PUBLICATIONS	STUDENT PAPERS

PRIMARY SOURCES

1	Xinru Tian, Shaowei Hu, Yaoqun Xu, Hao Qi, Xiang Xue. "Self-sensing study of stress in low-doped carbon fiber reinforced hydraulic concrete", Journal of Building Engineering, 2023 Publication	3%
2	Yunyang Wang, Liqing Zhang. "Development of self-sensing cementitious composite incorporating hybrid graphene nanoplates and carbon nanotubes for structural health monitoring", Sensors and Actuators A: Physical, 2022 Publication	2%
3	ijrpr.com Internet Source	1%
4	opus.lib.uts.edu.au Internet Source	1%
5	Wengui Li, Yipu Guo, Xuanrui Zhang, Wenkui Dong, Xiaohu Li, Tao Yu, Kejin Wang. "Development of self-sensing ultra-high-performance concrete using hybrid carbon	1%

black and carbon nanofibers", Cement and Concrete Composites, 2024
Publication

6	Mohammad H. Sarwary, Gürkan Yıldırım, Ali Al-Dahawi, Özgür Anıl, Kaveh A. Khiavi, Kenan Toklu, Mustafa Şahmaran. "Self-Sensing of Flexural Damage in Large-Scale Steel-Reinforced Mortar Beams", ACI Materials Journal, 2019 Publication	1 %
7	bradscholars.brad.ac.uk Internet Source	1 %
8	Jin Tao, Xiaohu Wang, Zhendi Wang, Qiang Zeng. "Graphene nanoplatelets as an effective additive to tune the microstructures and piezoresistive properties of cement-based composites", Construction and Building Materials, 2019 Publication	1 %
9	Guodong Qi, Qin Wang, Ruifeng Zhang, Zhixiang Guo, Dafu Zhan, Shuang Liu. "Effect of rGO/GNP on the electrical conductivity and piezoresistance of cement-based composite subjected to dynamic loading", Construction and Building Materials, 2023 Publication	1 %
10	hdl.handle.net Internet Source	1 %